Titanate nanotubes combined with graphene-based materials as a novel anode material for lithium-ion batteries

by
Anaguli Abulizi

Submitted to the Graduate School of Engineering and Natural Sciences
in partial fulfillment of
the requirements for the degree of
Master of Science

Sabanci University
August 2016

Titanate nanotubes combined with graphene-based materials as a novel anode material for lithium-ion batteries

APPROVED BY

Assoc. Prof. Dr. Selmiye Alkan Gürsel (Thesis advisor)	.....
Dr. Alp Yürüm (Thesis co-advisor)	.....
Prof. Dr. Ayşe Gül Gürek	.....
Assoc. Prof. Dr. Burç Mısırlıoğlu	.....

DATE OF APPROVAL: 10/08/2016

to my family

Acknowledegments

Before I express my sincere appreciation to any specific person, I would like to emphasize how grateful I am for being accepted to Sabancı University as a graduate student for Fall 2014. I feel very proud to be part of Sabancı University.

First of all, I would like to thank Prof. Dr. Yuda Yürüm for his kind support and help throughout my studies at Sabancı University. I am honored to be chosen to work in his research group. My deepest thanks goes also to my supervisor Assoc. Prof. Dr. Selmiye Alkan Gürsel, who has been constantly providing me with all possible support during my studies. She treats the students with great patience and makes a great effort to create a positive working environment for students. Her strict and valuable assessments on the quality of the presentation during each biweekly meeting have helped me to significantly improve my scientific presentation skills. I could not be more grateful for her supervision .

My sincere gratitude goes also to Dr. Alp Yürüm. As my daily supervisor, he has guided me through my studies and research work, for which I am truly grateful. His passion for research and enthusiastic commitment to the scientific discussions with students have inspired me to work hard and achieve my research goals. I would like to express my sincere appreciation to him for his guidance, support, and constant encouragement during the course of my two-year master's program at Sabancı University.

I wish to thank Dr. Emre Biçer. His extensive and deep knowledge on battery testing methods and his constructive remarks on the project helped me to work more efficiently. I would like to express my heartfelt appreciation to him for his assistance.

Furthermore, it would not have been possible to achieve the results in this thesis without the invaluable effort of following people: Miad Yarali (SEM, BET), Ad-

nan Taşdemir (battery test), Zahra Gohari Bajestani (BET), Ali Ansari (TGA/DTA, SEM/EDX), Sajjad Ghobadi (GO material supply), Ahmet Can Kırlıoğlu (N-doped GO material supply), and Parveen Qureshi (SEM). Thank you all for your tremendous technical support and fruitful discussions.

In many ways, I am indebted to some people to whom I could never express my earnest appreciation enough. These include Ashish Pandey, Reyyan Bulut, Ezgi Bakırcı, Stefan Räbiger, Muhammad Usman Ghani, Malek Ebadi, Dilek Çakıroğlu, Kush Kumar Upadhyay, and Masoumeh Ndi. Thank you all for your deep friendship and constant support, which have made this journey more meaningful.

Titanate nanotubes combined with graphene-based materials as a novel anode material for lithium-ion batteries

Anaguli Abulizi

Materials Science and Engineering M.Sc. Thesis, 2016

Thesis advisor: Assoc. Prof. Dr. Selmiye Alkan Gürsel

Thesis co-advisor: Dr. Alp Yürüm

Keywords: lithium-ion batteries, hydrothermal treatment, elongated titanate nanotubes, graphene-based materials

Abstract

Lithium-ion batteries are popular rechargeable energy storage devices due to their attractive properties such as good performance, high reliability, and affordability. Due to the problametic dentride growth present in typical anode materials for conventional lithium-ion batteries, graphene-based materials have gotten a wide attention as alternative materials for graphite oxide. Graphene features a high electrical conductivity and good mechanical properties. Also being able to be functionalized makes them very attractive as support materials for other electrochemically active anode materials. Due to titanium dioxide (TiO_2) being a non-toxic and cost-effective material with a capacity theoretically up to 335 mAh/g, it has become a hot research topic worldwide. Nevertheless, a poor electronic conductivity and a low rate capability are the main drawbacks which can be overcome by synergetic effects of composite materials.

Titanate nanotubes (TiNTs) are promising materials because of their special morphology and high specific surface area. We introduce a novel one-step hydrothermal method to obtain TiNTs&graphene-based composites as our anode materials. The self-organized TiNTs ($H_2T_3O_7$) are dispersed on the surface of various types of graphene-

based materials, namely graphene oxide (GO), reduced graphene oxide (rGO), nitrogen doped reduced graphene oxide (NrGO), popypyrrole functionalized graphene oxide (PPy-GO), graphene nanoplates (GNP), nitrogen noped graphene nanoplates (NGNP), and amino functionalized graphene oxide (GO-NH_2). Material characterization such as X-ray powder diffraction (XRD), Raman spectroscopy, Brunauer-Emmett-Teller (BET), scanning electron microscopy (SEM) are performed for all the as-prepared samples to examine the chemical compositions, elemental properties, and physical morphologies. Electrochemical characterizations such as charge and discharge, cyclic performance are conducted. The material characterization reveals well-aligned TiNTs which are homogeneously dispersed on the surface of the GO-based materials. A battery test is performed on four promising samples. Among all these samples, GO-NH_2&TiNTs at pH=4 yields the best electrochemical performance. It exhibits a high capacity retention with only 11% capacity fading after the first 4 cycles. Furthermore, its reversible capacity after 40 cycles is about 100 mAh/g with a high capacity stability. Charging and discharging cycle tests of our lithium-ion batteries reveal the anode materials have good stability in terms of capacity retention. Our findings suggest that the integrity of TiNTs are conserved well and the ion diffusion rate is in good balance with the electron transfer.

Lityum-iyon pilleri için özgün anot malzemesi olarak grafen temelli malzemelerle birleştirilmiş titanat nanotüpler

Anaguli Abulizi

Malzeme Bilimi ve Muhandisligi, Yüksek Lisans Tezi, 2016

Tez Danışmanı: Doç. Dr. Selmiye Alkan Gürsel

Tez Eş Danışmanı: Dr. Alp Yürüm

Anahtar Kelimeler: lityum-iyon pilleri, hidrotermal işlem, uzatılmış titanat nanotüpler, grafen temelli malzemeler

Özet

Lityum-iyon bataryaları iyi performans, yüksek güvenirlilik ve ucuzluk gibi cezbedici özelliklere sahip oldukları için şarj edilebilir enerji depolama cihazları olarak popülerdirler. Grafen içerikli malzemeler, geleneksel lityum-iyon bataryalarının tipik anot malzemelerindeki problemli dendrit büyümesinden dolayı grafen oksit için alternatif malzemeler olarak dikkat çekmektedir. Grafen iyi mekanik özelliklere ve yüksek elektrik iletkenliğine sahiptir. Grafenin fonksiyonelleştirilebilmesi, diğer aktif malzemeler için bir kaynak niteliği taşımasında cezbedici rol oynamaktadır. Teorik kapasitesi 335 mAh/ga kadar çıkabilen, toksik olmayan ve uygun maliyetli titanyum dioksit (TiO_2), son yıllarda dünya çapında pek çok araştırmaya konu olmuştur. Zayıf elektrik iletkenliği ve düşük hız kapasitesi gibi olumsuzlukları olsa da bunlar,kompozit malzemelerin sinerjik etkisi ile üstesinden gelinebilecek dezavantajlardır.

Titanat nanotüp (TiNT) ler yüksek özgün yüzey alanları ve özel morfolojilerinden ötürü ileriki çalışmalar için gelecek vaadeden malzemelerdir. Bu çalışmada anot malzemesi olarak TiNT&grafen içerikli malzemerlerin eldesi için yeni bir tek-adımlı hidrotermal metod gelirtirilmiştir. Kendiliğinden organizasyonlu TiNT'ler ($H_2T_3O_7$); grafen

oksit (GO), indirgenmiş grafen oksit (rGO), azot katkılandırılmış indirgenmiş grafen oksit (NrGO), polipirol katkılandırılmış indirgenmiş grafen oksit (PPy-GO), grafen nanokatmanlar (GNP), azot katkılandırılmış grafen nanokatmanlar (NGNP) ve amino katkılandırılmış grafen oksit (GO-NH_2) gibi çeşitli grafen içerikli malzemelerin yüzeyine dağıtılmıştır. Hazırlanan malzemelerin kimyasal kompozisyonları, elementel özellikleri ve fiziksel morfolojilerinin karakterizasyonu için; X-ışını toz kırınımı (XRD), Raman spektroskobu, Brunauer-Emmett-Teller (BET) ve Taramalı elektron miskrokobu (SEM) materyal karakterizasyon teknikleri kullanılmıştır. Malzemelerin şarj-deşarj ve döngüsel performansları gibi elektrokimyasal karakterizasyonları gerçekleştirilmiştir. Malzeme karakterizasyonları TiNT'lerin, GO içerikli malzemelerin üzerine homojen olarak dağıldığını ve iyi hizalandığını göstermiştir. Malzemeler arasından en umut verici dördü seçilerek bunlar üzerinde batarya testleri yapılmıştır. Bunlar arasından pH değeri 4 olan GO-NH_2&TiNT'ler malzemesi en iyi elektrokimyasal performansı sergilemiştir. Bu malzeme ilk 4 döngüden sonra yanlızca 11% kapasite sönümlemesi ile yüksek bir kapasite muhafazası göstermiştir. Buna ek olarak, 40 döngüden sonra ölçülen tersinebilir kapasite 100 mAh/g olup malzemenin yüksek kapasite kararlılığına sahip olduğu görülmüştür. Üretilen lityum-iyon bataryasının şarj ve deşarj çevirim testleri, anot malzemesinin kapasite muhafazası bakımından yüksek karalılığa sahip olduğunu göstermiştir. Bu çalışmada elde edilen bulgular TiNT'lerin bütünlülüğününün korunduğunu ve iyon difüzyon hızının elektron transferi ile iyi uyumlu olduğunu belirtmektedir.

Table of Contents

List of Figures

List of Tables

Chapter 1

Introduction

1.1 Motivation

Nowadays conventional energy, such as fossil fuel, serves as the prime energy resource for powering our devices. However, in the past decades a new class of energy - alternative energy, has emerged which covers wind, solar, biomass and geothermal energy amongst others. In contrast to the conventional energy it is renewable, which is of utmost importance considering the fact that every source of energy is needed to fuel our latest technology. Another problem of conventional energy is that it is distributed inhomogenously across the world, causing political conflicts.

A problem of alternative energy is its low conversion rate as opposed to conventional energy. Furthermore, the former is not available everywhere, i.e. it is utilizable in limited areas and times. But with the help of rechargeable batteries this problem can be circumvented because they can be charged whenever the energy is available and then this stored electrochemical energy can be distributed to any place and any time. Due to the wide range of potential applications, lithium-ion batteries (LIBs) are among the most preferred energy storage sources in terms of their lower weight, higher energy capacity and performance, their longer life time, lower cost, and greater reliability, when compared to the other types of rechargeable batteries.

1.2 Problem description

In this study, we tackle two problems. First of all, the tubular structure of titanate nanotubes (TiNTs) is difficult to obtain under general synthesis procedure reported by the other research groups. Normally the general synthesis procedure to produce titanium-based nanotubes&graphene oxide (GO) derivative composites is using a two-step hydrothermal treatment. Here we propose a new synthesis method where elongated TiTNs are grown on GO and GO derivatives in a one-step hydrothermal treatment. The treatment temperature and the treatment duration are crucial to preserve the complete structure of obtained TiNTs. 1) Can these parameters be optimized?

From the morphology point of view TiNTs are promising candidates for anode material in LIBs. However, TiNTs exhibit inherent low conductivity. Introducing conductive materials could overcome this obstacle. 2) Could graphene-based materials be suitable candidates?

1.3 Main results

The main contributions of this thesis are:

- halving the original synthesis duration but keeping the structure integrity of elongated TiNTs
- synthesized elongated TiNTs&GO-based composites show promising morphology and characteristics which are required for achieving a better performance

1.4 Thesis outline

Chapter 2 introduces the basic working principles of batteries and specifically focuses on LIBs. This is followed by a description on the preparation of anode composite materials for the characterized lithium-ion electrodes in chapter 3. Furthermore, it briefly outlines the methods involved in the characterization of the synthesized materials. A detailed discussion of the obtained results follows in chapter 4. Chapter 5

concludes this thesis by summarizing the main findings.

Chapter 2

Literature survey

This chapter briefly discusses the basics of batteries and the groups into which batteries can be subdivided. The remainder of this chapter focuses on explaining the working principle of LIBs and properties and synthesis of TiNTs&GO-based composites which are used throughout this thesis.

2.1 Introduction to batteries

A battery is an electrical energy storage device, which can be used to convert chemical energy into electricity. In general, a battery consists of several electrochemical cells, which are usually referred to as galvanic or voltaic cells. A galvanic cell is indeed a unit device, which can be electrically connected in series or in parallel in a certain type of battery pack [1]. More specifically, each galvanic cell consists of three major components: an anode, a cathode, and an electrolyte solution. The anode (negative terminal) and the cathode (positive terminal) of a cell are made of different materials, which are immersed into an electrolyte solution with an electrically isolated microporous separator: an electrolyte solution [2]. This electrolyte solution allows a smooth flow of the electrical charges, such as ions, between the anode and the cathode terminals. The oxidation reaction occurs at the anode, whereas the reduction process takes place at the cathode. The function of an electrochemical cell is either to produce electrical energy using chemical reactions or to promote chemical reactions by introducing elec-

trical energy. Usually, these electrochemical cells are categorized into two main groups: primary and secondary (rechargeable) cells [3].

2.1.1 Primary batteries

Primary batteries (disposable batteries) are generally designed for a single-use of the electrochemically stored energy until its complete depletion. In general, such batteries cannot be recharged with electricity because of the non-reversible electrochemical reactions occurring in the cell, which render recharging impossible. Commercially available primary batteries have different applications. Table 2.1 shows a list of several commonly used primary batteries.

Table 2.1: Features of several common types of primary batteries [4].

Battery type	Advantages	Disadvantages
Alkaline	Cost effective; leak-proof ; environmentally friendly; good safety record	High internal resistance; higher cost than Leclanché cells
Leclanché cells/zinc carbon	Long traditional reliability; low cost; higher energy density; better performance under heavy discharge condition; smaller leakage resistance	Sensitive to oxygen; Higher gassing rate; Poor low temperature performance
Lithium metal	Light; Less production pollution; high power; better durability	Safety issues
Silver oxide	Long operating life; high specific capacity; long shelf life	Expensive; limited cycle life
Zinc air	High energy density; low cost; available in various range and size; low self-discharge rate	Sensitive to humidity and extreme temperature; quick operating requirements

2.1.2 Rechargeable batteries

Rechargeable batteries (secondary batteries), as the name suggests, can be recharged and reused multiple times. Although rechargeable batteries produce current in the same way primary batteries do, the electrochemical reactions in rechargeable batteries are reversible and occur in both directions, allowing to recharge these batteries. More specifically, during the discharging process, electrochemical reactions happen in one direction and the battery gives out its energy. But the electrochemical reactions take place in the opposite direction when the battery undergoes the charging process. Some of the most commonly used rechargeable batteries are shown in table 2.2. They suffer from the same problem as primary batteries, namely that there is no single battery that can be used in all contexts.

Table 2.2: Features of several common types of secondary batteries [2, 4].

Battery type	Advantages	Disadvantages
Rechargeable alkaline	Cheap; easy manufacture; not requiring maintenance	Less capacity; limited cycle life; relatively high internal resistance; poor deep discharging performance
Lead acid	Long life cycle; low cost;	Minor leakage risk, heavy
Nickel Cadmium	Fast recharge time; long life time; low resistance	Costly; toxic material; memory effect
Nickel-metal hydride	High capacity and power density	-
LIBs	High voltage; long life time; low density; environment friendly material; good cyclic performance; no memory effect;	Costly; explosion risk; extra maintenance requirement

Two other key parameters for describing capabilities of rechargeable batteries are

volumetric energy density and specific energy density. They are of particular interest for portable and electric vechicles or hybrid electrical vehicles. Figure 2.1 illustrates a comparison among common types of rechargeable batteries regarding these two aforementioned factors.

Recently LIBs have emerged as promising candidates among rechargeable batteries, which are the focus in this study.

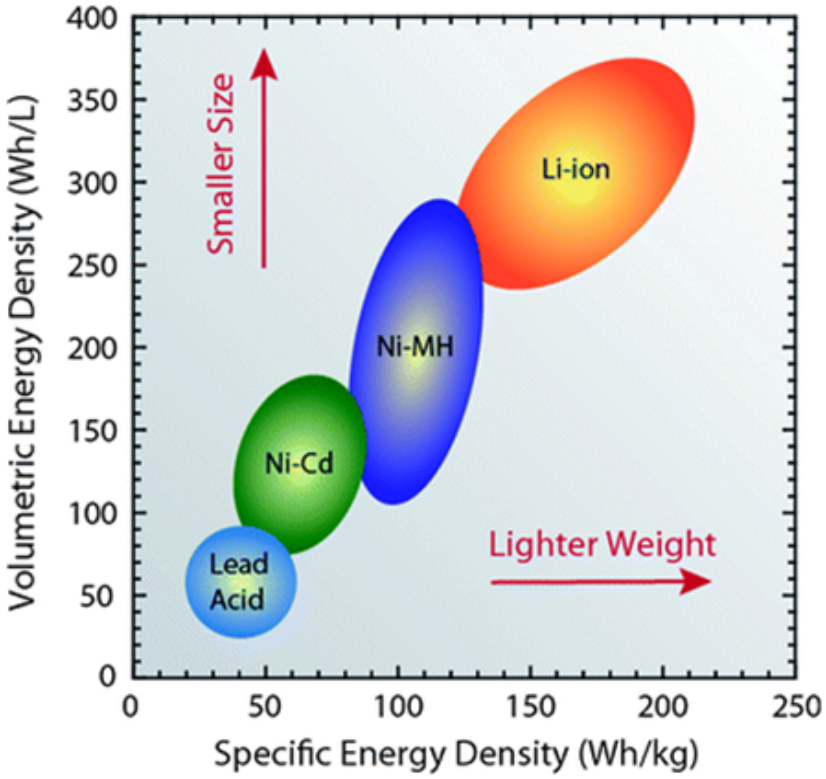

Figure 2.1: Comparison among the rechargeable batteries with regard to their specific energy and volumetric densities [5].

2.2 Lithium-ion batteries

The lithium-ion battery (LIB) was discovered by John Bannister Goodenough in 1970, and then commercialized by Sony in 1991 [2]. This battery was invented to replace the primary lithium battery in order to overcome safety risks associated with customers' usage since primary lithium batteries suffer from an overheating issue if charged quickly. This, in turn, leads to battery rupture, or in the worst case, even an

explosion. This safety issue has been controlled in LIBs at the expense of exhibiting a lower energy density compared to primary lithium batteries. Due to their many beneficial properties, LIBs have quickly gained popularity among rechargeable batteries. For example, because of their electronegativity of -3 V (measured against the standard hydrogen electrode), they are a good fit for storage devices with higher energy densities. Moreover, LIBs use non-aqueous electrolytes instead of the commonly used aqueous electrolytes to achieve operating voltages as high as 4 V [6]. Furthermore, these batteries exhibit common appreciative features, such as ideal capacity retention, low self-discharge and being cost-effective.

In general, a LIB shows three different electrochemical reaction mechanisms depending on the choice of both anodes and cathodes: alloying, insertion, and conversion [7, 8]. Both cathode and anode are comprised of chemicals with special structures, which can permit reversible intercalation and extraction of lithium ions. In theory, there are plenty of materials available for undergoing this dual intercalation, and they can be used as the electrode materials. But it is important to choose the anode and cathode materials according to the targeted performance by taking into account the total cost of LIBs.

There are mainly six types of LIBs. These include lithium cobalt oxide ($LiCoO_2$), lithium manganese oxide ($LiMn_2O_4$), lithium iron phosphate ($LiFePO_4$), lithium nickel manganese cobalt oxide ($LiNiMnCoO_2$), lithium titanate ($Li_4Ti_5O_{12}$), and lithium nickel cobalt aluminum oxide ($LiNiCoAlO_2$). According to the active materials, the names of the above mentioned six types of LIBs are further abbreviated as LCO, LMO, LFP, NMC, LTO, NCA, respectively [8, 9, 10]. We note that LCO, LMO, LFP, NMC, and NCA belong to cathode material for LIBs while LTO serves as anode material. The chemical structures together with the characteristic features of each above mentioned LIB are discussed in details below. Lithium titanate is explained in section 2.2.5.

Lithium cobalt oxide ($LiCoO_2$)

Lithium cobalt oxide (LCO) has a layered structure. This layered structure is preferred as a cathode because the surface of the layered structure provides a good number

of reaction sites for lithium ions when the battery discharges. In the reverse process, LCO releases the ions under external potential. LCO features high specific energy, which makes it a promising candidate for the portable electronics [8]. The main drawbacks exist in LCO are its specific power limitation, low load capability, lower thermal stability, and undesirable thermal stability.

Lithium manganese oxide ($LiMn_2O_4$)

Lithium manganese oxide has three-dimensional architecture with spinel crystal structure. This specific structure is ideal for facilitating the ion flow. Thus lower internal resistance plus elevated capability of current handling can be promised once the ion flow is improved. Therefore, LMO gain its popularity in terms of high power rate application usage. Unfortunately, the drawbacks exclaimed for t his type of battery is its calendar life and lower cyclic performance.

Lithium nickel manganese cobalt oxide ($LiNiMnCoO_2$)

NMC refers to lithium nickel manganese cobalt oxide which also known as lithium manganese cobalt oxide. Among cathodes for LIBs, NMC is favorable for its high current rate while discharging [8, 11]. Like LMO battery, it can be tuned to work in power devices. With its high energy density combined with lower cost, and good cyclic performance, it became one of the most well-known lithium ion systems.

Lithium iron phosphate ($LiFePO_4$)

Lithium-ion phosphate ($LiFePO_4$) cathode was made in 1996. It is also well known as lithium ferrophosphate (LFP) . In comparison to the other cathodes for LIBs, LFP has lower energy density but relatively good life span and higher power density, which make it applicable for power tools . In addition to that it shows enhanced lifespan. Apart from that LFP has good tolerance if it is fully charged and experience less stress. On the other hand, its drawbacks include usage limitation in certain condition such as cold temperature, and comparatively higher level of self-discharge.

Lithium nickel cobalt aluminum oxide ($LiNiCoAlO_2$)

Lithium nickel cobalt aluminum oxide (NCA) is a new generation of the NMC battery by adding aluminum into its cathode material, thereby enhancing the stability in its chemistry [12]. This type of rechargeable LIBs shares some similarity with NMC as both of them providing considerable specific energy (roughly around 250 Wh/kg) , good specific powder, and decent life span . It has been widely used in power trains by Tesla and medical devices.

Table 2.3: Comparison of six types of common cathode materials for LIBs in terms of their capacity performances [13]. replace table with original one related to battery

	Material	Specific capacity (mAh/g)	Main features
Lithium cobalt oxide	$LiCoO_2$	140	High specific energy
Lithium manganese oxide	$LiMn_2O_4$	100-120	High thermal stability and enhanced safety
Lithium nickel manganese cobalt oxide	$LiNiMnCoO_2$	160-170	Serve as energy cells or power cells
Lithium iron phosphate	$LiFePO_4$	150-170	Tolerant to full charge conditions
Lithium nickel cobalt aluminum oxide	$LiNiCoAlO_2$)	180-200	High specific energy, reasonably good specific power and a long life span
Lithium titanate	$Li_4Ti_5O_{12}$	175	high discharge current, high surface area, good performance at low temperature

Although there are six different types of LIBs, they share some common advantages and disadvantages [14, 15, 16]. The merits of LIBs are:

- LIBs are very light in comparison with the other rechargeable batteries based on the same with consideration. This light weight of LIBs surely promises a high energy density.

- Lithium used in the LIBs have a better electrochemical mobility.
- Self-charge is very low which was the main issue occurred in other types of rechargeable batteries.
- LIBs are free from memory effects which quite common on other rechargeable batteries. This also saved LIBs from high maintenance.
- LIBs can be cycled numerous times.

Drawbacks of LIBs are:

- Lithium is an expensive metal which keeps LIBs costly.
- Face quick aging issue. The lifespan is comparatively short with 2 to 3 years after manufactured. It does not matter whether or not the battery is being used.
- It requires some extra protection because of its sensitive to high temperatures. It will degrade very quickly if they are exposed to heat.
- Explosion risk exist although the possibility is not high so proper usage is required.
- It can get damaged after over-discharging.
- The LIB technology needs further development.

2.2.1 Working principle

A LIB is assembled with one or more power-generating components called cells. Each cell consists of an anode, a cathode, an electrolyte, and a separator, shown in figure 2.2. On charging a battery, the positive electrode (cathode) releases Li-ions, which migrate through the electrolyte and intercalated the negative electrode (anode). On discharging the reverse phenomena happens in which the Li-ions deintercalates from the anode and goes to the cathode and the current passes through the external circuit via load. The shutting phenomena of Li-ions between the cathode and the anode form the basis of how Li-ion functions as a power source. Therefore, in order to improve

the overall electrochemical performance of a LIB, the research should be more focused towards the improvement of anode based materials to enhance the Li-ion intercalation ability because the cathode material choice is limited. In terms of electrolyte, most of the LIBs use still organic or non-aqueous electrolytes, though solid state electrolytes promise better safety. Most used electrolytes have $LiPF_6$, $LiAsF_4$, and $LiClO_4$. All of these electrolytes are based on the mixture of multiple organic solvents dissolving lithium salts in. The most common multiple solvents are ethylene carbonate (EC), diethyl carbonate (DEC), dimethyl carbonate (DMC), propylene carbonate (PC), and ethyl methyl carbonate (EMC) [17]. Apart from the multiple organic solvents, a single salt chemistry can be used in LIBs. These carbonate based organic solvents improve both ionic and electronic conductivity. In order to prevent a short circuit, the separator is placed in between two electrodes.

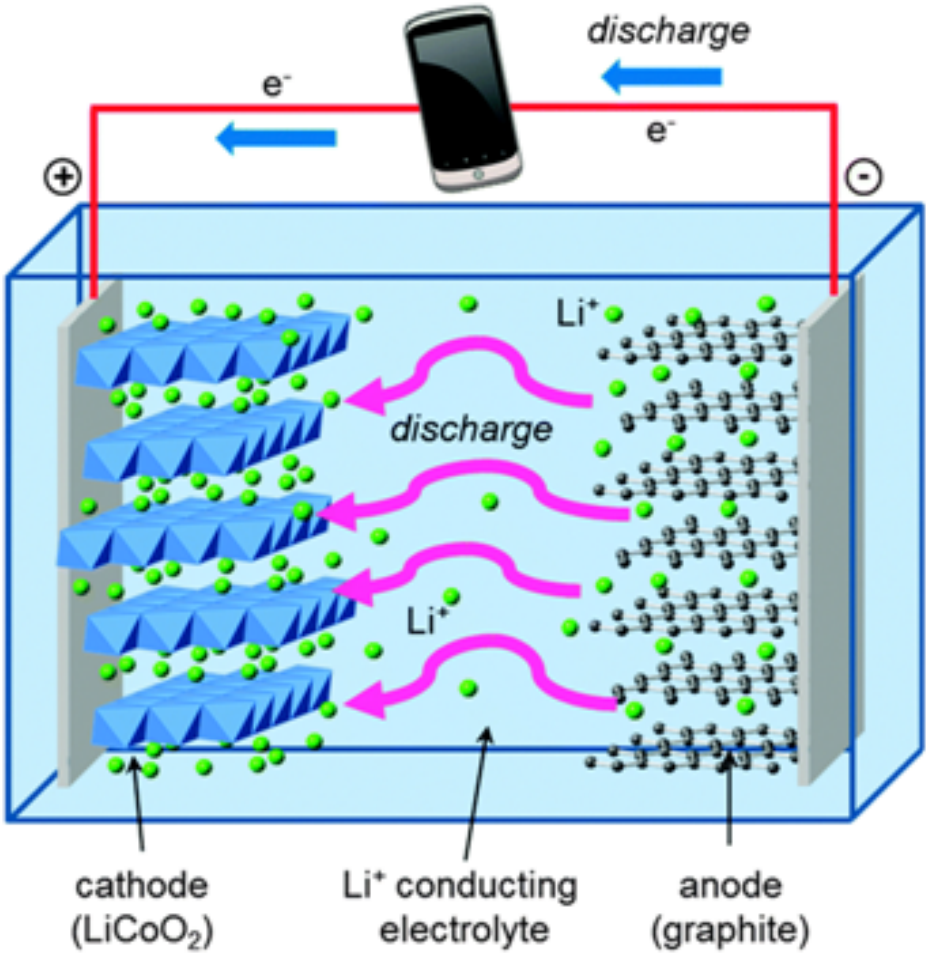

Figure 2.2: Schematic drawing of the working principle of a LIB [18].

The chemical reactions which occur in Li-ion battery are shown below where graphite is used as anode and Lithium cobalt oxide as cathode (equations 2.1-2.3).

$$\text{Cathode: } LiCoO_2 \rightleftharpoons Li_{1-x}CoO_2 + xLi^+ + xe^- \tag{2.1}$$

$$\text{Anode: } C_6 + xLi^+ + xe^- \rightleftharpoons Li_xC_6 \tag{2.2}$$

$$\text{Overall: } LiCoO_2 + C_6 \rightleftharpoons Li_{1-x}CoO_2 + Li_xC_6 \tag{2.3}$$

The overall cell potential equals to the potential difference between positive electrode (cathode) and negative electrode (anode) as shown in equation 2.4:

$$E^{\circ}_{cell} = E^{\circ}_{cathode} - E^{\circ}_{anode} \tag{2.4}$$

Basic concepts of LIBs

This section introduces important concepts of LIBs in more detail.

Charging

As opposed to the discharging process, in the charging process lithium ions move in reverse direction from cathode to anode. A conversion of electrical energy into chemical energy will occur.

Overcharging/discharging

It is an unfavorable process where the excessive charging/discharging of battery happens. This excessive charging/discharging goes beyond the capacity limit of the battery and poses a risk on shortening the life cycle of the battery (2.5-2.6).

$$\mathrm{LiCoO_2 + Li^+ + e^- \longrightarrow Li_2O + CoO} \tag{2.5}$$

$$\mathrm{LiCoO_2 \longrightarrow Li^+ + e^- + CoO_2} \tag{2.6}$$

Self-discharging

It is the capacity leaking process on its own. It is also a technique to study the capacity retaining behavior of the material. The self-discharge rate should be low for a material having good capacity behavior.

Open circuit voltage

The compatibility of the anode, cathode, and electrolyte as a whole determines the cell voltage. Especially, the differential change in between the anode and the cathode indicates the working voltage, also known as the open circuit voltage (OCV) [19].

Short circuit

It occurs when two terminals of the battery are connected electrically and the electrons are not well guided through external circuit. Due to this unintended path, the current flow may experience a low or even no electrical impedance.

Theoretical specific capacity

The theoretical specific capacity is calculated by equation 2.7:

$$Q_{\mathrm{TSC}} = 1000 \times \mathrm{F} \times \mathrm{n}/(\mathrm{M} \cdot 3600) \tag{2.7}$$

where $\mathrm{Q_{TSC}}$ is the theoretical capacity (mAh/g), n is number of electrons transferred, F is the constant of Faraday (As/mole) and M is the molar mass (kg/mole). The above equation can also be modified as $\mathrm{Q_{TSC}}$=26.8×n×100/M, where n denotes the electron transferred; M denotes the formula weight of the active material. Normally, the theoretical specific capacity is calculated to demonstrate the battery cell capacity. For instance, if $\mathrm{LiFePO_4}$ will be used as cathode, its theoretical capacity can be calculated by equation 2.7.

$$\mathrm{LiFePO_4} \longrightarrow \mathrm{FePO_4} + \mathrm{Li^+} + \mathrm{e^-} \tag{2.8}$$

Here n=1 and the molar mass of $\mathrm{LiFePO_4}$ is 157.7×10^{-3} kg/mole and Faraday constant is 96500 As/mole, by using equation 2.7, $\mathrm{Q_{TSC}}$=170 mAh/g.

Specific charge and specific discharge capacity

Specific charge capacity is also referred to as specific capacity. These terms come for distinguishing the practical specific capacity and the theoretical capacity. Each battery has some limitations such as its proper operation temperature, kinetic barrier, cutoff voltage etc., and therefore the practical calculated specific capacity is more reliable than the theoretical capacity for real application purposes. The specific discharge capacity can be understood in the same way as explained below. These two values can be obtained by using the equation 2.9 shown below.

$$Q_C \text{ (or } Q_d) = I \times t/m \tag{2.9}$$

Where

I: current (mA)

t: time (h)

$m(g)$: the mass of active materials.

Specific energy density

It is also called specific energy. There are two ways to calculate the energy density of the material. The one which is calculated considering the mass of the active material is known as gravimetric energy density (Wh/kg) and the other one calculated considering the volume of the active material is called volumetric energy density (Wh/l).

Specific power density

Power density is the measurement of the maximum power amount per unit volume. It is related to the energy density yet highlights the battery's ability of discharging rate. Its unit is W/kg. This is an expression for loading capability of the battery as well as an ability of the battery for taking on or delivering the power. The value of specific power density is useful for devices with a specific current demand. The power density of a battery is related to its energy density, as well as the ability of the battery to discharge quickly.

Rate capability

Rate capability can be written as C-rate indicating the charging and discharging speed of the battery. If the battery is charged or discharged in 1C, then it can be charged to full or discharged to empty status in 1 h. If we halve the C-rate to 0.5C, then the time for discharging is 2 h accordingly. For example, the calculated specific capacity for $LiFePO_4$ using equation 2.7 is Q_{TSC}=170 mAh/g.This yields: 1C=170 mA, assuming a mass of 1 g.

Irreversible capacity

Irreversible capacity is the capacity loss occurring during the process of battery cycling. The amount of irreversible capacity loss varies and this variation depends on several factors such as solid-electrolyte interphase (SEI) formation, types of electrode materials, performance of electrolyte, charge and discharge rate etc. The irreversible capacity leads to the capacity fading in the end.

Capacity retention

Capacity retention is one of the battery performance indicators. It expresses the capacity amount which can stay unchanged after certain times of charge and discharge cycles.

Coulombic efficiency

It is the capability to maintain its capacity after cycles of charging and discharging. This term also means Faraday efficiency. Equation 2.10 shown below can be used to calculate the coulombic efficiency.

$$\eta_c = \frac{Q_{out}}{Q_{in}} \tag{2.10}$$

Where

η_c : the coulombic efficiency

Q_{out} : charge amount while discharge cycle (C)

Q_{in} : charge amount while charging (C)

Li-intercalation chemistry

Based on the chemical mechanism involved in the Li-intercalation process, there are three types: alloying, conversion, displacement. These types are described in detail below.

Alloying

Alloying materials have been considered as one of the most promising electrode materials for next-generation LIBs due to their high energy densities, relatively low costs, environmental compatibility and safe operation potentials. The purpose of using compound alloys is to create a Li-insertion host that maintains a strong structural relationship with the intermediate and the lithiated phases to minimize the volume expansion during reaction. Alloying active elements with inactive elements can reduce volume expansion, leading to improved cycle life and it also maximizes the energy density. The disadvantages of alloy anodes include their short cycle life and high irreversible capacity loss as a result of the large volume expansion during lithium insertion. Alloying is the process in which Li can be inserted into the crystal structure of electrodes. De-alloying is obviously the extraction process of Li. The exact reaction can be explained by using equation 2.11:

$$\mathrm{Li} + \mathrm{xM} \rightleftharpoons \mathrm{LiM_x} \tag{2.11}$$

The reactant M in above equation can either be a compound or an element. During the reaction, the lithium ions are added into reactant phase. Thus, the reaction involves phase change from M to LiM_x [20].

Conversion mechanism

In conversion mechanism, decomposition and formation process takes place. the conversion reaction is also called lithiation reaction. During the process of discharging, lithium reduces the active material such as metal oxide (MO) into its metal form which dispersed into Li_2O matrix. While charging, the reaction will be reversed where elemental metal M alloyed with O and converted into MO and Li_2O components are converted into metal oxide.

Displacement mechanism

This mechanism can be called insertion and deinsertion mechanism as well. Materials like TiO_2, TiS_2, MoS_2 follow this type of reaction mechanism. What is good in this type of reaction mechanism is lithium can enter the lattice of host materials reversibly, as well as with less volume change [21, 22] like graphite. Less volume change means good structure stability. This might be good news to the application where needs good cyclic performance. Yet, capacity of such materials is quite low as in the case of intercalation and deintercalation mechanism.

2.2.2 Electrolyte

Apart from two electrodes, electrolyte is another key component which plays important role in the LIBs. The electrolytes used for LIBs are non-aqueous electrolytes, although semi-solid state and solid state electrolytes are available. Electrolytes are generally made of dissolving a single lithium salt in multiple component of organic solvent. Stability of these electrolytes is also a prime concern. And so its ionic mobility should be optimized to reduce the ionic resistance. Also the working potential window of the electrolyte has to be within its decomposition limit. The working in the potential limit will enhance the overall life cycle of the battery. Also, the melting and boiling point are another two key factors that should be taken care. This is because the higher value of these two critical factors can offer sufficient conductivity. In addition to that, a high range capability of melting point and boiling point can prevent thermal buildup which can increase explosion risk. Besides, solidification can also be prevented to some extent. Though electrolytes at solid state and gel state have been introduced, their ion conductivity is still much inferior then their liquid counterpart. Most of the LIBs are still manufactured using organic electrolytes despite of the appalling toxic problem it has. Therefore, introducing a non-toxic environmentally friendly electrolyte with low cost is a promising research target.

Lithium salt

So far, there are already numerous lithium salts commercially available such as $LiPF_6$, $LiAsF_4$, $LiClO_4$, and LiBOB [23]. These electrolyte proved to be least damaging and works well in wide potential range. But demerits are its low thermal stability and extreme sensitivity to water which restricts its uses. Furthermore, LiBOB was introduced and used together with $LiPF_6$ in a certain ratio based on their concentration. This is because it is demonstrated the controlled amount of LiBOB blending into $LiPF_6$ can attenuate both the cycling performance and power capability of the LIBs.

Organic solvent

In general, the organic solvents are used for LIBs. Mostly, they are either cyclic or linear carbonates. The multiple components of solvents for LIBs are ethylene carbonate (EC), Diethyl carbonate (DEC), dimethyl carbonate (DMC), ethyl methyl carbonate (EMC), propylene carbonate (PC), and γ-butyrolactone (GBL) [24]. Unlike the single solvent electrolyte system, the electrolyte in binary or ternary phase gives better electrochemical battery performance due to the decreased viscosity due to the presence of the cyclic and linear carbonates combination in the organic solvents. These special combinations give better performance especially in the low temperature situation.

Apart from organic solvents, ionic liquids are also used as solvent for LIBs. In comparison to organic solvents, ionic liquids can work in wider potential window. The working of these solvents however, depends on the used cathode materials. Therefore the electrode materials should be chosen wisely according to the electrolyte used. Moreover, unusual SEI formation due to failure on solvent selection is another critical issue which has to be avoided.

SEI is a passive protective layer formation which has ionic conductivity yet lacks electronic conductivity. It grows after the first cycle of charging and results in a significant amount of capacity loss. A thickness in certain ranges is favored as it can prevent the electrolyte undergo decomposition. However, an excess SEI layer thickness would cause the electrolyte to break. Besides, a SEI layer with unfavorable thickness affects battery performance significantly by inducing much higher internal impedance and it

further deteriorates the performance of the battery. Hence, an electrolyte should be chosen carefully.

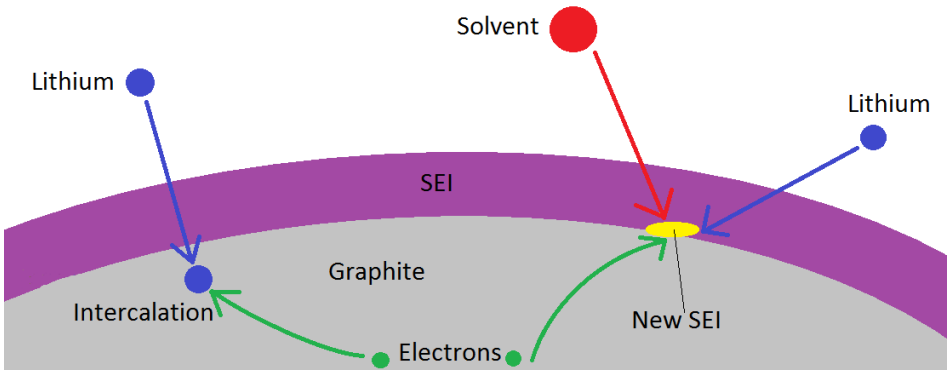

Figure 2.3: The desired electrochemical reaction is the intercalation of lithium, but lithium can also react with components of the electrolyte to form a solid-electrolyte interphase. Taken from [25].

2.2.3 Separator

A separator is a thin microporous film placed in between two electrodes. It is designed for the purpose of preventing any short circuit risk. Also it absorbs lithium ions easily and gives easy access to its migration. In general, it is made up of either flexible polymeric membrane or a non-woven fabric mat. The main sources of plastic films are PE (polyethylene), PP (polypropylene) or Nylon. It should be thin enough around 10-30 μm which can help in reducing the overall size of the battery. Some strict requirements that must be taken carefully for its efficient working are mentioned below:

- No electron conductivity
- Mechanical stability
- Low ionic resistance
- Chemical resistance in terms of electrolyte degradation, electrode reactants and impurities

- Working effectively to prevent species other than lithium ions passing through
- Good absorbent
- Smooth surface with uniform thickness
- Homogeneous in other properties

2.2.4 Cathode materials

A cathode determines the electrochemical performance of a battery significantly. And therefore the material selection for a cathode should be done wisely. Some intensively studied and widely used cathode materials are $LiCoO_2$, $LiMn_2O_4$, and $LiMPO_4$.

Initially, the research focus regarding cathode material selection was mainly on the transition metals. Then, research interest shifted to the oxide based materials. Transition metals are being preferred as the result of its intrinsic conductive and higher electrochemical capacity storage ability as well as their good thermal conductivity.

A promising candidate material of the cathode should exhibit some of features mentioned below:

- High capacity;
- High working potential window;
- Possesses good energy density;
- Thermal & electrochemical stability;
- Inexpensive;
- Environmental and consumer friendly;
- Keeps good reversible capacity retention as well as rate performance.

Nevertheless, we have to understand that it is not easy to find a material to have all these merits together. Thus some trade-off should be made according to the specific

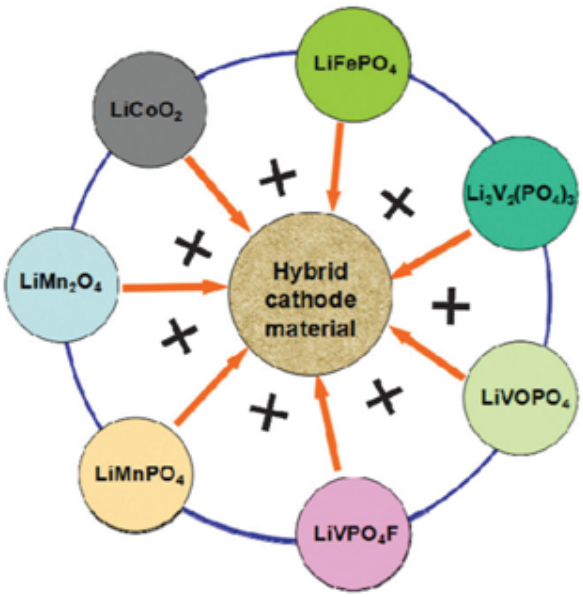

Figure 2.4: Schematic drawing shows the hybridized cathodes for LIBs with different types [26].

application of the battery. Luckily enough, researchers came up with new concept and had proposed hybrid cathode materials as shown in figure 2.4.

The cathodes for LIBs are classified into several groups depending on their crystal structure, chemical composition, and their microstructure. This is because these aspects have their special impacts on interested transfer processes, reaction occuring on the surface, and cyclic stability.

Layered cathode materials for LIBs

The most well-known layered cathode materials are $LiCoO_2$, $LiMnO_2$, $LiNiO_2$. Among them $LiCoO_2$ is widely used. The specific energy and specific charge for this material is 590 Wh/kg and 140 mAh/g, respectively. Though the material is promising, it still has some drawbacks. The raw material is not available easily. Apart from the toxicity, it suffers from degradation or failure when overcharged [27].

Olivine cathode materials for LIBs

$LiFePO_4$ belong to this olivine cathode materials family. With the discharge potential as high as 3.4 V versus Li/Li^+, it represent a potential candidate. $LiFePO_4$ is promising because of its low cost, good cycling performance, as well as high capacity around (170 mAh/g). Though they are commercially successful, they also have some drawbacks which limit their application in devices. They cause electrolyte experience thermal decomposition because of their high discharge voltage.

Spinel cathode materials for LIBs

This type of cathode material has a spinel structure. One of the representatives of this family is $LiMn_2O_4$. Unlike $LiCoO_2$, $LiMn_2O_4$ is less toxic, not expensive, rich abundance. However, this type of material suffers from elevated temperature which leads to serious capacity fade. Besides, the manganese used in the compound has inherent problems as dissolution. Moreover, in comparison with other materials mentioned above, it has less capacity around 120 mAh/g.

The crystal structures of LCO, LFP, NMC, NCA, LTO and LMO are depicted in figure 2.5.

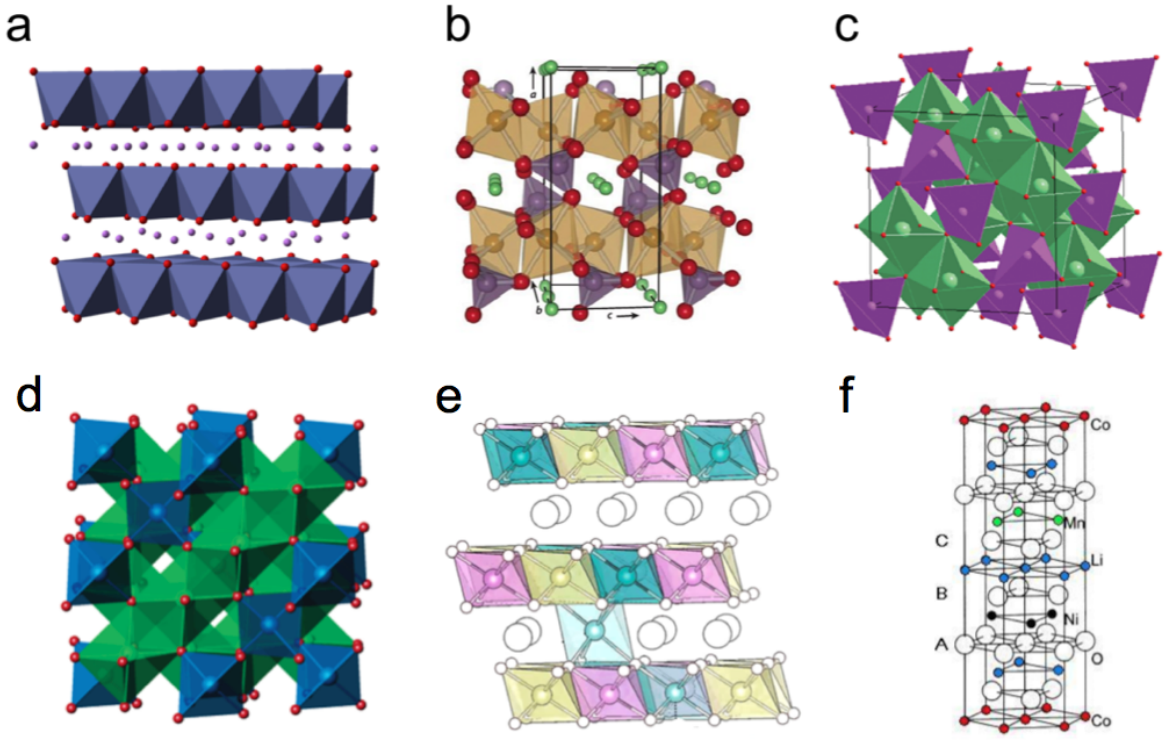

Figure 2.5: Schematic drawings of the crystal structures of: a) LCO (purple spheres show Li-ions; red spheres denote oxygen; blue octahedra represent cobalt [9]). b) LFP with orthorhombic olivine structure (the yellow area is exhibiting Fe octahedral; purple spheres are P tetrahedral atoms; green spheres are Li-ion; red indicates O atoms [15]). c) spinel crystal structure of LMO [14]. d) LTO (blue tetrahedra are lithium, green octahedra are disordered lithium and titanium [28]) e) NCA (white spheres are oxygen and lithium, blue, pink and green areas are nickel, aluminium, cobalt, respectively [29]) f) NMC (white spheres are oxygen; green spheres are manganese; black ones illustrate nickel; red spheres show cobalt [30]).

2.2.5 Anode materials

The LIBs give better performance in terms of energy density, good cyclic performance, as well as high rate capability depending largely on the chemical and physical properties of the electrode materials. The major requirements on structure stability, high potential, good lithium insertion performance expected from the cathode become a big obstacle to make a big progress. Meanwhile, this challenge mentioned above can be

one of the main reasons that explains the intensive interest of researchers in exploring the anode material, yet less in cathode research. Regarding the capability on storage lithium reversibly, however, anode material choices turned out to be much more than cathode material options.

- Li-alloy reaction mechanism
- Insertion reaction mechanism
- Conversion reaction mechanism

As a result, there are three types of anode materials [31]: insertion/deinsertion, alloying, and conversion, which are described in detail below.

Insertion/deinsertion anode materials

Carbon based materials are first grouped based on where insertion and desinsertion mechanisms happen. Later on transition metal oxide materials are included. Carbon based materials are basically categorized into two main groups - graphitic carbon and non-graphitic. Graphite as a graphitic carbon is an allotrope of carbon, which has been predominantly used as an insertion-type anode for Li-ion power packs. It shows a reversible capacity of 280-330 mAh/g, and Li discharge/charge plateaus are clearly observed below 0.2 V. However, it suffers from safety concerns due to serious dendrite formation. Because of that, graphene, a single layer carbon sheet (carbon atoms in a two dimensional honeycomb lattice), was introduced as a replacement. Hard carbon and soft carbon are the two main types which belong to the non-graphitic carbon group. Due to its low cost, being mechanically strong yet flexible for further modification to obtain a good rate capability and a higher energy capacity as well. It also features non-toxic, rich abundance, carbon based anodes are one of the most practical choice as electrodes for LIBs. Lithium is inserted into carbon during the insertion, also known as intercalation, processed without inducing any major structural changes. This intercalation process can be described as lithium as a guest species entering a host such as carbon with layered structures.

In addition to carbonaceous material, TiO_2 is also considered as a typical intercalation compound. Besides, it exhibits a good structural stability with lower than 4% of volume change during the insertion. The better structural stability and therefore enhanced cyclic performance is due to the slight lattice changes of titanium dioxide based structures. The anatase phase of TiO_2 has long been evaluated as a good insertion anode for LIBs for the reason of its numerous merits. Anatase TiO_2 shows the highest theoretical capacity among TiO_2 polymorphs while having a volume change as low as 3.7% during Li insertion/extraction. Meanwhile, TiO_2 comes in low price and rich abundance and does not harm the environment. Nonetheless, insertion/deinsertion anode materials have also drawbacks, such as low coulombic efficiency, high irreversible capacity, and high voltage hysteresis.

Alloying type of anode materials

Materials with lithium-ion (Li-ion) storage based on alloying mechanism have long been recognized as promising anode candidates with their much higher capacity to replace the commercial graphite anode which provides a much lower capacity about 372 mAh/g. Among the materials belonging to this family group IVA elements such as Si, Ge, Sn have a high volumetric and gravimetric capacity performance. Compared to the high capacities of Si (3579 mAh/g) [32], Ge (1600 mAh/g) [33], and Sn (994 mAh/g) [34], graphite has a much lower value. However, their commercial application is not going anywhere for the reason of serious pulverization they encounter due to large volume expansion up to almost 300%. In addition to pulverization, thick solid electrolyte interface (SEI) formation during the charging and discharging results in low coulombic efficiency as the result of quick capacity fading. Si being the one which gives the highest capacity, the charge and discharge potentials at the phase of $Li_{15}Si_4$ is lower than 0.5 V (vs. Li/Li^+). Recently, the research group of Yi et al. has published their study on porous micro-sized Si-C composite using SiO as the Si source [35]. The results reveal a very high capacity of 1459 mAh/g, a great coulombic retention of 97.8% after cycling of 200 times. Recent studies in regard to germanium, research group of Xue et al. [36] reported a novel material of Ge@C/RGO (reduced graphene oxide)

nanocomposite by using a simple synthesis method. A reversible capacity around 940 mAh/g was kept stable under the current density of 50 mAh/g after 50 cycles. A quite high capacity of 380 mAh/g was obtained even under a high current density of 3600 mAh/g.Concerning to tin-based materials, amorphous tin oxide provides a specific volume capacity of more than 2200 mAh/cm^3 with the reversible capacity more than 600 mAh/g. Wang et al. reported their research study on a set of MSn (M = Fe, Cu, Co, Ni) nanospheres by using the conversion chemistry [37]. They synthesized for the purpose of comparison in terms of their electrochemical performance. The theoretical capacities for those materials are as such CoSn3 (852 mAh/g) > $FeSn_2$ (804 mAh/g) > Ni_3Sn_4 (725 mAh/g) > Cu_6Sn_5 (605 mAh/g). This is the ordered list when theoretical capacities are compared, whereas in reality, the order of them is $FeSn_2$ > Cu_6Sn_5 ≈ $CoSn_3$ > Ni_3Sn_4. The authors claim that the good electrochemical activity in $FeSn_2$ is attributed to open channels in the structure and an effective SEI layer is responsible for the superior cycling performance. Furthermore, they observe that the small particle size is beneficial to cycling stability and Li^+ diffusion. However, the alloying type of anode materials also suffers from the following disadvantages: large irreversible capacity, huge capacity fading, and poor cycling.

Conversion anode materials

Conversion type of materials normally refer to transition metal-based compounds such as oxides, sulfides, phosphides, nitrides, as well as halides. This type of Li-ion storage mechanism is also known as replacement reaction. This type of anode materials were explored and later proposed as alternative anode materials for storing the Li-ion effectively. Materials, such as MoO_2 (capacity: 419 mAh/g) [38], V_2O_5 (capacity: 270 mAh/g) [39], and WO_2 (capacity: 248 mAh/g) [38] are from this family. The conversion mechanism is conceptually similar to the rocking chair. During the charging, the metal oxide will be reduced to its pure metal forms and lithium oxide is formed as well. During the discharging process, however, metal is again oxidized to its initial metal oxide form. The replacement process of lithium by metal oxide makes the sub-lattice of original oxygen stay unchanged in the lattice of the lithium oxygen. Recently, the oxide

compounds of tin, iron, nickel, and cobalt have also been hot research topics. Storage capacity as high as 1000 mAh/g has been reported for these materials. Miniaturization of them individually can mitigate the volume expansion problem during cycling process to some degree. Metal oxides such as SnO_2, Fe_3O_4, NiO, Co_3O_4 are from this group where the Lithium insertion mechanism is defined as conversion mechanism [40]. They are well-known material with such high theoretical capacity as 600-1000 mAh/g. On the other hand, two big challenges from this material - unwanted volume expansion and poor conductivity - remain. But, conversion anode materials also shows the following disadvantages: low coulumbic efficiency, unstable SEI formation, large potential hysteresis, and poor cycle life. To conclude this section, an overview of anode and cathode materials with their capacities are shown in figure 2.6.

In the past, graphite was used as a regular anode material for LIBs, however, lithium titanate (LTO) substituted it by replacing graphite at the anode part. In essence, LTO is developed based on the Li-ion battery technology. It is a spinel material with 3D crystal structure [41]. Unlike other LIBs, it does not use carbon particles. Instead, it utilizes nano-scaled LTO on the surface of a LIB. It features a high discharge current which is about 10 times higher than in all other types of LIBs. These alterations increase its surface area to $100m^2$ per gram. In addition to that, it comes with many other merits such as enhanced safety, long lifetime, and a good performance at low temperature.

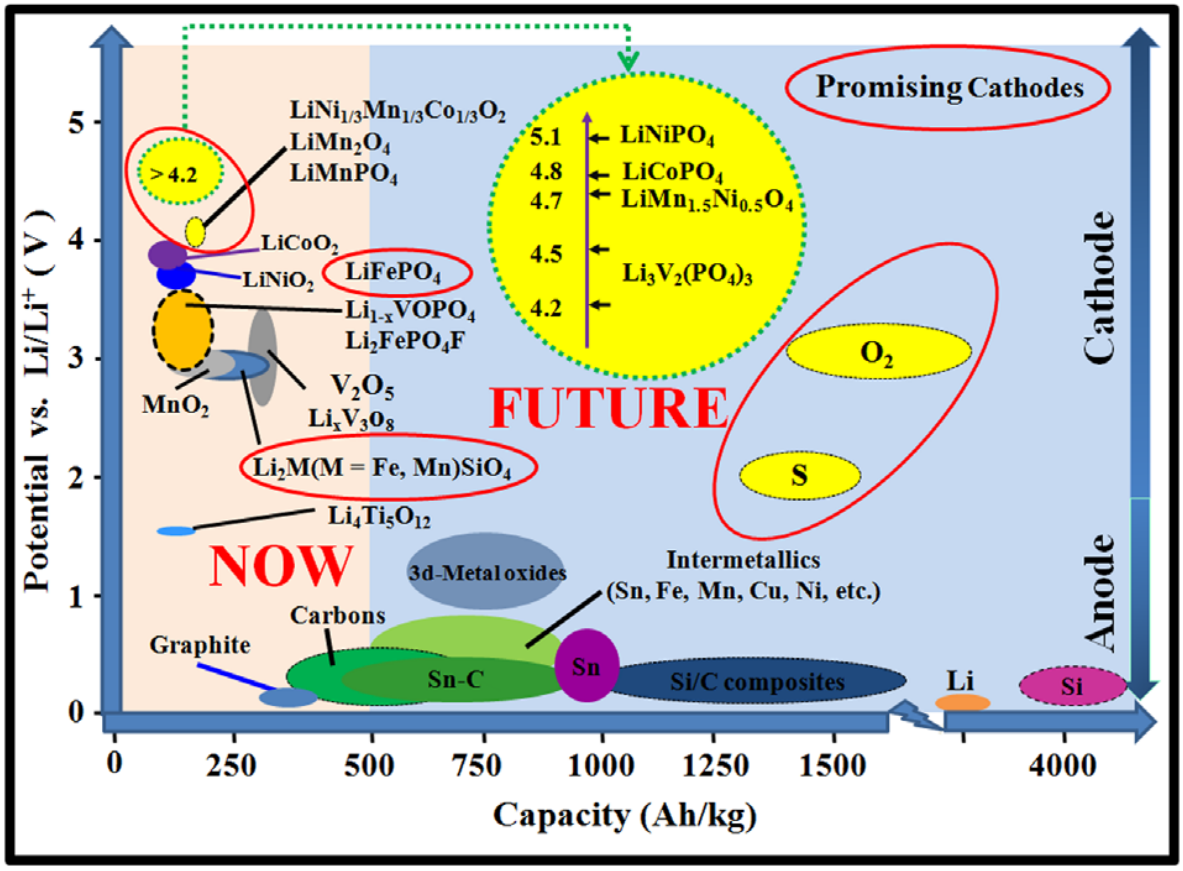

Figure 2.6: Overview of anode and cathode materials with their capacities in the current LIB generation. Taken from [42].

2.3 Titanium dioxide

Titanium dioxide (TiO_2) is a well-known metal oxide semiconductor, which has been used in many areas, for example, solar cells, water purification, supercapacitors, and batteries because of its promising properties, such as photocatalytic activity, nontoxicity, chemical stability, and abundance in various crystalline structures [43]. TiO_2 exists in many different morphologies, although only three of them occur naturally, while the others can only be obtained by synthesizing in certain conditions. These three natural forms of TiO_2 are rutile, anatase, and brookite. Among them, only rutile is thermally stable, and the other two are metastable. Besides, brookite is less studied in comparison with rutile and anatase due to its difficult synthesis process. One of the uncommon

forms of TiO_2 is TiO_2 bronze, which is now getting its interest because of its attractive features. The primary application of TiO_2 is to use it as white pigments by taking advantage of its high refractive index. For some special application purposes, the hydrophicity of anatase and rutile has been explored by studying the surface enthalpy and surface energy. It has been reported that anatase showed lower surface enthalphy and surface energy compared to that of rutile [44].

Figure 2.7 shows the crystal structures of rutile, anatase, brookite, and TiO_2 bronze. The corresponding lattice parameters and the densities are listed in Table 2.4. Rutile is a bulk material, which is composed of body centered unit cells known as a tetragonal structure, as shown in figure 2.7a. Anatase has a structure with a specific ordering of two different types of atoms and bonding between Ti and O, see figure 2.7b. Brookite has a distinct orthorhombic crystal structure, as shown in figure 2.7c, which makes it quite rare compare to rutile and anatase. The cell volume of brookite is quite large with such a complex crystal structure, where eight TiO_2 form one unit cell unlike four TiO_2 for anatase, and two TiO_2 for rutile. Although rutile is a stable phase at the atmospheric condition, it becomes metastable when the crystal size is decreased to a certain value, whereas anatase and brookiteare convert to the stable phases. Structure transformation from brookite to rutile occurs either directly or via the anatase phase when the temperature is increased. However, such transformation is influenced by several factors, such as crystallite size, the contact condition, and the size distribution. Unlike these three natural phases of TiO_2, TiO_2 bronze is normally synthesized using alkali hydrothermal method,where hydrogen titanates are first obtained by hydrolysis of $K_2Ti_4O_9$ and then thermal treatment is carried out to converte titanates into TiO_2 bronze at certain temperature. As a result, many different morphologies of TiO_2 bronze have been synthesized and analyzed [45].

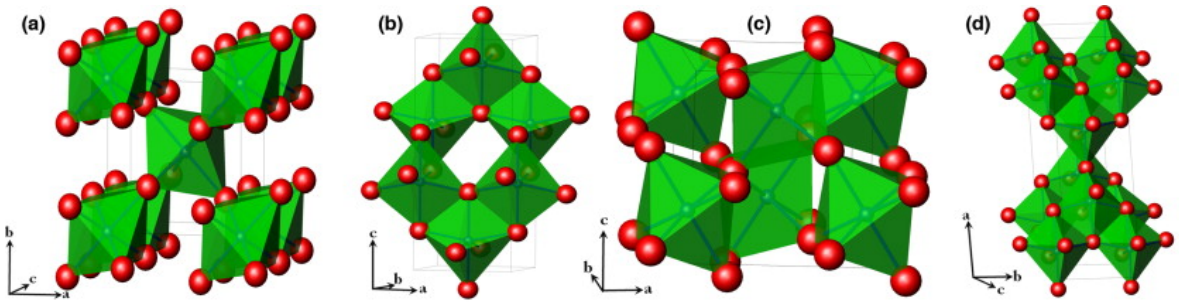

Figure 2.7: Crystal structure of a) rutile; b) anatase; c) brookite; d) TiO_2 bronze. Here, red and blue spheres represent the O and Ti atoms, respectively. This figure is taken from [46].

Table 2.4: Crystal structures and properties of rutile, anatase, brookite, and TiO_2 bronze. The numbers are taken from [47, 45, 48]

Crystal form	Rutile	Anatase	Brookite	TiO_2 bronze
Crystal structure	Tetragonal	Tetragonal	Orthorhombic	Monoclinic
Lattice parameters (Å)				
a	4.594	3.785	5.456	12.179
b	4.594	3.785	9.182	6.525
c	2.959	9.514	5.143	6.525
d				107.054
Density (g/cm^3)	4.13	3.82	3.99	3.64

Driven by the excellent works done in associate with carbon nanotubes [49], growing nanotubular shape of TiO_2 has been initiated because a relatively high rate capability is expected. TiO_2 nanotubes are easier to synthesize and are practical to manufacture than carbon based materials because of the diverse chemistry in regard of synthesizing methods and the low cost. Miniaturization has a significant influence on the electrochemical properties of TiO_2, especially on the performance of reversible capacity and Li^+ insertion and extraction. Enhanced electrochemical performance has been achieved by utilizing the obtained high surface area, effectively shortened Li^+ diffusion path, and the better controlled electron transport [48]. Numerous synthesizing meth-

ods have been reported for their structural dimensions, such as zero-dimensional (0D), one-dimensional (1D), and two-dimensional (2D) [48, 50]. These dimension tailoring is especially beneficial for effectively directing the charge carrier to move in straight path instead of isotropic transport. With the concern of intrinsic poor electronic conducting property that TiO_2 has, coating with carbon based conductive materials,such as caron blass, graphitic carbon, non graphitic carbon, graphene, and functionalized graphene, has been proposed and under extensive study. In addition to carbonaceous materials, noble materials, for example, gold, silver, and planium, are also used. However, these noble materials are too costly, which limits its practical application. Doping with materials, such as ruthenium and nitrogen, has been reported as well. These doped materials facilitate the ionic transport. As a result, a higher rate capability is expected for TiO_2 based materials [51].

2.4 TiO_2&GO-based materials as anode

Higher energy density and gravimetric power density are required for the development of energy storage and conversion devices nowadays. Due to high gravimetric capacities as well as high volumetric the transition metal oxides have, extensive research interest have been focus on them. Those proposed materials are more or less transition metal oxides They exhibits larger reversible capacity, better cyclic performance, enhanced rate capability due to synergic effect. Few examples of these materials are TiO_2, Fe_3O_4, Si, SnO_2, Mn_3O_4, Co_3O_4 etc. However, the major issues exist in the transition metals for its practical application in the field of energy are the poor ion diffusion rate and electronic conductivity. Among transition metal oxides, TiO_2 is a promising candidate because of various advantages it has. However, some main drawbacks remain to bulk TiO_2 and seriously affecting its effectiveness.

Hybrid materials or composite materials have been proposed with the aim to address those critical issues. Synergic effect triggered by combining the TiO_2 with carbonaceous materials contributes significantly. Carbon materials such as CNTs, CB (carbon black), coke, graphite which provide high electronic conductivity have been combined with

titanium dioxide on different polymorphs to form novel composites [52]. A composite of TiO_2/C has been reported exhibiting the better electrochemical performance in regard to higher rate capability and higher specific capacity owing to the electron contribution of carbon to the composite [53].

Graphene, a monolayer allotrope of carbon with large surface area, however, can be a panacea for these issue faced by transition metal oxides. Apart from the excellent electronic properties, the flexibility it has yet strong enough mechanically shows a good direction to the anode research. Meanwhile, the good thermal stability as well as the stable in-plane electrical conductivity together with all other properties, paved a way for graphene to be extensively employed in energy storage devices, especially LIBs. Tao Shan et al. reported a ternary composite material of TiO_2 (B)-CNT-graphene which exhibit very good rate performance. TiO_2 (B) refers to the bronze form of TiO_2. A capacity of 190 mAh/g was obtained after 200 cycles at 1C [54]. Recently, anode research group reported a novel composite of TiO_2-carbon-rGO (TCG) with the discharge capacity as high as 191 mAh/g at 0.2C after cycling 100 times [55]. Although the theoretical specific capacity of the graphene is much larger than other potential materials, the huge irreversible capacity poses a challenge for its efficiency as anode material for LIBs. Moreover, huge capacity loss lead to rapid capacity fading. In order to overcome these key issues, strategies of miniaturization and morphology designing partially solved the problem. Nanocomposite of TiO_2&graphene was proposed and claimed to better choice as the nanoscale can overcome the problem of properties constraints lies in the bulk counterpart of the transition metal anode materials. Graphene was proposed to be promising as a novel material for assisting the anode material TiO_2. Mengs group reported that TiO_2 nanosheets based on graphene was synthesized by utilizing the technology of atomic layer deposition. Their research study indicated that the temperature control of deposition process is the major factor to tuning the composite morphology [56]. Another research group of Gao has reported TiO_2-GO composite synthesized by reduction reaction which features a homogeneous distribution of TiO_2 nanoparticles on top of graphene layers and results in a high reversible specific capacity as well as great rate performance [57].

The graphene utilized as the component of composite anode material is almost its defective derivatives such as graphene oxide (GO) or reduced GO (rGO) [52]. The research group Dibakar et al. reports that the lithiation will not occur in the printine form of graphene. According to their observation, Li absorption was enhanced when defective graphene was utilized [52]. Therefore, functionalizing the surface of graphene based materials attracts the researchers attention and becomes the main research focus in the energy storage field. GO-based materials such as rGO, NrGO, PPy-GO GNP, NGNP, and GO-NH_2 are extensively studied regarding their electrochemical properties. Graphene can encounter fracture due to its single layer structure during the synthesis process. In addition to that, the thermally reduced graphene sheets are not stable results in restacking. Thus GNP (Graphene nanoplates) which has almost no difference from GO but the thickness of GNP is higher than GO is used as a substitute to the GO.

It has reported that the incorporation of NrGO with TiO_2 makes the photocurrent density of pristine TiO_2 enhanced more than 27 times due to its efficiency on separating and transporting charges [58]. Meanwhile, it is demonstrated that the rate capability and reversible capacity of the NrGO are higher than GO. In addition to that a better cycling performance for elongated time period is obtained for material incorporated with NrGO compare with GO compound [59]. Regarding polyporrole, a nitrogen rich material doped GO, after its fabrication with rGO makes the electrode more resistant to strain results in better stability on cycling [60].

As mentioned previously, a new hydrated form as protonated titanate produced by the alkaline hydrothermal process claimed to be better choice due to its layer sheet structure. It is reported that TiNTs exhibits the properties of both layered titante and TiO_2 nanoparticles. Meanwhile the surface area provides by the TiNTs is higher than TiO_2 nanotubes. Besides, TiNTs is favored due to its comparatively higher band gap of 3.87 eV.

2.5 TiNTs

Compared with its conventional bulk counterparts, NSMs shows distinct and promising properties in regard of physical, electronic, chemical, and magnetic properties. Nanostructured materials can be classified into 0D, 1D, 2D and 3D. Since the morphology tailoring idea proved to be very promising, the synthesis methods have been a big study topic. Both physical and chemical techniques have been under investigation to have a control on their shape, size, structure and dimensionality. Here below are the two separate list for physical and chemical synthesizing techniques, respectively [61].

Physical methods are less harmful because of non-toxic chemicals are used, thus it is known as a eco-friendly way to grow materials in various dimensions. A list of physical methods for synthesizing material in 0D, 1D, 2D, or 3D in the nanoscale is shown here below.

- Evaporation technique
- Sputtering technique
- Lithography processes
- Cold and hot plasma
- Spray pyrolysis
- Inert gas phase condensation technique
- Pulsed laser ablation
- Sonochemical reduction

Chemical methods are favored due to some advantages it has over physical methods for synthesizing nanostructured materials. First of all, the designing as well as synthesizing process are quite diverse. Secondly, a comparatively better homogeneity can be obtained. On the other hand, its drawbacks are also critical such as less eco-friendly and unexpected side reaction are involved which requires further purification. Here below is the list of chemical methods for synthesizing the nanostructured materials.

- Lyotropic liquid crystal templates (LLC)
- Electrochemical deposition
- Electroless deposition
- Laser pyrolysis
- Laser chemical vapor deposition technique
- Chemical vapor deposition(CVD)
- Sol-gel technique
- Hydrothermal and solvothermal techniques

Among all these approaches, as listed above, to synthesize TiNTs, hydrothermal treatment is intensively studied. Hence, we introduce this method in section 2.5.2.

2.5.1 Properties

In strike contrast to the nanotubular shape of the TiO_2 nanotubes, titanate nanotubes (TiNTs) consist of 2D TiO_6 octahedral host layers with a lepidocrocite (γ-FeOOH)-type layered structure (see figure 2.8), which have been confirmed by considering the Raman scattering properties of a restacked titanate prepared by assembling TiO_6 octahedral layers derived from the original scroll-like TiNTs [62]. This is illustrated in figure 2.9.

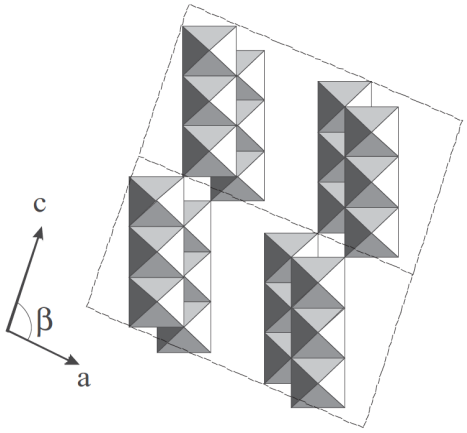

Figure 2.8: Crystal structure of monoclinic trititanic acid ($H_2Ti_3O_7$) in octahedral representation [62].

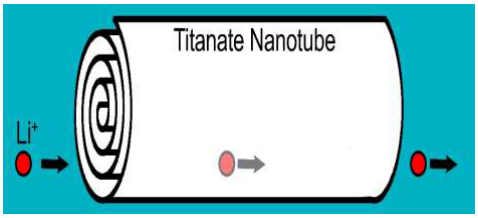

Figure 2.9: Schematic illustration of scroll-like TiNTs [63].

Equations 2.12 and 2.13 represent the reactions occurring during the TiNTs formation process via the hydrothermal method. More specifically, equation 2.12 shows the conversion from anatase to the titanate nanosheets occurring in the hydrothermal treatment. In contrast, equation 2.13 represents the ion exchange process triggered by mild acid washing. As it can be seen, Na-titanates are converted into H-titanate which is accompanied by the nanotube shape formation. As for the formation mechanism of TiNTs, there is a conflict among different research groups. Some reports that TiNTs are actually grown after hydrothermal treatment such that edge shared octohedral TiO_6 layers hold sodium cations in between which induce the surface energy. Due to higher surface energy, the layers scroll into tube shapes [64]. It was also claimed that tubes are formed after acid wash. The basic logic for such claims is described as such that acid washing sodium titanate nanotubes with acid will give rise to the replacement of sodium cation into hydrogen cation. During this process a distance shrinkage between

layers occurs which leads to the lower surface area. Thereafter the layers are forced to bend into tubular structures [65]. Meanwhile, the more opened layer distance could more efficiently contribute to gain a higher amount of reactions sites.

$$3\,TiO_2 + 2\,NaOH \longrightarrow Na_2Ti_3O_7 + H_2O \tag{2.12}$$

$$Na_2Ti_3O_7 + 2\,H^+ \longrightarrow 2\,Na^+ + H_2Ti_3O_7 \tag{2.13}$$

2.5.2 Synthesis mechanism - alkaline hydrothermal method

Numerous methods are available to form the titania and titanate nanostructures. These methods include anodic oxidation, templating, and chemical vapour deposition [66]. However, the precise control on the tubular structure of titanate can hardly be obtained by the aforementioned synthesis methods. Alkaline hydrothermal treatment was claimed to be a facile method to produce the elongated TiNTs. Meanwhile, it was also proved to be an effective method to have TiNTs with more desirable tube dimensions and length even without the requirement of templating.

The hydrothermal treatment method was widely used owing to some attractive advantages it possesses. It is claimed as a cost effective method due to the temperature required for the experiment is low. Meanwhile, the reactivity of the alkaline ion to attack the anatase TiO_2 particles is high. In addition to that, the precise control on the structural dimention and tube diameter is easily obtained. Anatase TiO_2 is used as a starting material to obtain the elongated TiNTs. The hydrothermal treatment is employed where an autoclave with a teflon beaker inside is used under certain pressure. Sodium hydroxide solution (NaOH) is used as the attacking alkaline ions and are mixed with anatase titania so that sodium titanate could be obtained through the hydrothermal treatment. It was reported that the concentration of NaOH solution should not be lower than 5 M and the temperature required for growing titanate with tubular structure has to be in the range of 110-150°C [67]. More specifically, 130°C is the optimal temperature to obtain the highest surface area and pore volume of TiNTs based on the

research findings [68]. After the hydrothermal treatment, acid washing is performed so that the sodium cations located between multilayers of TiNTs are replaced by the hydrogen cations [69]. Ion exchange gives rise to the a decrease on the interlayer distance of nanotubes because of the smaller ion radius of hydrogen compared with that of the sodium ion. Figure 2.10 schematically shows the mechanism of the scroll-like TiNTs formation.

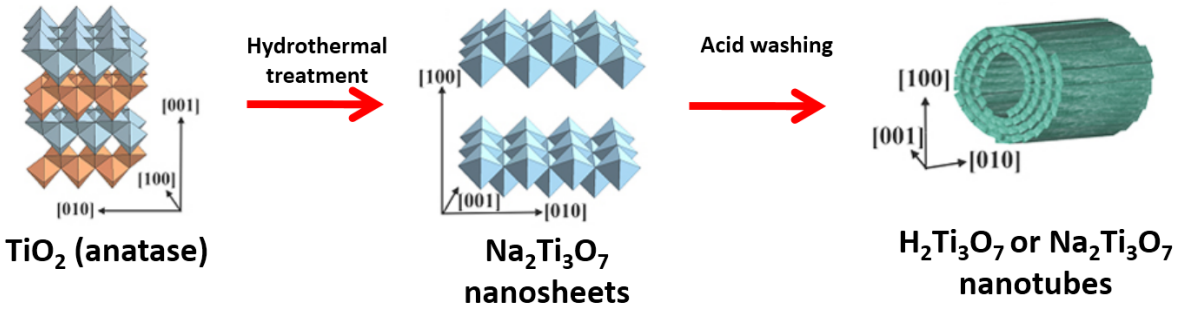

Figure 2.10: Schematic illustration of the mechanism to form TiNTs [70].

2.5.3 Application

TiNTs display a wide band gap which rendered it as semiconductor suitable for being a potential candidate in the application of photocatalysis [71]. Besides, properties such as good chemical and thermal stability up to 450°C, and good capability on ion exchange make TiNTs an attractive material as a supporting material for nanoparticle catalysts. [69]. Forthermore, research study reveals that the Co-doping can enhance the magnetic properties of TiNTs and make them a good material choice for electronic devices [72]. In addition to that, TiNTs possess a high surface area and open channels with mesoporous structure which is promising for energy storages and conversion applicatons. It was reported that TiNTs show a huge potential in electrochemical Li-ion storage and hydrogen storage as well due to their mesoporous adsorption characteristic [73]. It was also reported that the application of TiNTs can also be extended into dye-synthesis solar cells [74].

There are plenty of works using TiNTs as anode materials for LIBs due to their special layered structure which can facilitate the lithium ion insertion and deinsertion.

Meanwhile, the scrolled tube structure can guide more directed charge flowing while the redox reaction occurs. Besides, the reason for choosing titanate as a promising anode material is due to its pseudocapacity property occurring in the redox reaction, which induces a faster charge and discharge process. Many studies related to its electrochemical performance in LIBs have been tested. It was reported that TiNTs exhibit a relatively large reversible capacity and a good reversibility about 200 mAh/g after 80 cycles [75]. In another study it was reported that the initial discharge capacity of TiNTs is 282.2 mAh/g at a current density of 0.24 A/g, 210, 185.7 and 165.9 mAh/g at current density of 0.24, 1.0 and 2.0 A/g, respectively [76].

2.6 GO-based materials

Graphite is one of two naturally occurring polymers of carbon which exhibits a 2D planer crystal structure. Due to various favored properties such as good electricity and heat conductivity, high mechanical strength, chemical, and thermal stability it has been widely used in many different fields. Moreover, graphite has been a common anode choice for the LIBs due to its relatively high specific capacity of about 350 mAh/g. Graphite is the parent material for obtaining GO-based materials such as graphene and graphene oxide. Graphene is a layer tightly packet of carbon atoms bonded with a hexagonal honeycomb lattice. Layers of graphene which are stacked up form graphite. Graphene oxide comes from graphene by modified Hummers' method [77]. Graphene and graphene oxide share the basic properties of graphite, yet exhibit some other enhanced electrochemical properties which makes them good candidates for further developing them into other GO-based materials and employing them as anode materials in LIBs.

Seven types of GO and GO-derivatives are used in our study, namely, graphene oxide, reduced graphene oxide (rGO), nitrogen doped rGO, graphene oxide/polypyrrole nanocomposites, graphene oxide/polypyrrole nanocomposites, amine functionalized graphene oxide (GO-NH_2), exfoliated graphite nano-platelets, and doped graphene nano-platelets. Their properties (see section 2.6.1), synthesis processes (see section 2.6.2), and appli-

cations (see section 2.6.3) are explained below.

2.6.1 Properties

Typical characteristics of the used materials are listed in this section.

Graphene oxide (GO)

GO is a graphite-based material with a single layer. It is viewed as a unique material for having some various functional groups, such as epoxide, carbonyl, carboxyl and hydroxyl groups (shown in figure 2.11). Due to these functional groups it possesses, it can be dispersed easily in solvents and matrixes. Possessing functional groups is a major benefit which makes it possible to combine the material with other ceramics or polymers to obtain better mechanical and electrical properties.

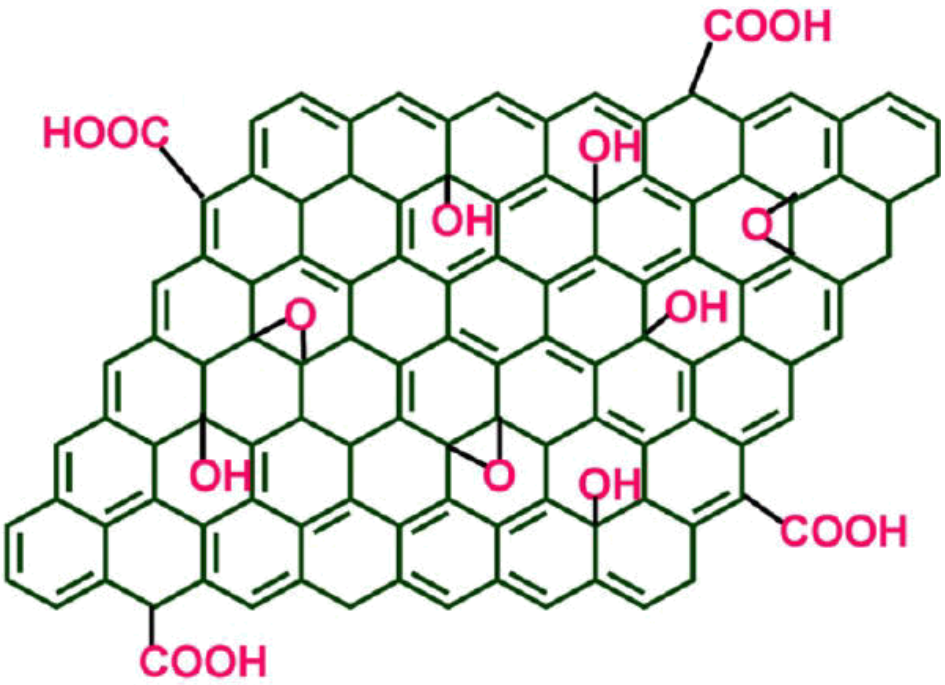

Figure 2.11: Schematic representation of GO.

Graphite was once chosen as a common anode material for LIBs, yet utilizing graphene oxide as anode has also been widely investigated. It was reported that

graphite and graphene oxide were synthesized as composite materials and employed as high capacity and binder-free anode materials for LIBs [78].

Reduced graphene oxide (rGO)

rGO is derived from graphene oxide and it has much better electrical conductivity due to the reduction of the functional groups. Moreover, reduced graphene oxide is a preferred conductive agent for various applications, especially for LIBs. Battery research by using rGO as anode has also been studied. It was claimed that Si/rGO films applied as free-standing anodes in LIBs can exhibit a high reversible specific capacity about 2 times higher than the theoretical value of the graphite anode (904 mAh/g at 200 mAh/g). Also Si/rGO films maintain a long cycle life such as 650 mAh/g after being tested for 150 cycles [79]. Another research group reported a 3D TiO_2-carbon-rGO (TCG) composite as an anode for LIBs. They claimed that it exhibited a higher specific discharge capacity of about 191 mAh/g after 100 cycles at a current rate of 0.2C [55].

Nitrogen doped rGO (NrGO)

Due to several crucial properties of NrGO (shown in figure 2.12) such as high catalytic activity, prolonged stability as well as superior electrocatalytic activity, it was intensively studied and exploited to substitute the expensive Pt-supported electrocatalysts for oxygen reduction reaction (ORR). Apart from that, the research study reveals that nitrogen doping could introduce the defects into carbon which could facilitate the ORR process. Therefore, NrGO could be good candidate to substitute conventional noble metal catalyst for the ORR process and lead to easy fabrication of next generation of fuel cells [80].

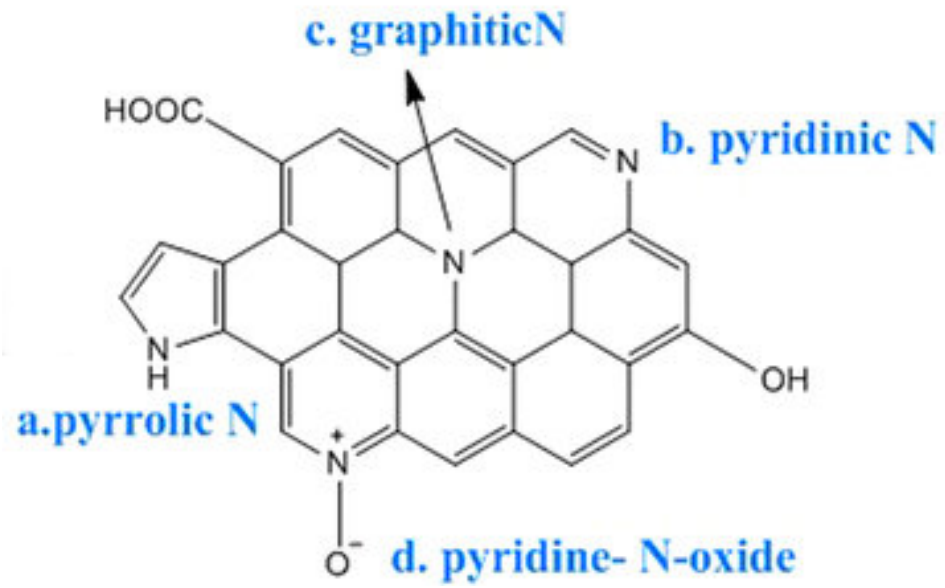

Figure 2.12: Schematic representation of NrGO.

It is known that doping the carbon with nitrogen could effectively modify the chemical and electrical properites of GO. Therefore the electrochemical performance of LIBs is enhanced due to the more activated space which aids the easy transport of electrons and lithium atoms on graphene [81].

Graphene oxide/polypyrrole nanocomposites(GO-PPy)

Conducting polymers such as polyacetylene, polypyrrole, polyaniline, polythiophene have attracted extensive research interest owing to their superior electrical, thermal, magnetic properties. Polypyrrole (PPy) was studied intensively due to good electrochemical performance, facile synthesis process, and low energy consumption [82]. It was reported that PPy with different morphologies exhibit redox properties differently [83]. In another study, it was reported that implementation of graphene nanosheets (GNS)&PPy results in a high capacitance up to 482 Fg^{-1} at a current density of 0.5A/g [84]. The composite of GO/PPy is considered as promising anode materials for LIBs due to the reason that graphene has a good electrical conductivity and PPy exhibits a good redox capability [85].

Amine functionalized graphene oxide (GO-NH_2)

Compared with the oxygen groups present on the GO surface, the nitrogent atom provided by the amine proved to be more nucleophilic. Therefore, it was proposed that functionalizing the graphene oxide with the amino group [86]. Functionalizing GO with amino groups proved to be efficient to enhance the electrochemical properties such that the amino groups can reversibly react with Li^+. Therefore the lithiation and delithiation of GO in LIBs can be improved [87].

Exfoliated graphite nano-platelets (GNP)

GNP is another new type of nanoparticles synthesized from graphite. It is different from graphite in terms of its stack size and layer thickness. It was reported that the GNP stacks are smaller than graphene which falls in a wide range from sub-micrometres to 100 mm. And the layer thickness is about 1-15 nm [88]. Though the interplanar distance is similar to that of the parent graphite, the platelet shape of the GNP provides more edges where the modification is prone to be done chemically for the purpose of enhancing its dispersion in the polymers. Apart from the naturally occurring function groups on the GNP such as hydroxyls or carboxyls, ethers, the sites present at the edges of the platelets after functionalization are found to be capable of hydrogen or covalent bonding. Figure 2.13a presents the TEM image of GNP and figure 2.13b illustrates the unique structure of GNP. A research study proved that GNP shares some similarities with carbon nanotubes in terms of thermal and mechanical properties [89]. Yet GNP exhibits a higher surface area and a higher aspect ratio. Furthermore, the authors reported that GNP can be a good anode due to its higher electrochemical activity and its larger potential window.

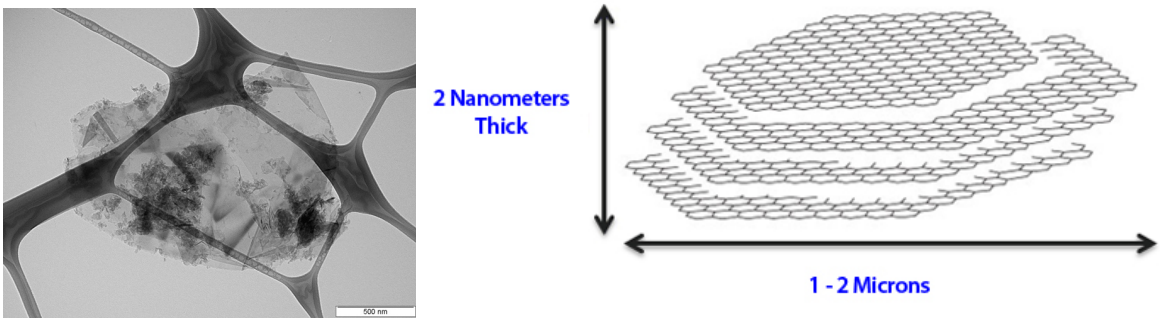

(a) (b)

Figure 2.13: a) Transmission electron microscopy of GNP. b) Thickness and platelet scale of GNP.

Nitrogen doped graphene nano-platelets (NGNP)

NGNPs have been under intensive investigation due to the unique structure of nanoparticles. The nitrogen doping of the GNP known to promote the faradaic pseudocapacitive reactions. Besides, these two main functional groups such as pyridinic and pyrrolic improves the capacity properties, whereas nitrogen and pyridinic-N-oxide are helping to facilitate the electron transfer [90]. Nitrogen doping of the graphene platelets is reported to enhance the electrical properties of graphene nano-platelets and make them a more attractive materials choice for energy-related applications [91].

2.6.2 Synthesis method

Hummers' method is used to synthesize graphene oxide from graphite oxide. The specific procedures are as such: H_2SO_4 treatment is used to intercalate the commercial graphite, followed by three times oxidation with $KMnO_4$ to obtain a fully oxidized graphite oxide. The resultant slurry is washed by water a couple of times for obtaining a neutral pH. Consequently, the suspention is dialyzed for more than 60 days to get rid of salt [92].

GO

It was reported that GO was synthesized simply by performing a sonicaton process for graphite oxide where distilled water was chosen as solvent for dispersing it. Therefore, to obtain GO, Hummers' method should be utilized first to synthesize the graphite oxide [93]. In general, Hummers' method is a widely used chemical process where graphite oxide can be generated by adding potassium permanganate into the solution sodium nitrate, sulfuric acid and graphite [94].

rGO

There are three main techniques available to synthesize the rGO. They are namely, chemical reduction , thermal reduction, and electrochemical reduction. One of the most cost-effective techniques is chemically reducing GO [95]. The general idea of chemically synthesizing rGO follows such steps as oxidation of graphite to graphite oxide, then GO is exfoliated, which is followed by a reduction of GO into rGO. Graphene converted chemically is suited to scalable and cost-effective production. Unfortunately, rGO produced by chemical reduction yields a relatively low surface area as well as lower electronic conductivity. The thermal reduction method at high temperatures up to 1000℃ or more give much better results in terms of surface area which comes even close to that of pristine graphene. Additionally, the electronic conductivity of the rGO synthesized via thermal reduction turns out to be much better [96].

NrGO

A facile chemical method such as thermal annealing of GO in the presence of ammonia was developed for obtaining NrGO sheets [97]. It is reported that the oxygen groups in GO are the main reaction sites for NH_3 and C-N bonding. The synthesis procedures of NrGO are shown in figure 2.14. The annealing of GO with NH_3 are performed by tube furnace with vacuum systems under gas flow. More specifically, GO samples are located in a quartz boat which is further placed in the center of the tube furnace. Initially, the furnace is flowed with NH_3. Then its temperature is increased. Conse-

quently, the temperature of the furnace is increased to the desired reaction temperature and samples are taken out once the furnace has cooled down to room temperature.

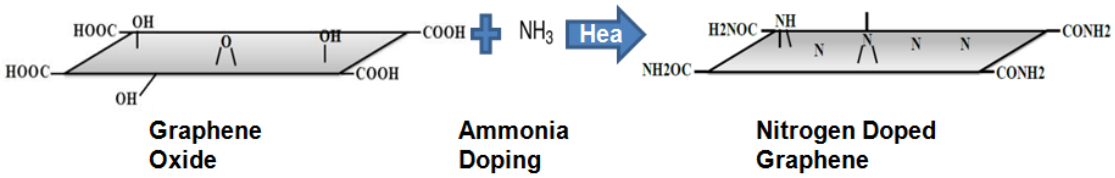

Figure 2.14: Schematic illustration of the synthesis process of NrGO.

GO-PPy

The reaction between the graphite oxide and amino acids takes place in the alkaline solution of amino acids. It is the epoxide groups on the graphite oxide where nucleophilic attack of the ANH_2 occurs. The systhesis process is shown in figure 2.15. More specifically, GO is first dispersed in dichloromethane (DCM) under ultrasonication. Icy water is used to prevent the solvent evaporation. Then N,N'-dicyclohexylcarbodiimide (DCC) is added as a catalyst. Subsequently, p-phenylenediamine is homogeneously mixed in the above suspention. The reaction is continued under stirring and heating. Once the reaction is completed, the DCM is evaporated. The sample is centrifuged, followed by ethanol washing. In the end, the resultant product iss dried in the oven.

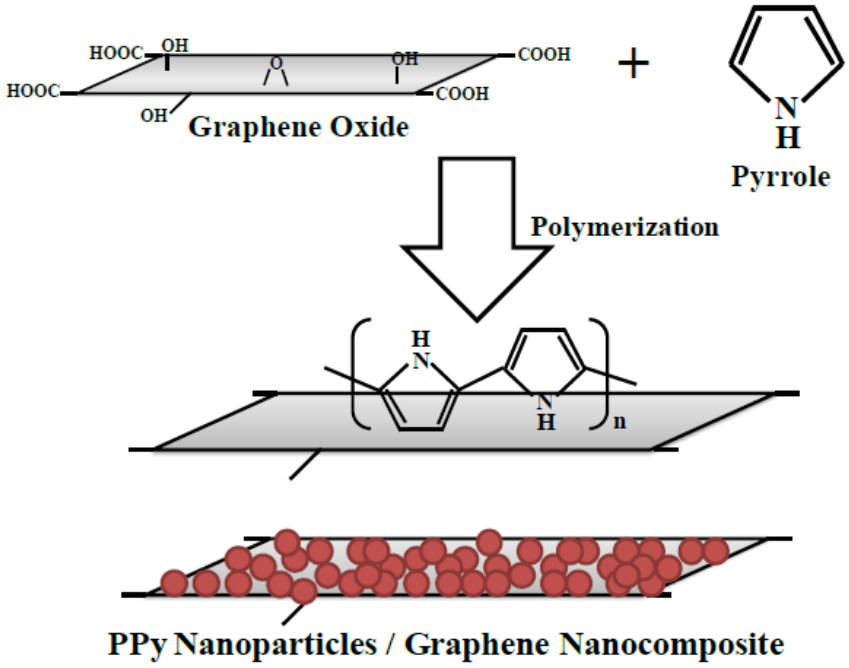

Figure 2.15: Schematic illustration of the synthesis of GO-PPy nanocomposites.

GO-NH_2

The synthesis of nanocomposite GO-PPy is carried out via in-situ polymerization of pyrrole monomer on commercial GO. Catalyst ferric chloride ($FeCl_3$) and dopant sodium p-toluenesulfonate (NapTS) are necessary for this chemical oxidative polymerization. More specifically, GO is first dispersed in water, followed by mixing it with catalyst and dopant. Subsequently, pyrrole monomer iss added slowly into the mixture from the previous step at lower temperatures. Harsh stirring is performed to complete the polymerization reaction. The samples are collected after centrifuging and subsequent ethanol washing. In the end, the sample iss put in the oven for final drying. Figure 2.16 is the schematic illustration of the synthesis of GO-PPy nanocomposites.

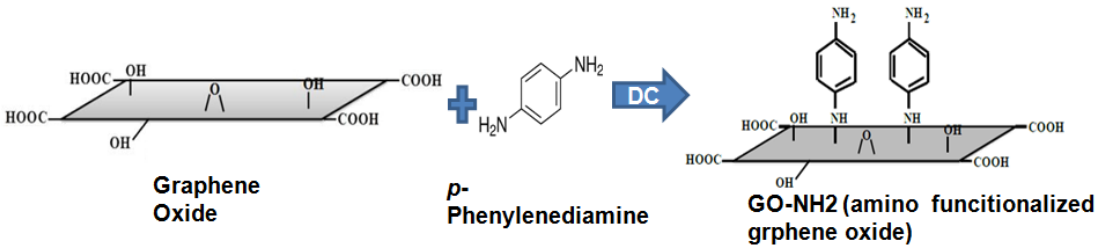

Figure 2.16: Schematic illustration of the synthesis process of GO-NH_2.

GnP

For synthesizing GNP, the intercalant in the graphite intercalation compounds is evaporated at an elevated temperature. Thereafter a sonication is carried out to the thermally exfoliated graphite in acetone for the further exfoliation purpose [98].

NGNP

The specific synthesis procedure for NGNP is as follows. GNP is first located in a ceramic boat. Then it is placed on the loaded boat in a quartz tube furnace for vacuum drying in order to remove the water. Subsequently, the sample is flowed with Ar to purge the oxygen residues. Then, NH_3 gas flow is introduced and a temperature is set which can be ramped up to a predetermined reaction temperature.

2.6.3 Application

This section explains common application scenarios of our used materials.

GO

GO materials are used in a wide range of applications. GO has been used as component materials for some electronic devices such as graphene based field effect transistors, field effect transistors and biosensors [77]. GO is also used as a component in drug delivery systems. Moreover, GO has emerged as a starting materials to provide scalable and cost-effective production of graphene-based materials. Although GO possesses many

good features, the end application of it still needs specific modification such as functionalization and furthur dispersion. Several techniques are available for the desired modifications of GO such as spin-coating, layer-by-layer assembly and filtration. It is of crucial importance to functionalizing GO as this can prevent the restacking and agglomeration of the graphene layers. Therefore the intrinsic properties of GO can be maintained and enhanced as well [99]. GO has been reported as anode materials for LIBs by many research groups. It was reported that electrochemical tests of graphite and graphene oxide composites reveal a reversible capacity of more than 690 mAh/g at the rate of 372 mA/g, simultaneously with outstanding cycle performance and rate capability [78].

rGO

rGO is generally used in the following applications: high capacity energy storage in LIBs. Combine with other components, reduced graphene can also used to improve the overall properties of the resultant composites. Moreover, rGO also displays a saturable absorption which makes it a good candidate for passive mode-locking of lasers [100]. Plenty of research studies have been reported for rGO as an anode material for LIBs. rGO/porous Si composite was obtained by the research group of Hua, Tao. et al. The composite of rGO&Si delivers a reversible capacity of about 815 mAh/g at a rate of 100 mA/g in the voltage range of 0.01-1.5 V after 50 cycles [101]. Another research study reports that SnO_2-reduced graphene oxide nanoribbons as anode for LIBs exhibit a high reversible discharge capacity up to 1,027 mAh/g at 0.1 A/g after 165 cycles and 640 mAh/g at 3.0 A/g after 160 cycles with current rates ranging from 0.1-3.0 A/g and it shows no capacity decay after 600 cycles in comparison with the second cycle at a current density of 1.0 A/g [102].

NrGO

NrGO is very much of interest for oxygen reduction reactions as it exhibits excellent electrocatalytic activity. It was reported that nitrogen doping, especially pyridinic and graphitic N, could offer more reaction sites for oxygen reduction reaction [103].

A study about pure NrGO as anode material for LIBs has been reported by M. Du et al. [104]. They reported excellent reversible capacity of 600 mAh/g at a current density of 0.1 C (1 C=372 mA/g) after 60 cycles for pure NrGO. They also reported that NrGO&Fe_2O_3 shows outstanding proformance. D. Li et al. have obtained TiO_2/NrGO which shows improved cycling performance and rate capability [105].

PPy-GO

PPy-GO shares some special properties due to this new composite structure. Compared to the parent GO, the conductivity of the PPy-GO composite was enhanced by four orders of magnitude. Apart from that, the thermal stability of the composite is improved as well compared to that of the pristine PPy. This improved thermal properties are especially noticeably in elevated temperature range of 430-700°C. A research study done by R. Liu et al. reports a ternary anode of SnO_2/rGO/PPy ternary anodes which reveals an improved cycling stability and an enhanced rate capability [106]. Another work done by Y. Yang et al. obtained a polypyrrole/reduced graphene oxide (PPy/rGO) composite film which exhibits substantially improved electrochemical properties such as good cycling stability and high rate capability [107].

GO-NH_2

Among a wide variety of modified graphene by functionalizing with other materials, GO-NH_2 is used widely as a good component candidate for some composite materials. Such a wide range of applications is due to its good dispersity, synthetic convenience, and scalable production at lower cost [108]. Besides, like all the other nitrogen atom doping in graphene based materials, it contributes to the composite materials for having better conductivity with its high amount of positive surface. It was reported that the Si@NH_2/GO electrode delivered a reversible capacity of 1000 mAh/g after 400 cycles at a current of 420 mA/g with almost 100% capacity retention [109].

GNP

Due to the unique platelets structure and specific nanoscale size, GNP was widely used to composite with various of polymeric materials such as themalset and thermoplastic composites, adhesives, coatings and paints. More specifically, GNP are proves to be a promising reinforcement material for Cu-based metal matrix composites [110]. According to the research study conducted by M. Agostini et al., the electrode combined with GNP delivers a capacity of the order of 150 mAh/g with an efficiency approaching 100% [111].

NGNP

NGNP has proved to be useful as an additive for composite materials. More specifically, it can be a potential component in batteries and super capacitors. Besides, it is used as a conductive components in adhesive and e-inks. On the other hand, it has also been used as an additive in impermeable packaging due to its mechanical properties. According to a recent research work, NGNP can also be utilized in highly sensitive bio-sensors thanks to its conductively and processed surface with sensitized molecules [112]. It was reported that platinum loaded nitrogen doped graphene and platinum loaded graphene nano-platelets as ORR yield a power density of 440 and 390 mW/cm^2, respectively [113]. This finding motivates the idea to use pure NGNP as an anode material for LIBs.

Chapter 3

Materials and synthesis

3.1 Synthesis of TiNTs&GO-based composites as anode

3.1.1 Two-step hydrothermal treatment

To prepare a novel composite of TiNTs combined with graphene-based materials, a two step hydrothermal treatment process was carried out.

The first step hydrothermal treatment was conducted for the purpose of growing TiNTs. The typical synthesis procedures are as follow. First, 40 g NaOH (Aldrich CAS no: 1310-73-2) solid was added into 100 ml distilled water to have 10 M NaOH solution. Then 0.5 g of commercial anatase powder (P25 Aldrich CAS no: 1317-70-0) was dispersed into the above 10M of NaOH solution under the constant stirring condition for half an hour. The above mixture was transferred into a high pressure autoclave with teflon beaker (figure 3.1) which was being sealed in autoclave thereafter. Afterwards, autoclave moved into oven (figure 3.2) and kept under the temperature of 130°C for 49 h. During this process anatase TiO_2 nanoparticles are transformed into sodium hydroxide ($Na_2Ti_3O_7$). Autoclave was taken out after 49 h and precipitated white $Na_2Ti_3O_7$ flack was filtered by filtered followed by overnight hot-plate drying at 100°C. The collected particles are grand into fine powder. The process is presented here below in figure 3.3.

Figure 3.1: Image of the autoclave and Teflon beaker used for hydrothermal treatment.

Figure 3.2: Oven used for hydrothermal treatment.

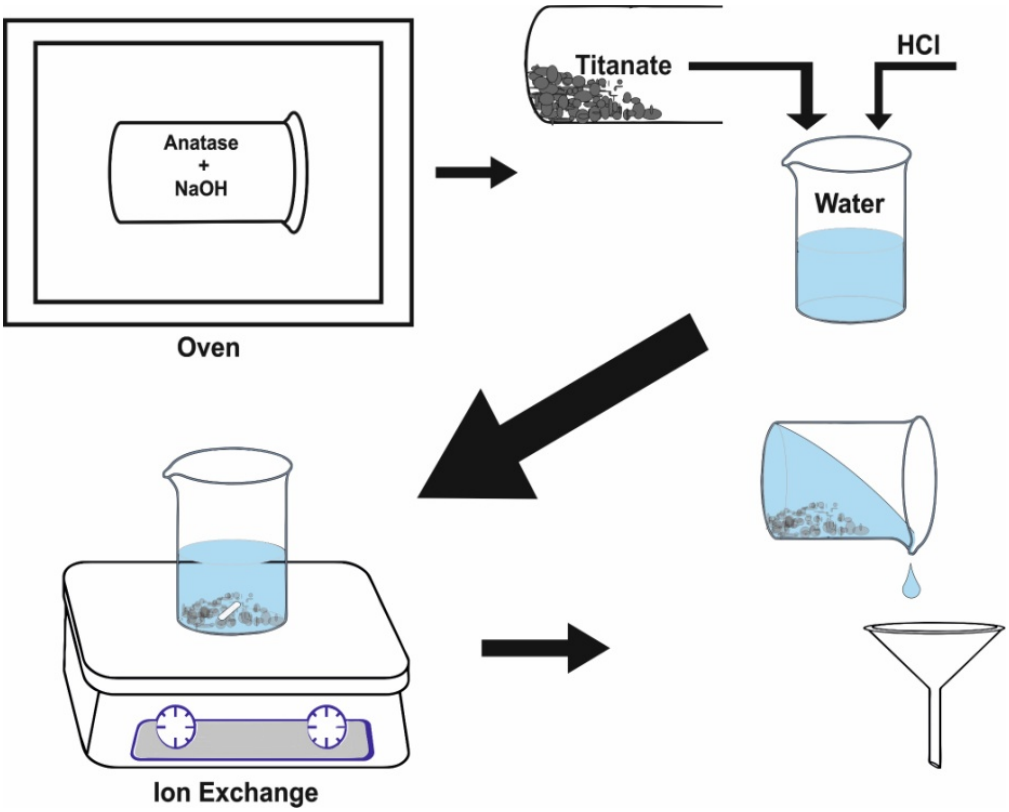

Figure 3.3: Schematic illustration of the first step hydrothermal treatment.

The second step hydrothermal treatment had been conducted to in-situ grow the TiNTs on the surface of GO based material. Figure 3.4 illustrates the synthesis processes which is similar to the first time hydrothermal treatment. The specific synthesis procedures are as follow. Firstly, 140 mg GO based materials was dissolved into 100 ml of distilled water followed by a 4 h probe-sonication under ice condition. Then a homogeneously dispersed mixture was prepared by adding the as-prepared TiNTs powder in to the above probe-sonicated GO-based suspension. A 0.5 h of constant stirring is carried out to obtain uniform dispersion. Thereafter, the mixture was transferred into autoclave in the same way as the first time hydrothermal treatment. Then the sealed the autoclave was moved into oven under the temperature of 130°C for another 49 h. After hydrothermal treatment, precipitates are collected by filtering and dried overnight at 100°C. The dried bulky powder was powdered finely using mortar. Afterwards the collected fine powder was dissolved into 1 L of distilled water followed by mild acid wash using 0.1 M HCl. Note that the HCl has to be added in dropwise because there

might be a sudden change in the pH of the solution. Besides, a harsh acid washing would destroy the newly grow nanotubes. The pH of the solution was set to 4 or 10.

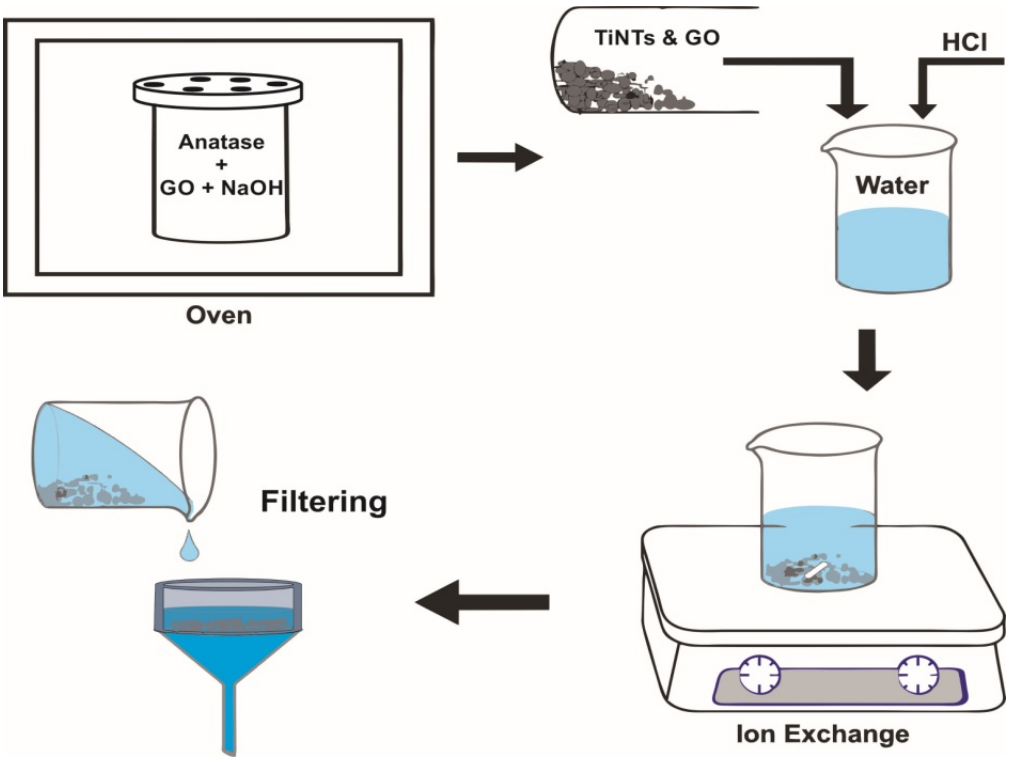

Figure 3.4: Schematic illustration of the second step hydrothermal treatment.

3.1.2 One-step hydrothermal treatment

One-step synthesis

Novel nanocomposites of TiNTs&GO-based are synthesized with hydrothermal method. Unlike the two step process as mentioned in previous section, one step hydrothermal synthesizing was adopted. They typical procedure is going as follows. 150 mg commercial graphite oxide was first dissolved in 50 mL of distilled water then undergoes 4 h probe-sonication. Secondly, 0.5 g of commercial anatase powder (P25 Aldrich CAS no: 1317-70-0) used without any purification treatment as a starting material and added together with 10 M of NaOH (Aldrich CAS no: 1310-73-2) into sonicated GO suspension under 0.5 h of harsh stirring condition. Then above dispersion was transformed into a stainless steel autoclave with a Teflon beaker of 200 mL volume. A hydrothermal

process of 48 h at 130°C was carried out for the above dispersion. After a following process of natural cooling in room temperature, the precipitates were collected using filter flask under vacuum pressure. While filtering, DI water washing of multiple times was also done for the purpose of illuminating excess sodium content. Filter paper with precipitates on it went for overnight drying at the temperature of 100°C. In the end, the bulk material was grounded into fine powder using a mortar. The resultant solution was then filtered and dried at 100°C overnight. The dried bulk flack sample ($Na_2Ti_3O_7$) was powdered and added to 1L water under acid environment (the pH was adjusted using 0.1 M HCl slowly) for 1.5 days in for the purpose of ion exchange between Na^+ and H^+ . Finally the washed sample was again filtered and dried overnight at 100°C to obtain hydrogen titanate ($H_2Ti_3O_7$). Figure 3.5 shows the one-step hydrothermal treatment process.

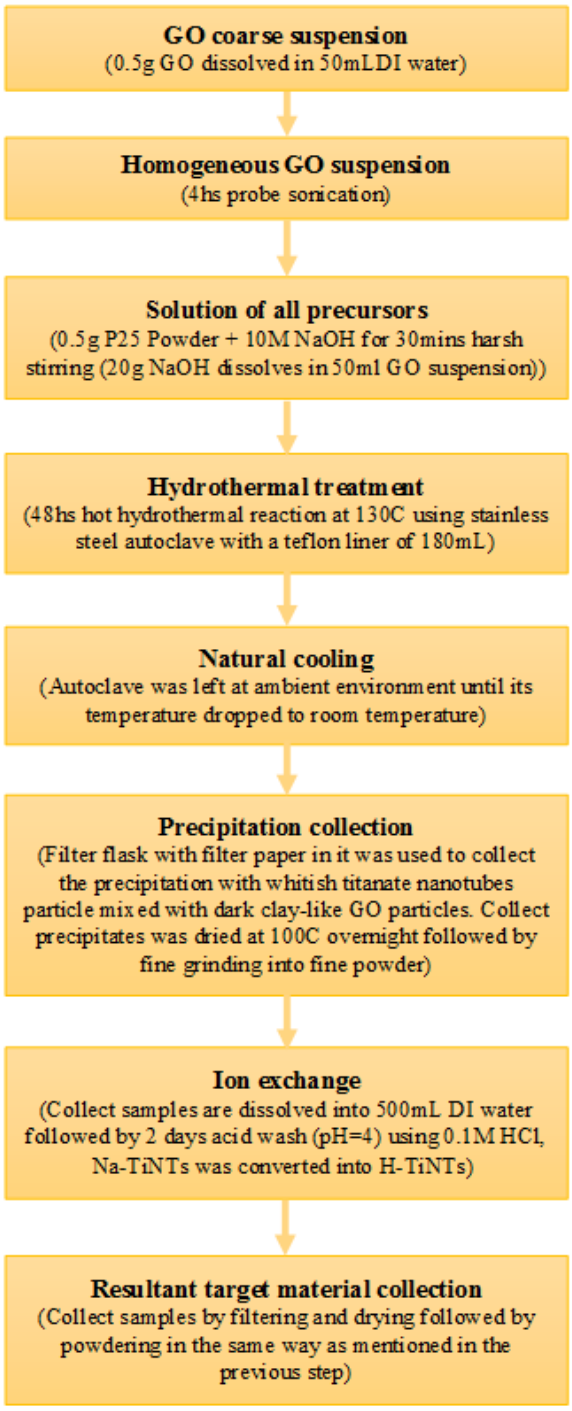

Figure 3.5: One-step hydrothermal treatment process.

3.2 Structure characterization

XRD is a material characterization technique commonly used for studying the crystal structures and atomic spacing of the targeting material. For the elemental analysis necessity, XRD analyzing was performed in this study. XRD features one of the few non-destructive test methods by which elemental information can be obtained from the diffraction pattern it provides. A Rigaku Rint 2000 diffractometer with a monochromatized CuKa irradiation (λ = 0.15405 nm) had been used for all samples synthesized in this research study. Data was taken for the 2 range of 2° to 90° with a step of 0.01°. The novel composite investigated in this study is TiNTs combinded with GO-based material. Raman spectroscopy is a device widely used for characterizing crystal structure, defects and disorder in graphene or graphene-based materials [114]. Based on the intensity ratio of the two main peaks named D band and G band, the reduction process of GO-based material can be presented. In addition to that, Raman spectroscopy can also be used to identify frequency modes as vibrational, rotational etc. The information obtained as such considered as a fingerprint of specific molecular. Raman spectra were recorded for all as-prepared sample on Renishaw inVia with excitation of 514.5 nm.

Surface areas of both GO-based materials and TiNTs are a critical factor that affects the battery performance. In addition to that, the pore size of the TiNTs is another significant factor which has to be examined properly. Thus the surface area and the pore size analyzer (Quantachrome NOVA 2200e) were utilized in boiling N_2 temperature (77 K) for examining all 24 h of degasing at 150°C was chosen for examining all the samples.

Investigations of the morphology of the as-prepared samples are important because the battery performance is significantly related to the in-situ growing and homogeneous distribution of TiNTs on the surface of GO-based materials. For analyzing the morphology structure of as-prepared samples, scanning electron microscopy (SEM) (Zeiss LEO Supra 35VP SEMFEG) was operated. The surface chemistry of the selected composite of TiNTs&GO (pH=10) had been examined by X-ray photoelectron spectroscopy (XPS). X-ray photoelectron spectroscopy was used for the purpose of investigating and

confirming the bond state between the TiNTs and the carbons.

3.3 Electrochemical characterization

Electrode preparation

A whole LIB cell is made up of four main components as mentioned before. Therefore electrode preparation is very critical. However, the electrodes are a mixture of multi-components. Besides the key component of active material such as TiNTs&GO, other ingredients of the mixture are a binder, a solvent and an additive. PVDF is the abbreviation of polyvinylidene fluoride resin which is a common binder choice for most of the LIBs. Binder is used for the reason of mechanical integrity of electrodes which can prevent the delamination and provide a good contact among each electrode components. N-Methyl-2-pyrrolidone also named in short as NMP used as the solvent. NMP is preferred in most of the rechargeable batteries due to the fact that it is an extremely powerful and versatile aprotic solvent. An additive such as carbon black is needed for enhanced conducting properties. For both electrodes, the mixture components are more or less same only with active material being different. Among the content of active material of electrode, the binder are normally fall in the range of 3% - 15%. Although a higher amount of binder can help to enhance the adhesion, it may harmful to the battery performance yet.

The problem induced from loose inter-particle contact between active materials has to be taken seriously. While preparing the slurry, carbon black was dispersed prior to adding the solvent. This is because internal resistance can be reduced and electrochemical performance can be enhanced due to agglomeration was prevented and therefore a better uniformity has been achieved. Due to the mixture of heterogeneous solid particles whose size varies from nano- to micro-scales, these component powders are bound together with a binder in an organic solvent. Thus the mixing condition has great influence on the performance of the battery. Normally, viscous slurry is prepared so as to be coated on top of the copper foil homogeneously. Meanwhile, a thorough mixing in highly viscous media will aid the mechanical integrity of the

electrode after being dried. The method for obtaining a well-mixed slurry has been explored extensively. Yangs research group reported that it might be better in terms of enhancing the life of batteries if all the component powders mixed in dry state first then introducing the solvent NMP to finely mix under a harsh stirring process. It said that the viscosity of the solution will drop gradually first then stay stable once reached its limiting value despite of long mixing time period. Apart from that, a higher stress yield may be problematic if the reduced amount of solvent is too much according to report from research group led by Ligneel.

After coated copper was prepared, it must be noted that a slow drying is preferred. This is because drying in elevated temperature may pose challenge on integrity of electrode. Instead drying on lower temperature will keep better interconnect among all components in the mixture.

Electrode preparation procedure in our study

Active material of GO&TiNTs, conducting additive of carbon black, and PVDF binder are mixed in mass ratio of 85:10:5 restrictively in NMP solvent. The amount of NMP is decided according to viscosity of the slurry (figure 3.6). The thoroughly mixed slurry with ideal viscosity was obtained under s harsh stirring condition for one day. Round copper foils were prepared by a disc cutter (figure 3.7). Then the slurry was cast finely onto the copper foil with approximately the same loading (figure 3.8). After that coated copper foil was left for drying at 50° on hot plate for one day. A PP/PE/PP tri-layer round shape separator (25 μm thick x 85 mm W x 60 mL, Celgard) was placed in between the anode and lithium cathode. 1.0 M lithium hexafluorophoshate ($LiPF_6$) dissolved in an equal volume mixture of ethylene carbonate (EC) and dimethyl carbonate (EC/DMC=50/50 (v/v), (battery grade-746711-100ML Sigma - Aldrich) was used as the electrolyte and slowly poured on both sides of the separator. The so-arranged cell stack was packed in stainless steel split-up flat test cell. Here below is the schematic description of the material and process as well.

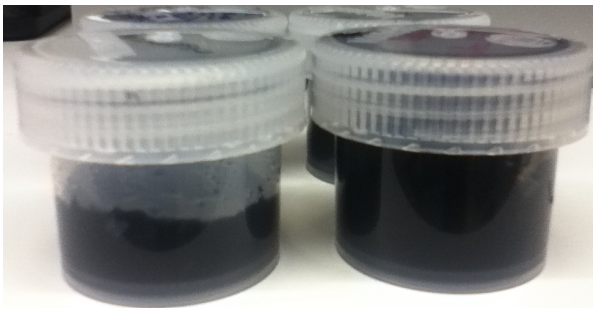

Figure 3.6: Slurry prepared by mixing the conducting additive of carbon black, PVDF binder in a mass ratio of 85:10:5 in a NMP solvent.

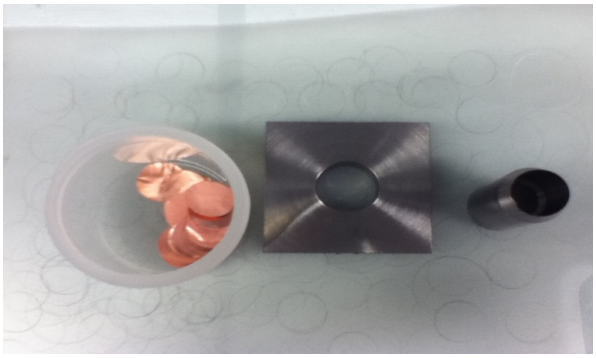

Figure 3.7: Manually cut copper foils prepared for the electrode.

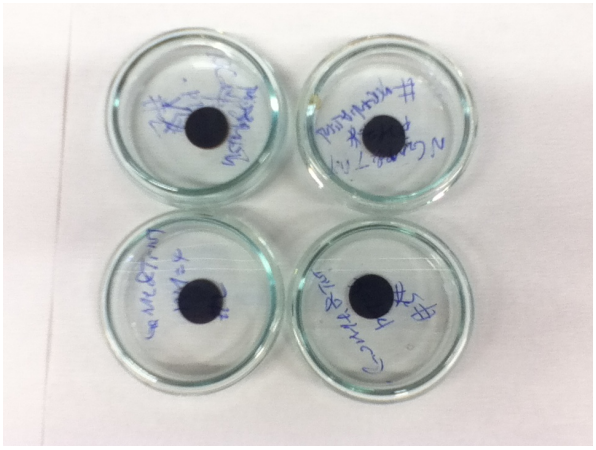

Figure 3.8: Image of some anodes: copper foil coated by as-prepared slurry.

Cell fabrication

Figure 3.9 shows a three electrodes test cell, with the lower side being the anode, upper side being the cathode, and the middle one is the reference electrode. All the prepared anodes were tested by this splitable designed cell which gives user an easy access to assembling and reassembling the electrodes. Note that the reference electrode is used for voltage variation monitoring purpose. This three electrode splitable flat test cell can allow electrodes with 15 mm in diameter and 24 mm separators.

Figure 3.9: Stainless steel three-electrode split test cell.

Assembly in glovebox

The test cell was assembled in an argon filled glovebox due to the sensitivity of the lithium hexafluorophoshate ($LiPF_6$) electrolyte and lithium metal to the oxygen and humidity. A low moisture and low oxygen amount lower than 1 ppm (v) was achieved by the incorporated humidity control system and oxygen analyzer by sensing the level of both of them continuously. Figure 3.10 shows the configuration of the glovebox used in our research study.

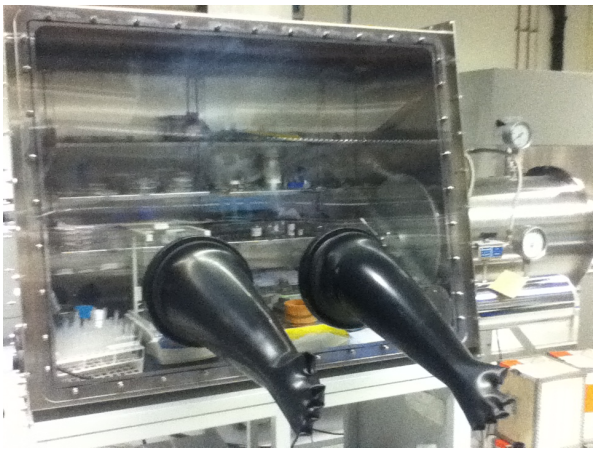

Figure 3.10: The glovebox used for assembling the battery cells.

Battery test

The galvanostatic charge and discharge were tested for the assembled battery at current densities of 0.1C and 1C between voltage limits of 1-3 V (vs. Li) at ambient environment. The specific capacity of TiNTs&GO-based composite was calculated based on the mass of TiNTs. Figure 3.11 shows the battery test station.

Figure 3.11: Battery test station for discharge and charge measurement.

Chapter 4

Results & discussions

To characterize our composite materials, we performed XRD, Raman spectroscopy, XPS, BET, SEM. Furthermore, we carried out electrochemical characterization and battery tests. A section is dedicated to each of the aforementioned methods and the obtained results are discussed therein.

4.1 XRD results

Titanate nanotubes (TiNTs) are the essential component of our final composites and the existence of the expected nanotubes structure is ascribed to the improved electrochemical performance of LIBs. Therefore XRD was performed to examine the chemical composition and phase change of all as-prepared samples.

Anatase TiO_2 was used as the starting material for synthesizing the as-prepared TiNTs by 48 h hydrothermal treatment at 130°C. It was reported that the starting material has a significant impact on the resultant material morphology. Moreover, the existence of rutile phase together with anatase phase in a different ratio would cause the morphology of a final product to vary from nanosheet, nanoplates, to nanotubes. Moreoever, pure nanotubes can barely be synthesized in such case [115]. Therefore, XRD was performed for examining the exact phase of the starting materials. Figure 4.1 presents the XRD pattern of the anatase TiO_2 used as starting material in this study. Three main peaks shown at 25.5°, 37.8°, 48.0° are ascribed to the characteristic

anatase phase of (101), (004) and (200) [116]. This result demonstrates that the starting materials used in this study were pure anatase.

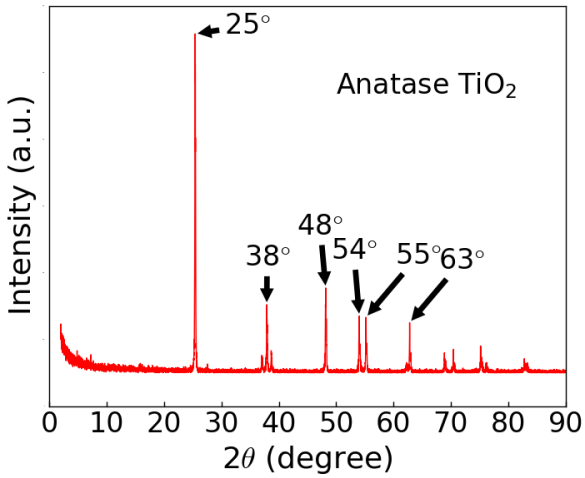

Figure 4.1: XRD pattern of anatase TiO_2 used as the starting materials for TiNTs synthesis.

TiNTs at pH values varying from 4 to 7 have been prepared by using the two-step hydrothermal treatment followed by ion exchange. This pH range was chosen according to the research report done by Yarali et al. [117]. In their study, a pH range from 2-13 was investigated for the purpose of tracking the interlay distance of elongated TiNTs. Their research illustrates a lower pH below 3 brought in a phase change from titanate to anatase TiO_2. Although TiNTs grow through the hydrothermal process, the ion exchange followed by hydrothermal treatment determines the interlayer distance of the TiNTs. The reason for such a result is due to the ion replacement occurring between atoms with different radii. Based on the literature, Na-O bond in $Na_2Ti_3O_7$ has a length above 2 Å, whereas the H-O in $H_2Ti_3O_7$ has a bond length of only about 1 Å[118].

Figure 4.2 shows the XRD pattern of the as-prepared samples with the pH values differing from 4 to 7. The patterns shows several clear peaks at 10.0°, 24.2°, 28.3°, and 48.0° for all samples except the one at pH=4. These peaks can easily be indexed to the layered TiNTs ($Na_2Ti_3O_7$-JCPDS: 31-1329, $H_2Ti_3O_7$-JCPDS: 41-1092) as those peaks are all in good agreement with the characteristic peaks of the TiNTs [117, 119]. Specifically, the peaks located at 9.6° refer to the (200) plane which is considered as

the critical peak for differentiating between sodium TiNTs and hydrogen TiNTs. It is reported that the shift on peak positions occurs if the interlayer distance decreased due to sodium ions replaced by hydrogen ions [120]. Since the pH investigated in this study is lower than 7, the slight changes are negligible. Moreover, it was reported that the presence of sharp peaks located at 2θ=25°, 31° in addition to a new peaks located at 35° demonstrates nanoribbons and nanowires [121]. From the pattern in figure 4.2, we can assure that the titanate nanostructures synthesized in this study are pure nanotubes with the absence of these characteristic peaks.

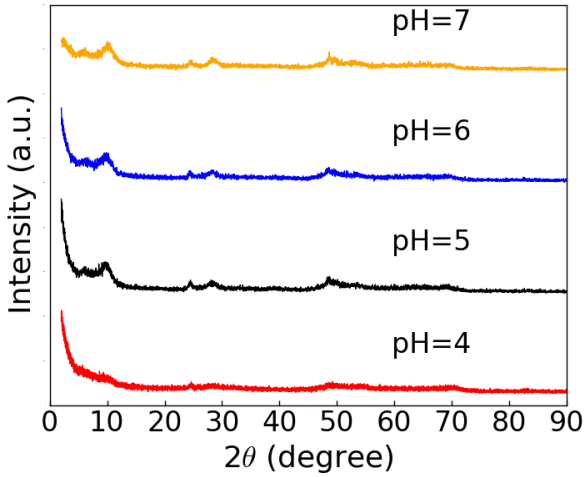

Figure 4.2: XRD patterns of the TiNTs at various pH values which were synthesized by hydrothermal treatment.

TiNTs (pH=4) synthesized from the first step of hydrothermal heat treatment were blended separately with 4 difference types of GO-based materials. They are graphene oxide (GO), graphene nano-plates (GNP), nitrogen doped reduced GO (NrGO), and polyporrole functionalized GO (PPy-GO). Figure 4.3 shows the XRD patterns of these 4 types of GO-based materials.

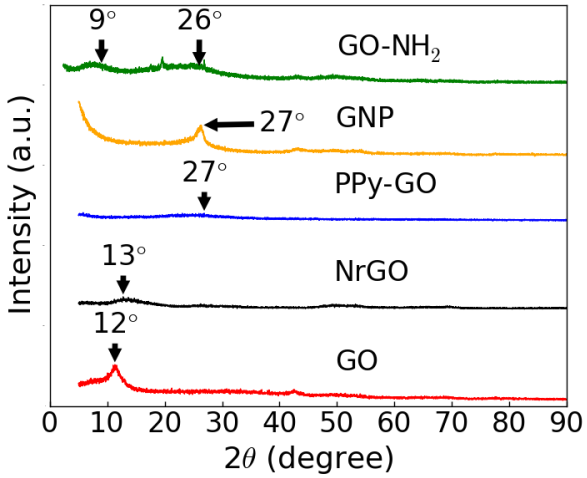

Figure 4.3: XRD patterns of the four types of GO-based materials, they are graphene oxide (GO), nitrogen doped GO (NrGO), polypyrrole functionalized GO (PPy-GO), graphene nanoplates (GNP) from the bottom to the top in the order.

As can be seen, each graphene based material has been marked right on top of each corresponding XRD pattern. For graphene oxide (GO), a strong peak located at 12° corresponds to an interlayer spacing of 8.47 Å. As opposed to graphene which has its characteristic peak located at 26.45°, a larger interplanar spacing in GO is due to the oxygen bonding on both side of GO sheet which opens the layer. After reduction, a higher 2θ value can be expected which are the case for the rest three patterns. In the NrGO pattern, two peaks can be observed though they are not not strong enough. The first broad peak located near to 12° corresponds to the crystal plane of GO. Yet its broadening is caused by the Nitrogen doping. Another one is barely visible around the characteristic peaks of GO (26.45°) corresponding to the (002) plane [121]. This pattern can be considered as nitrogen doped GO which has no effective oxygen reduction [122]. Polypyrrole functionalized GO shows comparatively much lower intensities due to the further broadening effect induced from the low intensitive reflection of reduced GO [123]. Another low intensity peak can still be observed around 24.30°. This smooth pattern is because of the amorphous nature of conductive polymer polypyrrole in addition to the less crystalline nature of the graphene. Regarding the graphene nano-plates (GNP), there is a strong x-ray diffraction located at 2θ=27.0°. This corresponds to the XRD

reflection of the (002) crystal diffraction plane of GNP [124]. And also the pattern illustrates that the GNP used composed of few layer sheets which imply an intact graphene structure. [110]. The interlayer spacing is much shorter than that of GO.

A second time hydrothermal treatment was performed for each mixture under same condition with previous hydrothermal treatment. Figure 4.3 shows the XRD results of our final composite materials. As shown from the XRD pattern, six samples were tested. Except four composites, commercial TiO_2 without hydrothermal treatment but ion exchange to pH=4 together with TiNTs pH at 4 were tested by XRD for the purpose of comparison. The figure 4.4 shows TiNTs combined with GNP, GO, NrGO, PPy-GO, respectively. As can been seen, the main characteristic peaks of tubular titanate nanostructures located at 10.0°, 24.2°, 28.3°, and 48.0° are obtained in all the as-prepared samples, though the intensity of the crystalline reflection has slight differences among one another. In comparison with the TiNTs, the characteristic peak of reduced graphene 2θ=26.0° (200) has disappeared in XRD pattern for all the composites. This is due to the TiNTs completely covering the surface of GO-based materials. The XRD reflection of GO-based materials was blocked. In addition to that, the peaks for reduced GO or GO overlapped with the main characteristic peaks of TiNTs at 2θ=10°, 24.2°.

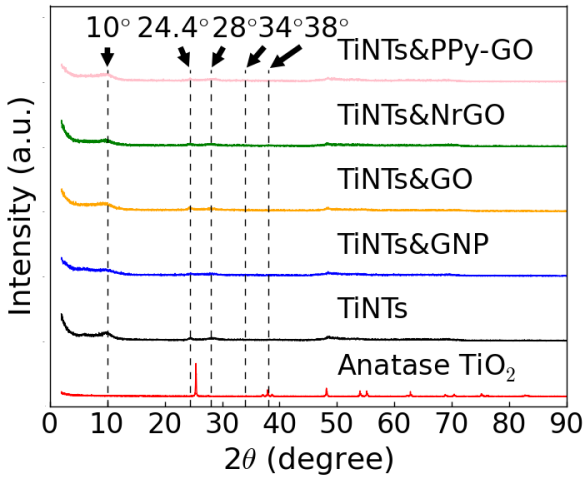

Figure 4.4: XRD pattern of the nanocomposite of TiNTs (at pH=4) synthesized by two-step hydrothermal treatment. Black color represents the TiNTs at pH=4, whereas the red line denotes the XRD pattern of commercial anatase.

One-step hydrothermal treatment has been utilized to synthesize our composite material TiNTs&graphene-based. This one pot synthesis was experimentally proved to be not only time-efficient but also effective in in-situ tubular structure growth compared with the two-step hydrothermal treatment. Two weeks of experimental process can be shortened into one week with much higher percentage of TiNTs aligned on the surface of graphene-based materials. Figure 4.5 represents a close comparison among the material being used, and visual explanation on the structural changes occurred after each experimental steps. As can be seen, after hydrothermal treatment, there is a peak broadening.This broadening induced by overlapping of the characteristic peaks GO (2θ=11°) and TiNTs (2θ=9°). Meanwhile, there is a conversion from anatase TiO_2 into TiNTs based on the position changes occurring at the XRD peaks.Figure 4.5 shows the XRD patterns of TiNTs pH at 4 blended separately with GO, rGO, NrGO, NH_2-GO, GNP, N-GNP. When compared with samples prepared by two-step synthesis method, more smooth XRD patterns are obtained for the samples prepared with one-step synthesis process. Those 4 main peaks 2θ=10.0°, 24.2°, 28.3° and 48.0°, which are characteristic for tubular TiNTs, are observed for all the sample as can been seen in figure 4.5. A week peak can be observed around 2θ=7° for the composite samples in this graph. This result may suggest that the thick alignment of TiNTs in between the layers increased the interlayer distance of the GO-based materials.

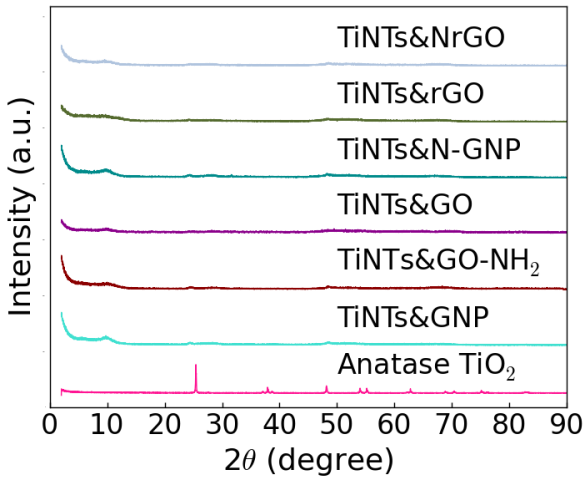

Figure 4.5: XRD pattern of the nanocomposite of TiNTs&GO-based (at pH=4) synthesized by one-step hydrothermal treatment.

In this study, TiNTs blending with GO-based materials at pH=10 have also been investigated. Figure 4.6 shows the XRD pattern of the composite TiNTs&GO-based materials synthesized by one-step synthesis method, all at pH=10. The names are all marked on top of the their corresponding XRD pattern. As can been observed, TiNTs&GO-NH_2 has the sharpest first characteristic peak, followed by TiNTs&NGNP has second sharpest same characteristic peaks compared with TiNTs&GO. This is due to the higher percentage of TiNTs in-situ grew and occupied the GO surface area.

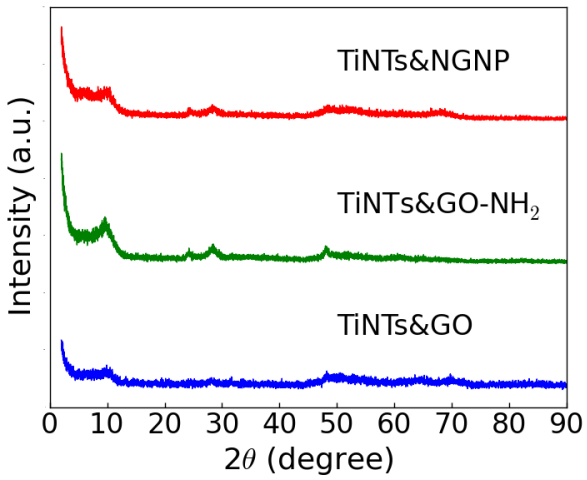

Figure 4.6: XRD pattern of the nanocomposite of TiNTs&GO-based (at pH=10) synthesized by one-step hydrothermal treatment.

4.2 Raman results

Raman spectroscopy was performed for analyzing and confirming the chemical composition of the products. The Raman spectra of the GO and the GO derivatives are presented in figure 4.7. Two main characteristic peaks around 1357 cm (D band) and 1595 cm (G band) are revealed in all examined Raman graphs in the GO-based materials. The D band is related to the disorder of the hexagonal lattice of the carbon, whereas the G band is induced by the vibaration of sp^2 carbon materials [125]. In addition to the position of these two bands, the intensity of the ratio of D band over G band (I_D/I_G) gives significant information regarding the disorder level. Raman spectroscopy provides clear information of N doping in the graphene lattice. Moreover, electron donation induced by N heteroatomes could induce a further blue shift in G band in compare with GO. Moreover, the intensity ratio of I_D/I_G increases after reduction and I_D/I_G=1.12 was reported for NrGO [126]. As can be seen from figure 4.7, NrGO has a relatively high D band which refers to a higher disorder degree as compared with the GO. In another report, the I_D/I_G for GO-NH_2 is 1.03. This large I_D/I_G indicates the additional disorder presence in carbon edges and the existence of the functional groups [127]. Regarding the PPy-GO, an intensity ratio of about 0.8 can be observed, which confirms the lesser amount of disordered graphene in PPy-GO. In addition to that, a down shift of the G band peak can be observed which further confirms a GO reduction [128]. For GNP, the intensity ratio of I_D/I_G observed in this study is in good agreement with the results I_D/I_G=0.57 obtained by another research group [129]. The intensity ratio of I_D/I_G is nearly equal to 1 according to the result for NGNP in figure 4.7. It said that structural defects and edge distortion are the main two reasons for this intensity ratio for NGNP [130]. 4.1 lists the intensity ratios of the D/G band in various GO-based materials used in our study. The Raman results of the GO-based materials indicate that the starting materials are not all fully reduced, yet at acceptable levels.

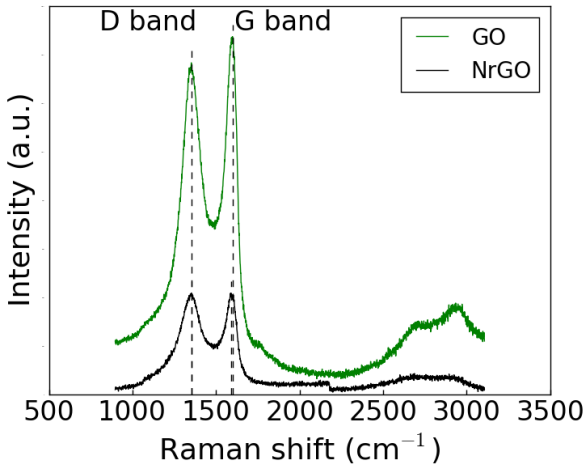

Figure 4.7: Raman spectra of the GO-based materials used in as-prepared TiNTs&GO-based composites.

Table 4.1: Intensity ratios of D/G band in various GO-based materials used in our study.

Samples	Intensity ratio (D/G)
GO	0.93
rGO	0.80
NrGO	1.12
PPy-GO	0.80
NGNP	1.05
GO-NH_2	1.03

Figure 4.8 represents the TiNTs&GO-based composite materials at pH=4. All materials in figure 4.8 were synthesized by the two-step hydrothermal method and the corresponding Raman spectra were recorded for each of them. Here below, a) shows the lower range of Raman spectra for examining the tubular structure of titanate in a close investigation on their characteristic peaks located in the range of 100-700 cm^{-1}. Raman spectrum of b) shows the higher range of whole Raman spectrum of the same composite as that of the a). The whole Raman spectra are split into two parts as such with the purpose of examining the tubular structure of titanate in a close-up in-

vestigation on their characteristic peaks located at lower range of 100-700 cm^{-1}, and the presence of graphene based materials on the higher range of D-band (1357 cm^{-1}), G-band (1595 cm^{-1}) of Raman spectra. Besides by the checking the higher range of Raman spectra, we can see how the lattice order of GO based material are affecting by embedded with the TiNTs. In addition to that, we can observe and confirm the phase and structure conversion occurred in each pattern with extensive comparison among each other. It was reported, the characteristic peaks for protonated titanatestructure are located at 275 cm^{-1} and 449 cm^{-1}. However, a) shows raman peaks which is identical to the anatase TiO_2 with 5 main peaks situated at 153, 206, 391, 505 and 615 cm^{-1}, respectively. Combined with XRD results with the Raman results of corresponding composite, they can be assumed as-prepared composites are anatase type of tubular TiNTs [131]. Compared with the pristine GO-based counterparts, the intensity ratio of the D band (1357 cm^{-1}) and G band (1595 cm^{-1}) arises due to an increase of disorder in sp^2 lattice specific for the carbon systems. This increases the intensity ratios of all these three patterns in figure 4.8b due to the incorporation of TiNTs in the lattice of GO and GO derivatives.

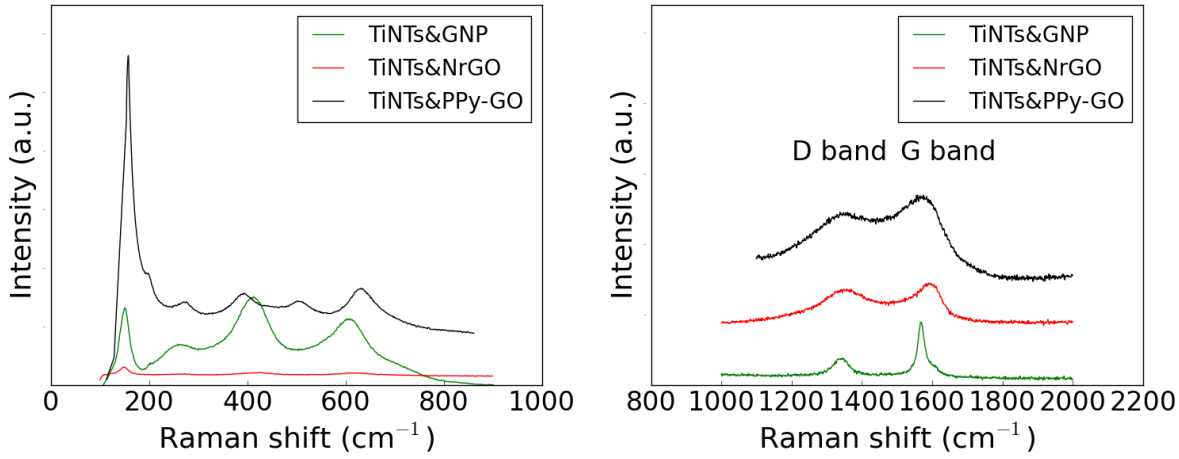

Figure 4.8: Raman spectra of TiNTs&GO-based composite materials synthesized by the two-step hydrothermal method at pH=4: a) lower range of the Raman shift and b) higher range of Raman shift.

Figure 4.9 shows the TiNTs&GO-based composite materials prepared by one-step sysnthesis method via hydrothermal treatment at 130°C for 48 h. As can be seen, 3 types of composites were prepared with each type adjusted to two pH values of 4 and 10. Figure 4.9a shows, except for TiNTs&GO-NH_2 pH=10, typical TiNT peaks (275 cm^{-1}, and 449 cm^{-1}). However, the other four composites TiNTs&NGNP pH=10, TiNTs&NGNP pH=4, TiNTs&GO pH=10, TiNTs&GO-NH_2 pH=4 indicate anatase TiO_2 with typical peaks located at 153, 206, 391, 505 and 615 cm^{-1}, respectively [132]. Besides, TiNTs&GO pH=4 are showing the characteristic peaks of both anatase peaks at 153 cm^{-1}, and that of trititanate peaks with a slight down shift to a lower value. A similar Raman spectrum has also been reported as rutile type of TiO_2 nanotubes [133]. Besides, the peak located around 630 cm^{-1} is a broad peak occupying a large range. Based on the report, it can be indicated as Hydrogen type of TiNTs [134]. Moreover, it was observed that the composites with the same formula, but with pH=10, have higher intensity ratios compared to their counterparts with pH=4. Such systematic intensity increase of D band over G band with the increase of pH values is due to the increase of defect induced by the bonding of TiNTs with carbon, which is shown in figure 4.9b. The Raman spectrum of the ambient H-Ti-NT powder has a somewhat broader band in the 600-720 cm^{-1} range than the Raman spectrum of the ambient Na/H-Ti-NT powder.

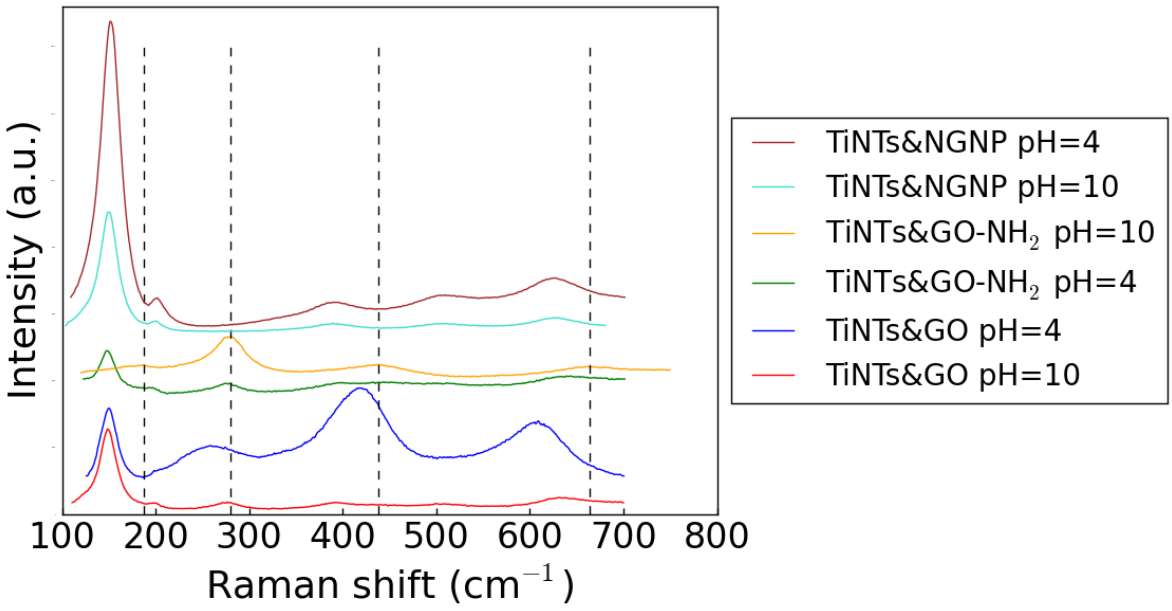

(a)

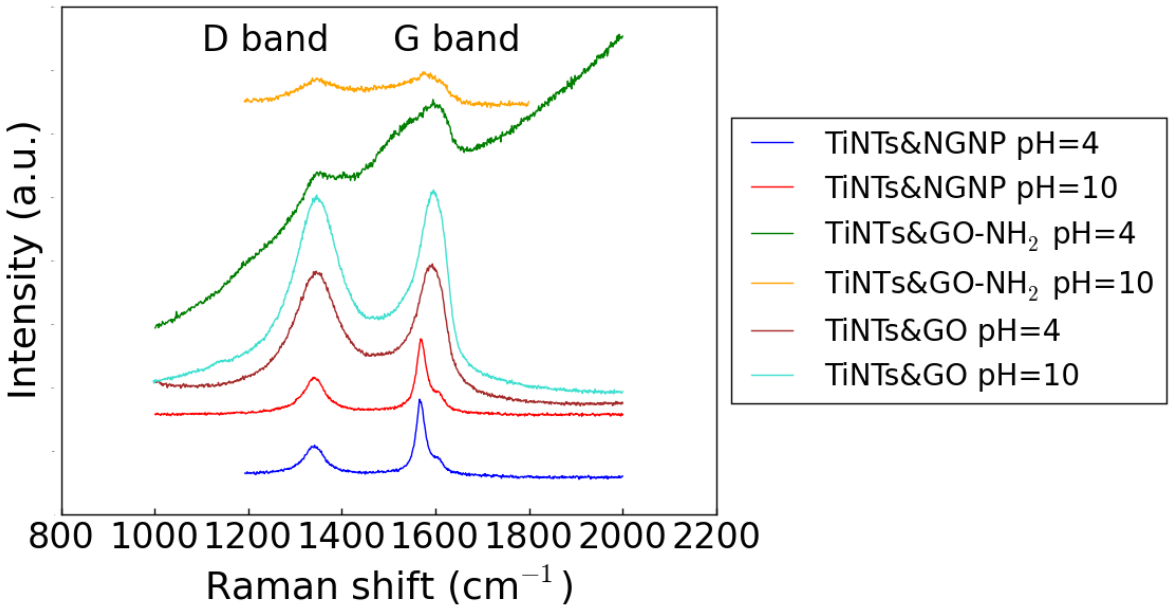

(b)

Figure 4.9: Raman spectra of TiNTs&GO-based composite materials synthesized by one-step hydrothermal method at pH=4 and pH=10: a) lower range of the Raman shift and b) higher range of Raman shift.

4.3 XPS results

The results obtained from scanning electron microscopy (SEM) indicate that TiNTs&GO at pH=4 has the highest amount of homogeneously aligned TiNTs on both sides of the GO surface. Therefore, XPS spectroscopy was performed for the purpose of analyzing the chemical state of the main components in this specific sample TiNTs&GO at pH=4. Figure 4.10a provides the O 1 s patterns which refer to the lattice oxygen Ti (IV)-O (528.5 eV) and Ti (III)-O (513.2 eV), respectively. Figure 4.10b represents the C 1 s where COOH, C=O, C-O, C-C bonds are located at the higher banding energy ∼289.5, 287.9, 286.1 eV, and 284.2 eV. Besides, we can observe the two bondings Ti-O-C and Ti-OH were superimposed over the C-O bonding signal at ∼531 eV. Two peaks situated at about 282.5 eV and 513.2 eV were attributed to Ti-C and C-O -Ti bonding. The presence of these two peaks are of significant interest as their presence indicates that a strong bond between TiNTs and carbon atoms has formed. These bonds between carbon and TiNTs are preferred as they can give rise to faster conduction and transport of charges. In addition to that, the small bonds ascribed to COOH, C=O, C-O, and C-C functional groups exist on the edge or on the surface of GO sheets [131, 135].

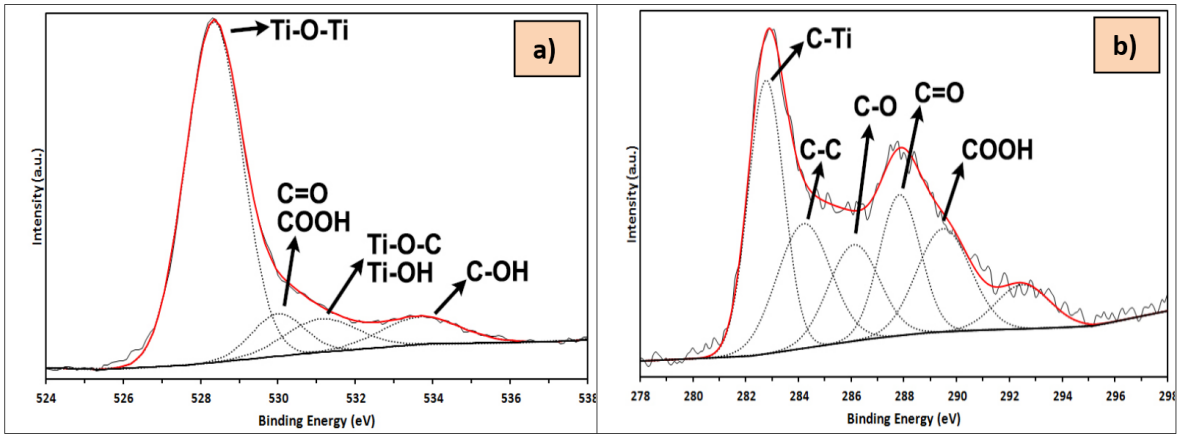

Figure 4.10: XPS spectra of TiNTs&GO composite at pH=4: a) O 1 s and b) C 1 s.

4.4 BET results

Physical examination on the surface area and the porosity of the TiNTs&GO-based composites

BET surface and BJH isothermal analysis were performed for obtaining information about the surface area and porosity of as-prepared composites. Surface area determines the amount of active sites, yet the active sites require the porosity texture of the material where molecular transport may occur. Therefore the surface area measurement and porosity examinination are two critical interests in this study. Meanwhile, the pore size distribution was also examined for the purpose of investigating the tubular structure of titanates more in detail. This is due to the inner diameter and the outer diameter of nanotubes together with the type of texture shape will confirm and complement the morphology of samples obtained from the SEM analysis [136]. Table 4.2 depicts the surface areas and pore radii of TiNTs prepared by hydrothermal heat treatment. As can be seen, 4 samples at a pH of 4, 6, 7, and 10 were listed in the table in ascending order with their corresponding surfaces and pore radii shown as well. Nitrogen adsorption analysis for all the samples show type IV adsorption isotherm corresponding to a mesoporous texture. Table 4.2 illustrates that increased pH values induce growing surface values. This is in complete agreement with the literature [69]. The replacement of Na^+ by H^+ induced a lower tubular pore diameter. According to the literature [117], the inside wall of the tubular structure contributes mostly to the surface area. Therefore it is understandable that the highest surface area was obtained at pH=4.

Table 4.2: TiNTs (hydrothermal treatment).

Samples (TiNTs)	Specific surface area (BET)(m^2/g)	Pore radius (Å)
pH=4	216	10
pH=7	155	10
pH=10	104	12

Table 4.3 shows the surface areas and pore radii of TiNTs&GO-based nanocompos-

ites prepared by two-step hydrothermaltreatment. We found that the maximum surface area was obtained for TiNTs&GNP. It was reported that TiNTs provide a surface area between 200-300 m^2/g (BET surface area) when based on the calculation from nitrogen adsorption isotherm. For the composite of TiNTs blend with GO based material, the dominant surface contributor are TiNTs, less contribution comes from GO-based materials [137]. Thus, despite that GO-based material feature a high surface area, a comparatively lower surface area around 150 m^2/g was obtained for these composites. The maximum specific surface area of 263 m^2/g was obtained for TiNTs&GNP.

Table 4.3: TiNTs&GO-based composite (Two-step hydrothermal treatment method).

Composite samples (pH=4)	Specific surface area (BET)(m^2/g)	Pore radius (Å)
TiNTs&GNP	263	12
TiNTs&NrGO	95	12
TiNTs&PPy-GO	106	12

Table 4.4 represents the surface areas and pore radii of TiNTs&GO-based nanocomposites prepared by one-step hydrothermal treatment. Four composite materials are analyzed, and the highest surface area was found for TiNTs&NGNP. Moreover, all the tested samples display a homogeneous pore radius with a similar range from 12-15. Such a radius value is preferred as it can facilitate the charge transfer.

Table 4.4: TiNTs&GO-based composite (one-step hydrothermal treatment method).

Composite samples (pH=4)	Specific surface area (BET)(m^2/g)	Pore radius (Å)
TiNTs&GNP	263	12
TiNTs&$NrGO_2$	61	15
TiNTs&GO-NH_2	228	15
TiNTs&PPy-GO	106	12

BJH pore size distribution curve (PSD curve)

Figure 4.11 shows the BJH pore size distribution curve for all three sets of samples. Figure 4.11a represents the TiNTs with a pH of 4, 7, and 10; figure 4.11b depicts TiNTs&GNP, TiNTs&NrGO, and TiNTs&PPy-GO all at pH=4 synthesized by the two-step hydrothermal method; figure 4.11c is about composites synthesized by the one-step hydrothermal method which includes TiNTs&GO, TiNTs&GO-NH_2, TiNTs&NGNP, and TiNTs&NrGO, all at pH=4. As can be seen from figure 4.11a, all the samples are having a pore size distribution range from 5-50. However, the main distribution range is 7-25 Å with a maximum pore radius of 12 Å. In figure 4.11b similar results are represented, which is in complete agreement with the pore size distribution of a typical TiNT [138]. In figure 4.11c, TiNTs&NrGO have quite a large range of pore size distribution ranging from 10-50 Å with the main point falling around 23 Å while the other three are having a similar distribution range of 7-25 Å. This is due to the tubular structure converted into spherical structure as observed in the SEM analysis. The results obtained for the as-prepared composite materials agree with the literature results because firstly, typical surface area values are reportedly in the range 150-300 m^2/g and secondly, a total specific pore volume range of 0.60-0.85 cm^3/g was reported for nanotubes [62]. The high pore volume of TiNTs&GNP composite can be explained by the SEM results where materials shows more porous morphology compared with other composites.

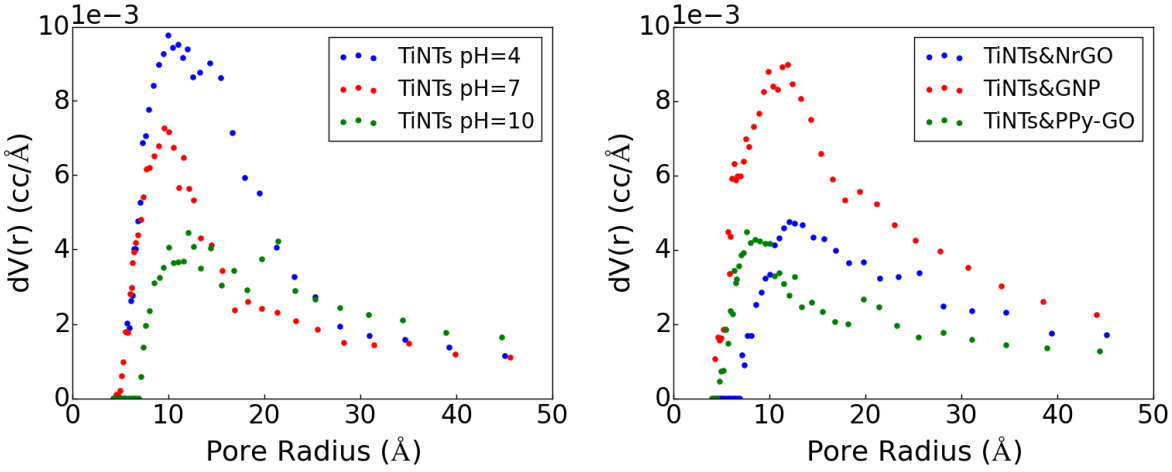

(a)

(b)

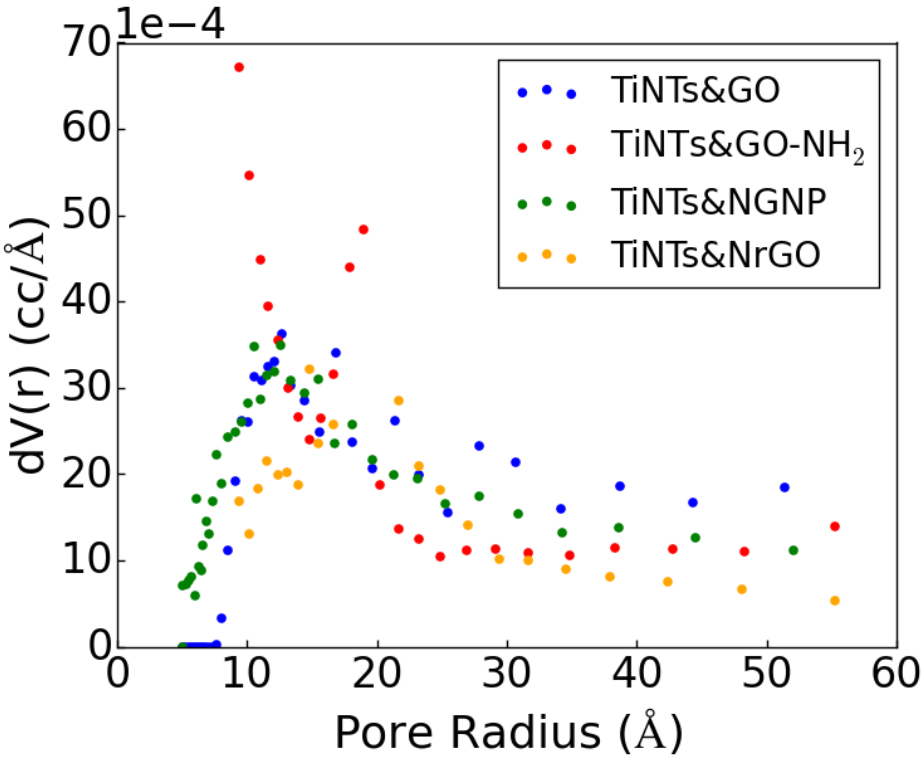

(c)

Figure 4.11: BJH pore size distribution curve of three sets of samples. a) TiNTs at pH values 4, 7, 10. b) TiNTs&GO-based material synthesized with the two-step method at pH=4. c) TiNTs&GO-based material synthesized with the one-step method at pH=4.

4.5 SEM results

To confirm the morphology of the precursor materials, all GO-based materials and titanate precursor have been investigated by performing the A Leo G34-Supra 35VP field emission scanning electron microscope (SEM). And the corresponding SEM images have been collected. Figure 4.12 shows the SEM image of 6 types GO or functionalized GO materials. Figure 4.11a reveals a flower-like morphology with relatively small grain size (<1 μm). It is obvious from this image that, the layers of the GO are quite open with no close attachment among layers. Figure 4.11b represents reduced GO with a large and smooth surface. The size of the graphene sheets vary from several hundred nanometers to few micrometers. No agglomeration or restacking of GO sheets can be observed from the SEM image. Figure 4.11c reveals nitrogen doped reduced GO with a clear paper-like morphology with small size of open gaps in between layers. The SEM image of NGNP (figure 4.12d) shows unique emerged spherical shapes with a very smooth surface. These unique nanoparticles observed on the image are formed by platelet-shaped graphene comprised of short stacks [113]. It is said that graphene nano-platelets are special in terms of enhancing the properties of many favorable polymeric materials due to their unique shape, nano-scale size, and special nitrogen doped material composition. In addition to that, the reported surface area can vary from 300-500 m^2/g based on the difference of width of the layers [139]. Figure 4.12e shows the morphology of polypyrrole functionalized GO (PPy-GO). The SEM image reveals that PPy has nearly a spherical shape with a diameter around 180 nm. It can be observed that PPy was dispersed on top of the reduced graphene sheets [140]. Figure 4.12f. shows the aminated GO. Amino functionalized GO sheets seem to form the tangled patches with ripple-like shapes on the surface. Between the crosswise edges of the multi-layer of amino functionalized GO, a porous network of few hundred nm can be observed. It was reported that functionalizing of GO with amino can cause hydrogen bending which can induce morphology with such specifications. It has also been mentioned that the wrinkled morphology structure of amino functionalized GO can provides a big surface area which is favorable for getting a high capacity for energy storage devices.

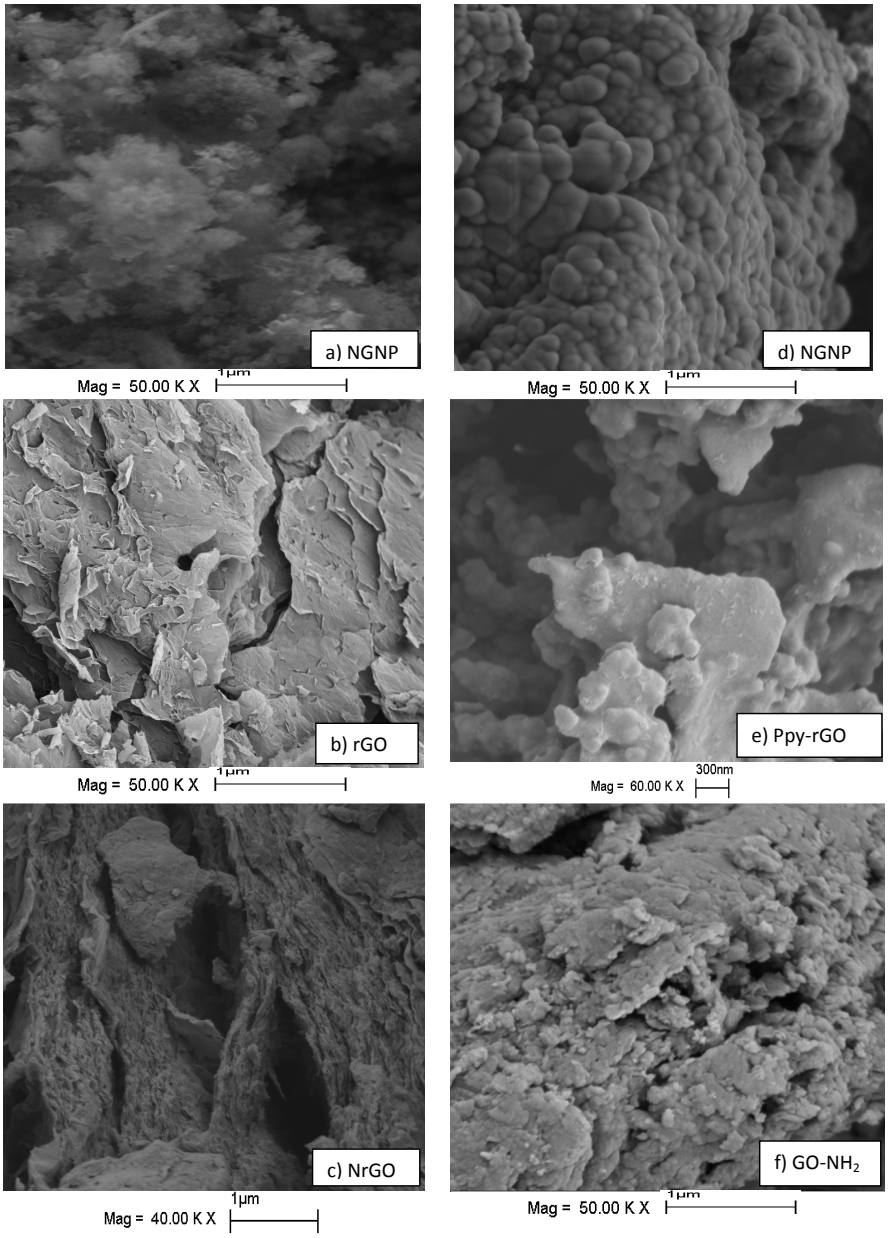

Figure 4.12: Scanning electron microscopy (SEM) images of the GO-based materials: a) GO, b) rGO, c) NrGO, d) NGNP, e) PPy-GO, and f) GO-NH_2.

Beside GO-based materials, the TiNTs produced by the one-step hydrothermal method with a pH of 4, 7, and 10 were also examined by SEM. Figure 4.13 shows the collected SEM images for four products. Figure 4.13a represents the morphology of the commercial anatase TiO_2. It is clear that in the figure 4.13 TiNTs at pH=4 (figure 4.13b) and 7 (figure 4.13c) show clearly tubular structure with homogenous size of tube diameter. The diameters of the tube sizes for both TiNTs at pH=4 and at pH=7 are around the range 10-20 nm, respectively. However, the TiNTs at pH=10 (figure 4.13d) shows a rod shape of nanostructures. Such kind of morphology conversion from nanotubes to nanorod at elevated pH value up to 10 is well supported by the literature [117]. In addition to that, we can observe the agglomation of nanotubes in some areas, which is due to the acid washing. Based on report from another group, it was claimed that the tubular structure of alkaline titanates is very sensitive to inorganic acid [69]. From the SEM results, we can conclude that the well-aligned tubular TiNTs with uniform tube diameter are obtained via hydrothermal treatment.

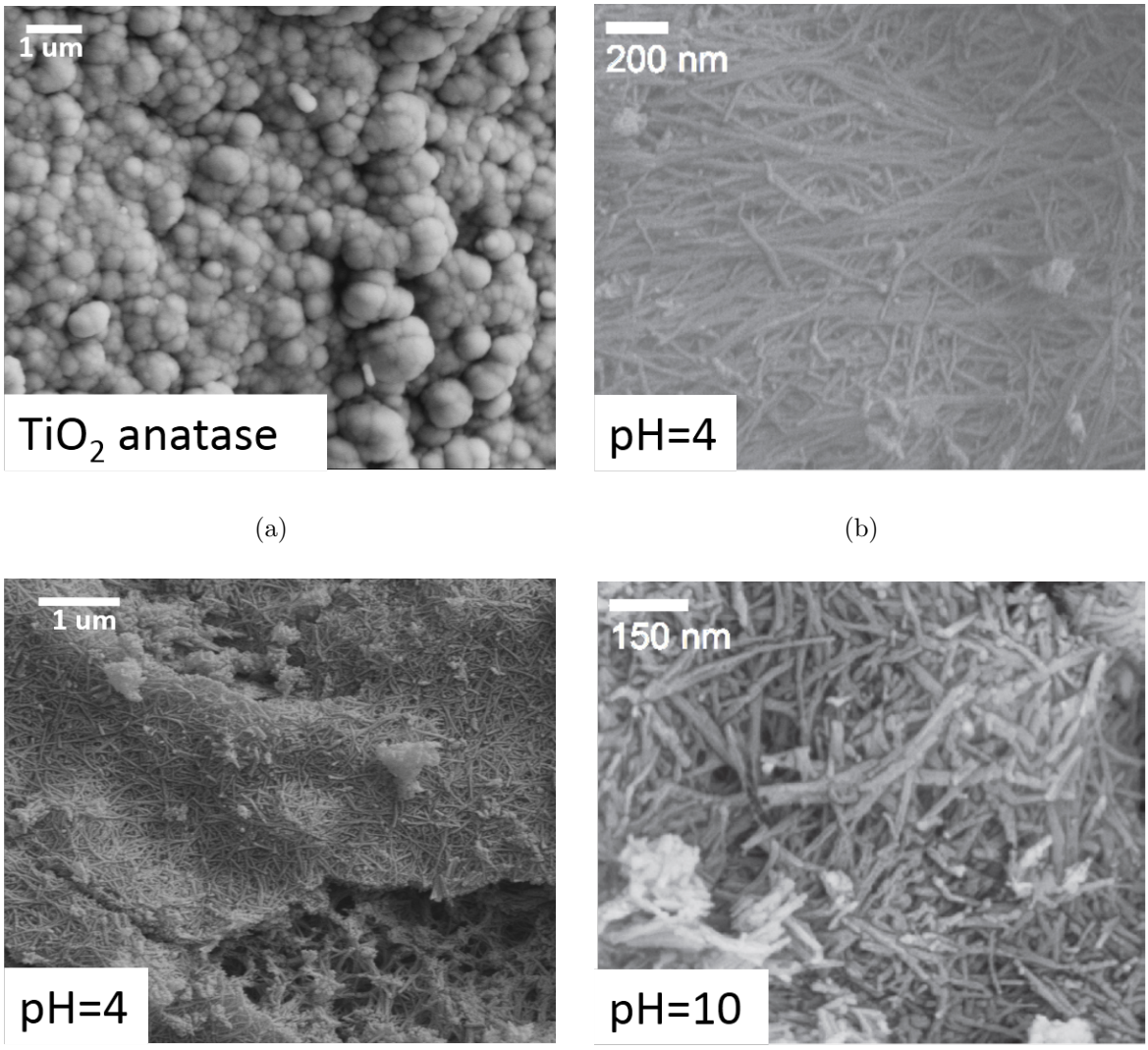

(a) (b)

(c) (d)

Figure 4.13: Scanning electron microscopy (SEM) images of: a) Commercial anatase TiO_2, b) TiNTs pH=4, c) TiNTs pH=7, and d) TiNTs pH=10.

The surface morphologies of the samples synthesized by two-step hydrothermal treatment are presented in figure 4.14. These three TiNTs&GO-based composites are synthesized by hydrothermal treatment by mixing the TiNTs at pH=4 with the GO-based materials, namely graphene nanoplates (GNP), nitrogen doped reduced GO (NrGO), and polypyrrole functionalized GO (PPy-GO), respectively. From the SEM image of TiNTs&GNP in figure 4.14a, the tubular structure under a pressed surface is

observable. The amorphous surface shown in the image may be caused by tubular structure collapse induced by the second time hydrothermal treatment. In the second time hydrothermal treatment, the pH changed to 7 because water was used as the solvent as opposed to the first time where NaOH was used as a solvent. Combined with the BET and Raman results, we assume that the acid content in the layers of TiNTs induced the partial phase conversion from tubular titanate to anatase TiO_2 nanoparticles, as well as partial tubular structure deterioration. Figure 4.14b reveals the morphology of TiNTs&NrGO at pH=4. As can be seen that the nanotubes grew by first step hydrothermal treatment are not aligned firmly on the surface of NrGO. In addition to that, the amount of the nanotubes on the surface of NrGO is very low compared with the starting nanotube materials for producing composites. Therefore we can conclude that most of the nanotubes are severely damaged. A serious agglomeration of the nanotubes can also be observed for TiNTs&NrGOs. The cracking of the NrGO may be due to the heavy loading of the agglomerated amorphous TiO_2. However, the XRD results show the characteristic peaks of the TiNTs. Meanwhile, we can still observe some nanotubes from the SEM image. Therefore, it is clear that the nanotubes are either destroyed or broken into ones of shorter lengths on the surface, whereas in between the layers, nanotubes are protected by NrGO layers mechanically. Figure 4.14c represents the TiNTs&PPy-GO at pH=4, in which nanotubes with shorter lengths were observed.

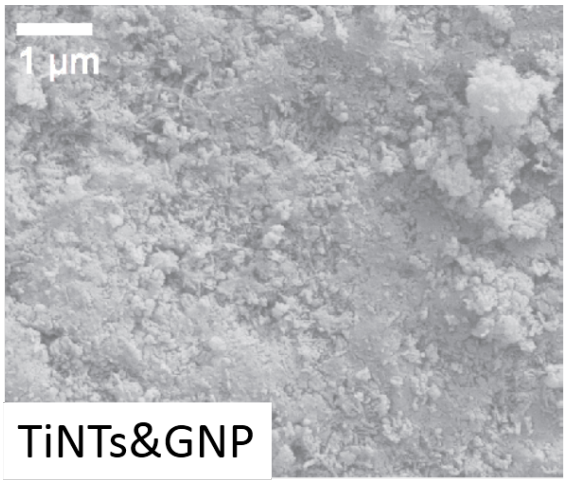

(a)

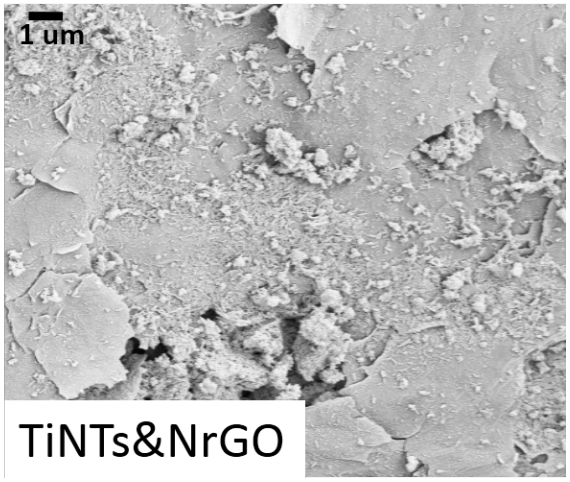

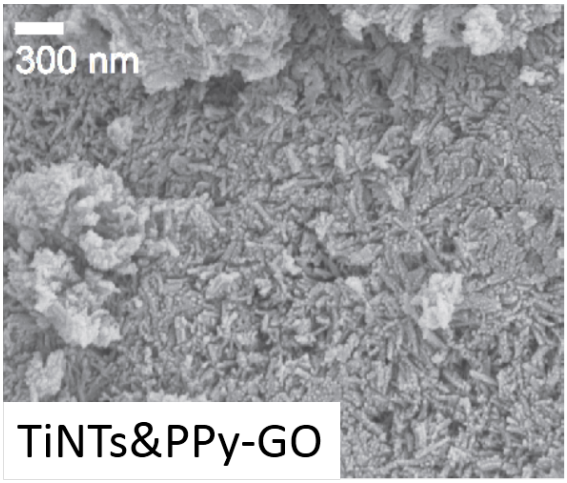

(b) (c)

Figure 4.14: Scaning electron microscopy (SEM) images of the TiNTs&GO-based (two-step synthesis): a) TiNTs&GNP pH=4, b) TiNTs&NrGO pH=4, and c) TiNTs&PPy-GO pH=4.

Figure 4.15 presents the SEM images of TiNTs&GO-based materials synthesized by the one-step hydrothermal method. The SEM images collected from these 6 types of TiNTs&GO nanocomposites reveal that the tubular nanotubes are successfully grown and well-aligned on the surface of the GO-based materials. By comparing the composites with similar components but at different pH, it can be observed that, the prolonged TiNTs grew at lower pH levels. In addition to that, agglomeration of TiNTs is observed

in each composite but to a different degree. Although the agglomeration degree is mild in each of these nanocomposites, it is still observable at some area. According to SEM, we can see TiNTs&GO-based materials is showing the least amount of agglomeration, whereas the TiNTs&NGNP shows the highest agglomeration. Based on the results obtained from BET together with SEM results, we realized that the agglomeration at lower pH levels is more severe than at higher pH levels such as 10. Similar results were reported by other research groups as well [117]. This is due to sodium TiNTs being more stable at higher temperatures and less sensitive to the acid environment. It is interesting that the amino functionalized GO shows almost similar morphology with no observable change in its tube length and tube diameter.

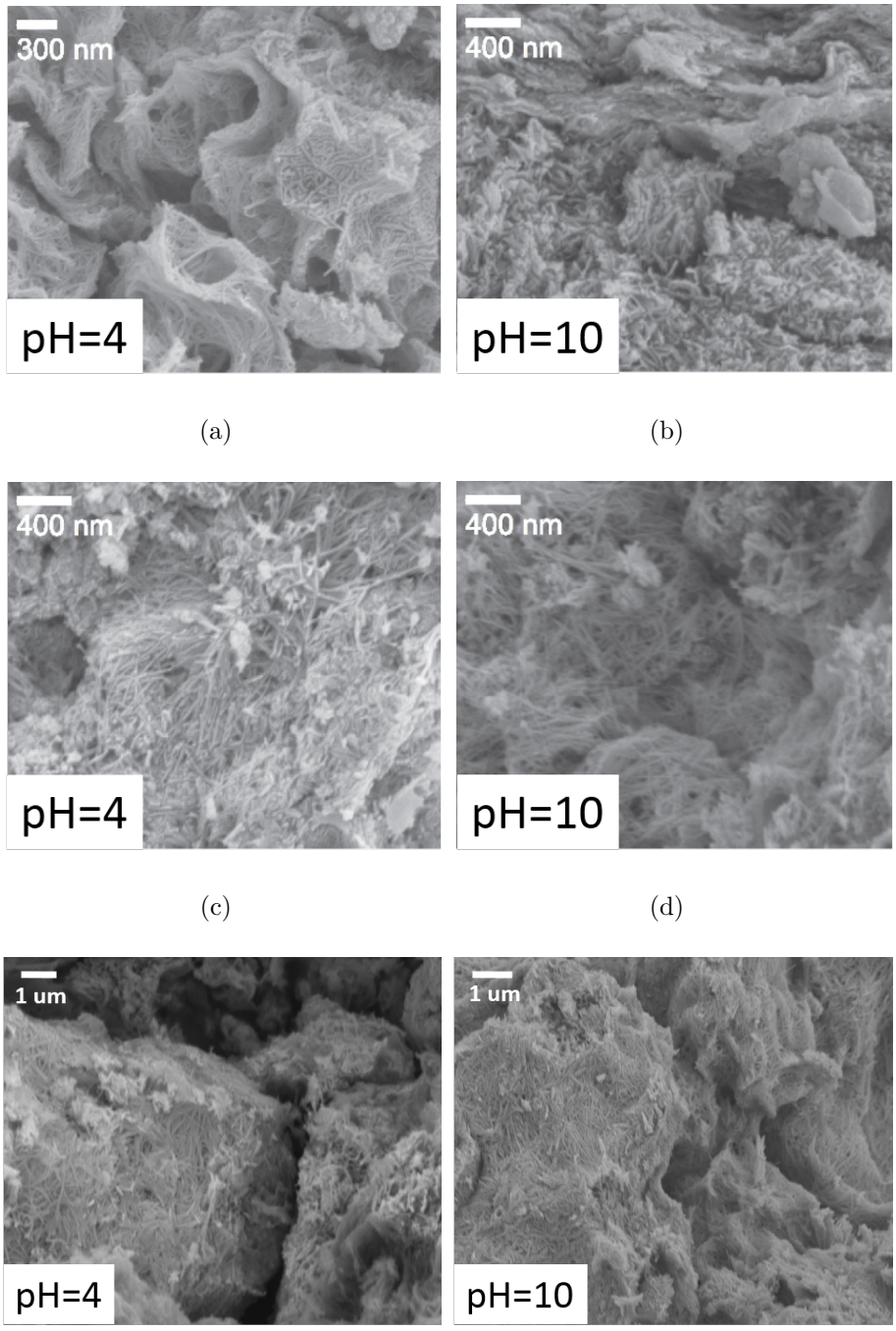

Figure 4.15: Scanning electron microscopy (SEM) images of the TiNTs&GO-based (one-step synthesis): a) TiNTs&GO pH=4, b) TiNTs&GO pH=10, c) TiNTs&NGNP pH=4, d) TiNTs&NGNP pH=10, e) TiNTs&GO-NH_2 pH=4, and f) TiNTs&GO-NH_2 pH=10.

4.6 Electrochemical characterization of TiNTs&GO-based nanocomposites

The cyclic voltammetry (CV) measurement was performed on TiNTs pH=4 at a scan rate of 5 mV/s in a range of 1-3 V vs. Li/Li^+. Figure 4.16 shows two main oxidation-reduction (redox) peaks with the reduction peaks located at 1.7 V, whereas the main oxidation peak is located at 1.55 V. These two peaks infer to the voltage of redox reaction where the lithiation process occurs. Moreover, the redox voltage is used as a reference for the charging and discharging test. The broad peaks obtained for the TiNTs are the results of the easy lithiation and de-lithiation process occurred due to the nanostructure and 1D tubular structure of titanates. The big area circled by the redox lines denotes the high amount of the charge stored by the TiNTs.

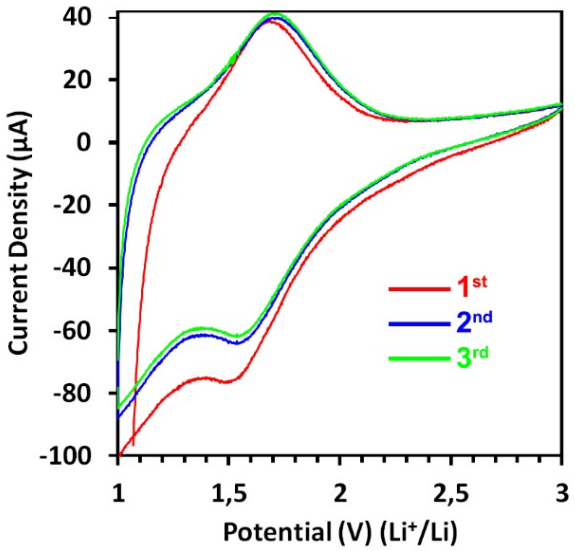

Figure 4.16: Cyclic voltammogram of TiNTs pH=4 at a scan rate of 5mV/s in a range of 1-3V vs. Li/Li^+.

4.7 Charge and discharge cycle results

Anodes were prepared by a slurry mixture of active materials: (TiNTs&GO-based composites) (85%), carbon black (CB) (10%), and binder polyvinylidene uoride (PVDF)

(5%). A split test cell was assembled in the argon-filled glove box with specific control on humidity (H_2O< 0.1 ppm) and oxygen amount (O_2 <0.1 ppm). In the first part of this study, the cyclic voltammagrams were recorded for two samples which were synthesized by the two-step hydrothermal treatment method. The two samples, namely carbon black&TiNTs and TiNTs&rGO, were tested with a voltage range of 0-3.0 V (versus Li/Li^+), respectively. A current rate of 0.1C was chosen for galvanostatically charging and discharging these aforementioned samples. Reversible capacities of these two samples were also investigated by charging and discharging for 8 consecutive cycles. Figure 4.17. shows the charge and discharge curves collected for the TiNTs mixed only with conductive materials of carbon black (CB). A large capacity of 800 mAh/g was achieved for the initial discharging. However, a 400 mAh/g of irreversible capacity loss had been observed from the second discharging test. A capacity loss of 100 mAh/g was also observed for the third time discharing. The large surface area TiNTs are attributes to the large initial irreversible capacity loss. However, the irreversible capacity losses are slowed down in the follow-up cycles. The mitigated capacity loss is due to the tubular structure of the titanate as it provides a larger interlay distance and more directed and much shortened passage for the charge transferring. Figure 4.18 represents the charge and discharge curves recorded for the TiNTs combined with the reduced GO (rGO). The initial discharge capacity is as high as 2206 mAh/g. However, the reversible capacity of the second time discharging drops to 191 mAh/g. This huge irreversible capacity loss is due to the solid electrode interphase (SEI) formation built after initial cycles. SEI formation is typical for the GO-based materials because of their huge surface area available for the reaction. Also we assume that side reactions induced by the oxygen functional groups on the surface of the GO-based materials are contributing to the irreversible capacity loss. From figure 4.18 we can also observe that the reversible capacity for the TiNTs&rGO composite is similar with the TiNTs&carbon black except that a huge initial discharge capacity was obtained for TiNTs&rGO.

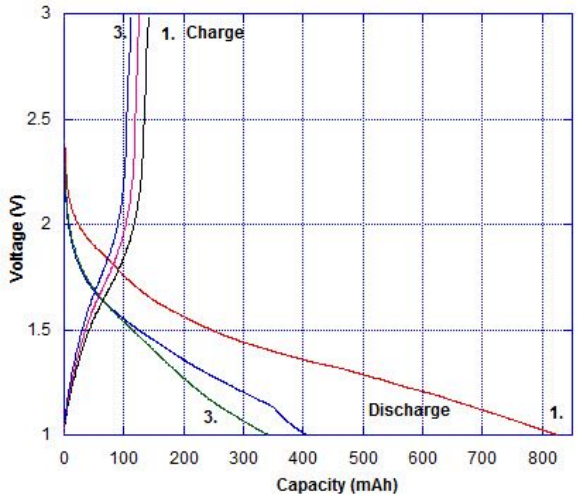

Figure 4.17: Charge and discharge curves of the TiNTs at 0.1C

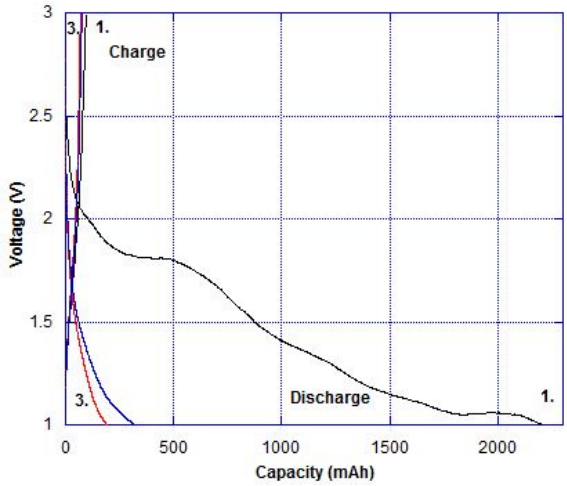

Figure 4.18: Discharge and charge curve of the TiNTs&rGO (pH=4) at 0.1C.

Figure 4.19 shows the cyclic performance of these two aforementioned samples. Cyclic performance can indicate the capacity retention which is of critical interest of knowing whether it can used in practice, also the electronic structure can be analyzed with the help of the information obtained from the cyclic performance. From the comparison of these two samples, we see that the larger amount of irreversible capacity occurred in the TiNTs blend with rGO, whereas the sample of TiNT&carbon black show a comparatively better stability of capacity retention and relatively higher reversible capacity after the second cycle until the 8th cycle of discharging. This may be due

to a tubular structure collapse of titanate in the composites synthesized by two times hydrothermal treatment based on the observation of the SEM image. However, the structure integrity of TiNTs does not occur for the sample of TiNT&carbon black.

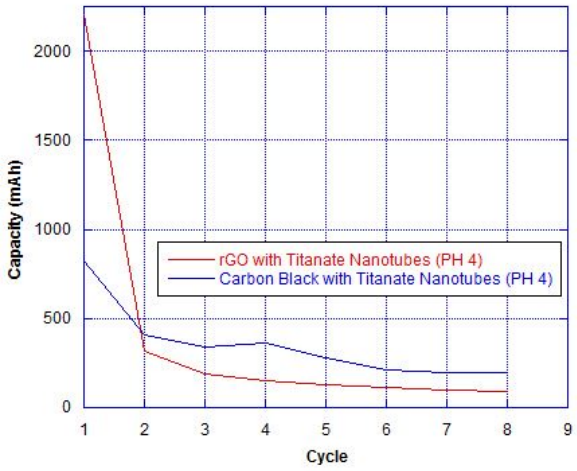

Figure 4.19: Cycle performance of the TiNTs (pH=4) (blue curve) and TiNTs&rGO (pH=4) (red curve).

Figures 4.20-4.26 depict the discharge and charge curves and cycle performance plots collected from the samples synthesized by the one-step hydrothermal treatment method. In figure 4.20, the TiNTs&GO at pH=10 was investigated with respect to its discharge and charge capacity for the first 3 cycles at a current density of 1C. TiNTs&GO pH=10 exhibits a reversible capacity of 150 mAh/g, 368 mAh/g, 144 mAh/g for the first 3 cycles. As can be seen, that discharge processes of TiNTs&GO exhibits a discrepancy on the irreversible capacity loss. This is further confirmed by the cyclic performance presented in figure 4.21. It is observed that the irreversible capacity of initial discharging was recovered in the second discharging. This recovery may contributed by the unreleased ions which was stuck in between the multi-layers of TiNTs in the first discharging process. However, the same ion releasing delay occurred in the follow up discharging process. Based on the both discharging curves and cyclic performance plot, we assumed such systematic delay on the ion delivering may be caused by the high current rate where the diffusing rate cannot follow up the electron transferring.

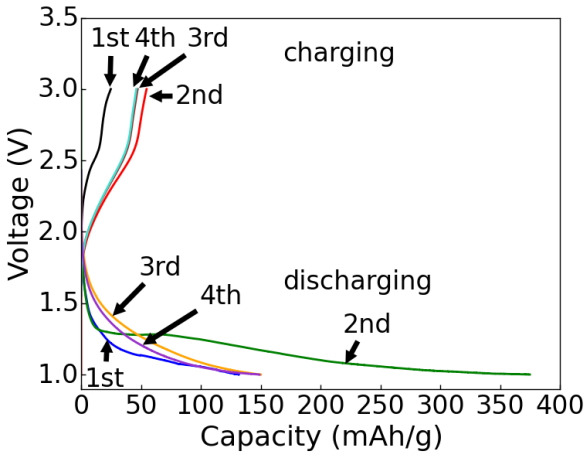

Figure 4.20: Charge and discharge curves of TiNTs&GO at pH=10 at a current density of 1C.

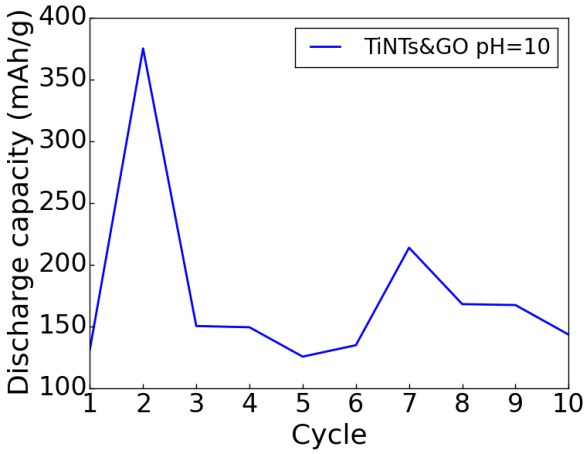

Figure 4.21: Cycle performance of TiNTs&GO pH=10 at a current density of 1C.

Figure 4.22 represents the discharge and charge curves obtained for TiNTs&GO-NH_2 at pH=10 with a current density of 1C, whereas the cycle performance of the corresponding samples is shown in figure 4.23. It can be seen that TiNTs&GO-NH_2 at pH=10 exhibits a low reversible capacity around 55-68 mAh/g for the 3 discharging processes after initial discharging at the current density of 1C. Although it exhibits a stable capacity retention, the reversible capacity is quite low. Meanwhile, the low capacity is due to the conduction problems of materials, a common observation for all the composites studied in this research work. Therefore the only contributor to the

capacity are TiNTs Therefore the voltage of the test was fixed to the range 1-3 V vs. Li/Li^+ where the lithiation reaction of TiNTs occurs. Based on the cyclic performance, we observe that capacity dropped to 20 mAh/g after 40 cycles.

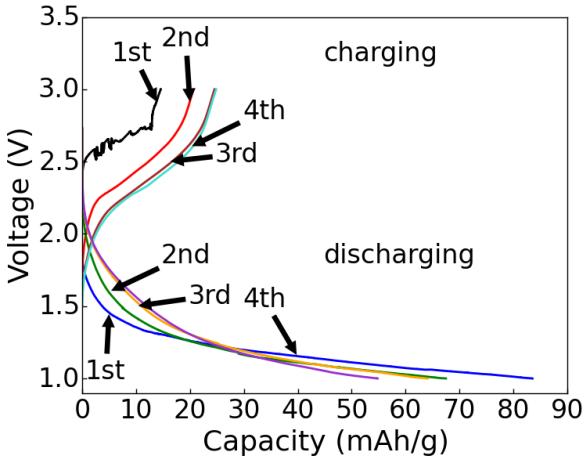

Figure 4.22: Charge and discharge curves of TiNTs&GO-NH_2 pH=10 at a current density of 1C.

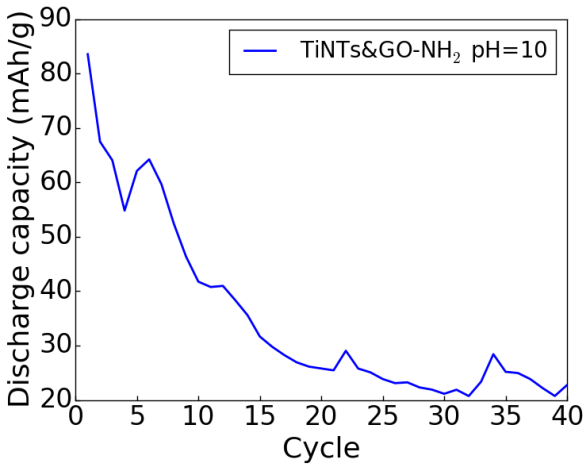

Figure 4.23: Cycle performance of TiNTs&GO-NH_2 pH=10.

Figure 4.24 reveals the discharge and charge curves obtained for TiNTs&NGNP with pH=4 at a current density of 1C while the performance of the corresponding samples was plotted in figure 4.25. According to figure 4.24 we can see the reversible capacity obtained for first 4 cycles are quite high as 355 mAh/g, 243 mAh/g, 201 mAh/g, 181 mAh/g, respectively. For the first 18 cycles, the minimum capacity was as high as

150 mAh/g. Based on the cyclic result in figure 4.25, however, the reversible capacity started to drop drastically and down to 67 after 40 cycles. The cyclic performance shown in figure 4.25 exhibits an unstable capacity retention due to the imbalance occurred between ion diffusion rate and electron transfer rate.

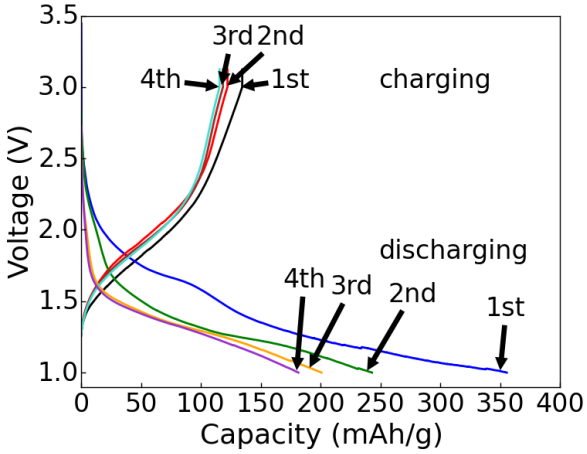

Figure 4.24: Charge and discharge curves of the TiNTs&NGNP pH=4 at current density of 1C.

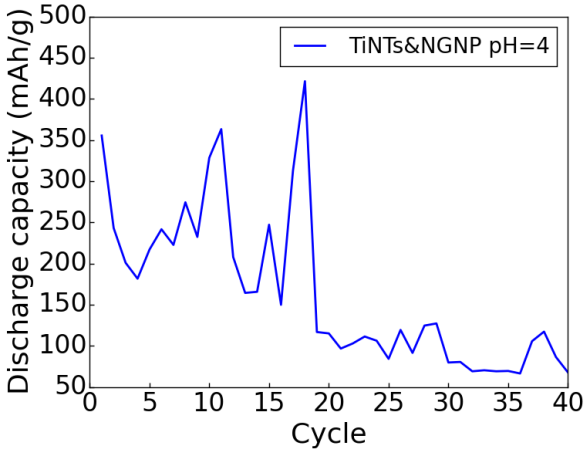

Figure 4.25: Cycle performance of TiNTs&NGNP pH=4.

Figure 4.26 displays the discharge and charge curves obtained for TiNTs&NGNP with pH=4 at a current density of 1C. The reversible capacities for the first 4 cycles are 177mAh/g, 180 mAh/g, 166 mAh/g, 157 mAh/g, respectively. Reversible capacities obtained for these four cycles exhibit only 11.2% capacity fading after the 4th cycle.

Figure 4.27 reveals that the reversible capacity after 40 cycles about 100 mAh/g with a high capacity stability. This result confirms that the integrity of TiNTs are well-conserved and the ion diffusion rates are in good balance with the electron transfer.

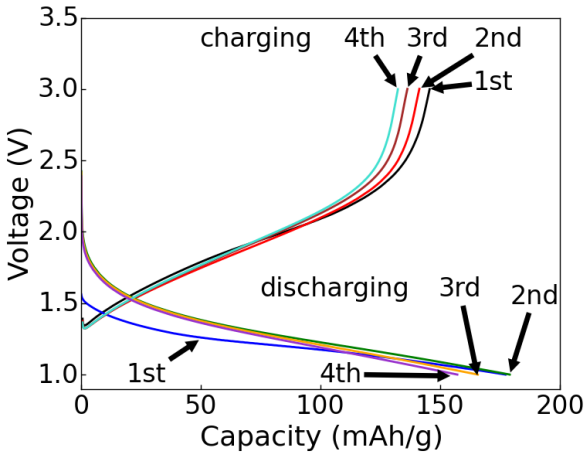

Figure 4.26: Charge and discharge curves of TiNTs&GO-NH_2 with pH=4 at a current density of 1C.

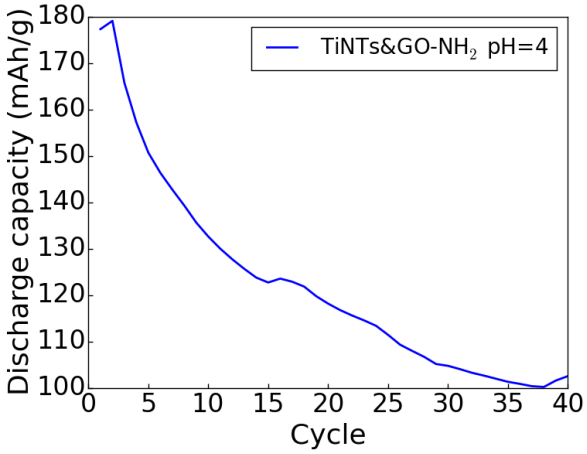

Figure 4.27: Cycle performance of TiNTs&GO-NH_2 pH=4.

Battery testing summary

The battery test results are summarized in table 4.5. They indicate that a conducting problem exists in all the as-prepared samples. Therefore, further work has to be focused on exploring the reason behind it and modify the sample preparation process

accordingly. Besides, it is clear from the table that the highest specific capacity, about 356 mAh/g, was obtained for TiNTs&NGNP, while TiNTs&GO-NH_2 shows a comparatively stable battery performance. The obtained results indicate that the utilization of elongated TiNTs with nitrogen doped graphene composites have a potential for Li-ion batteries but further research is necessary.

Table 4.5: Summary of battery testing results.

Battery samples	First cycle discharge capacity (mAh/g)	Last cycle discharge capacity (mAh/g)
TiNTs&GO (pH=10)	130	85
TiNTs&NGNP (pH=4)	356	68
TiNTs&GO-NH_2 (pH=4)	177	103
TiNTs&GO-NH_2 (pH=10)	84	23

Chapter 5

Conclusions and outlook

This chapter summarizes this thesis by emphasizing our main contributions to the study of lithium-ion batteries and outlining our approach.

5.1 Findings

Due to the wide range of potential applications lithium-ion batteries (LIBs) are among the most preferred energy storage sources in terms of their lower weight, higher energy capacity and performance, their longer life time, lower cost, and greater reliability, when compared to the other types of rechargeable batteries. Due to the problematic dendrite growth present in typical anode materials for conventional LIBs, graphene has been used as a replacement material for graphite oxide. Graphene exhibits high electrical conductivity and a good mechanical property. Also being able to be functionalized with other functional groups makes graphene attractive as a support material for other electrochemically active anode materials. With a capacity theoretically up to 335 mAh/g, TiO_2 has been chosen as a promising anode materials candidate for LIBs, provided that a complete reduction from Ti^{4+} to Ti^{3+} could be exploited. Meanwhile, its environmentally benign nature makes it a hot research topic worldwide. TiO_2 is non-toxic, as well as cost effective. Nevertheless, poor electronic conductivity and low rate capability are the main drawbacks which can be overcome by synergistic effects of material composites. Anatase TiO_2 was processed with hydrothermal treatment to ob-

tain microsize titanate nanotubes (TiNTs). TiNTs are promising materials because of their special morphology and high specific surface area. The nanotubes are formed by rolling-up of titanate nanosheets via hydrothermal treatment method followed by ion exchange process. Then self-organized TiNTs ($H_2T_3O_7$) are dispersed on the surface of various types of graphene based materials, namely graphene oxide (GO), reduced GO (rGO), nitrogen doped reduced GO (NrGO), polypyrrole functionalized GO (PPy-GO), graphene nanoplates (GNP), nitrogen doped graphene nanoplates (NGNP), and amino functionalized GO (GO-NH_2).

Material characterization techniques such as XRD, Raman, BET, SEM were utilized for all the as-prepared samples to examine their chemical compositions, elemental properties and physical morphologies. Electrochemical characterizations such as charge, discharge, and cyclic performance were investigated as well. The material characterization results regarding TiNTs produced by the hydrothermal treatment method at 130°C for 48 h in the autoclave environment, yield well-aligned TiNTs with a few hundred μm in length and 10-20 nm in tube diameter.

The TiNTs&GO-based composites prepared by mixing the TiNTs at pH=4 (prepared from the first step of hydrothermal treatment) with GO-based materials for the second step hydrothermal treatment exhibit a low amount of TiNTs and a poor attachment between each component of composites in the resultant materials. Based on the morphology examination provided by the SEM images, the main reason for such structure failure are pH changes induced by the second time hydrothermal treatment because the newly grown tubular structure of hydrogen titanate is susceptible to high temperature and encountered a serious integrity collapse. The failure of in-situ growth of TiNTs is further confirmed by the battery test. According to the charge and discharge results, the charge and discharge curves recorded for the TiNTs combined with the reduced GO (rGO), the initial discharge capacity is as high as 2206 mAh/g. However, the reversible capacity of the second time discharging drops to 191 mAh/g. This huge irreversible capacity loss is due to the solid electrode interphase (SEI) formation built after initial cycles. SEI formation and side reactions of the oxygen functional groups on the surface of the GO-based materials are contributing for the irreversible

capacity loss.

With respect to the samples prepared via one-step hydrothermal treatment, the material characterization reveals well-aligned TiNTs dispersed homogeneously on the surface of the GO-based materials. BET results confirmed the mesoporous nature of the composites with the tube diameter falling between 10-40 nm and with the dominant peak dropping to 12 nm. The SEM shows well-grown TiNTs with a wide distribution and thick covering on the surface of the GO-based materials. Motivated by the expected morphology, the corresponding battery tests were performed with the 4 most promising samples at a current density of 1C. Moreover, a poor conductivity of TiNTs and GO-based materials was observed for all the composites studied in this research work. Therefore, we set the voltage from 1-3 V vs. Li/Li^+, where the lithiation reaction of TiNTs occurs. The charging and discharging results exhibit a reversible capacity of 150 mAh/g, 368 mAh/g, 144 mAh/g, 140 mAh/g for the first 4 cycles of TiNTs&GO pH=10. Meanwhile, a systematic delay on the ion delivering was also observed for the samples caused by the high current rate where the diffusing rate cannot follow up the electron transfer. TiNTs&GO-N_2 at pH=10 exhibits a low reversible capacity around 55-68 mAh/g for the 3 cycles of discharging processes after initial discharging at the current density of 1C. Although it shows good stability with regard to the capacity retention, the reversible capacity is still low. Concerning to the cyclic performance, we observed that capacity dropped to 20 mAh/g after 40 cycles for the TiNTs&GO-NH_2 at pH=10. A minimum capacity of 150 mAh/g was obtained for TiNTs&NGNP at pH=4. However, it exhibits an unstable capacity retention due to the imbalance occurring between the ion diffusion rate and the electron transfer rate. For TiNTs&GO-NH_2 pH=4, reversible capacities obtained for its first four cycles exhibit a high capacity retention with only 11.2% capacity fading. It also showed for the same sample a reversible capacity of about 100 mAh/g with a high capacity stability after 40 cycles. This result confirms that the integrity of TiNTs is well-conserved and that the ion diffusion rate is in good balance with the electron transfer.

5.2 Conclusions

We introduced a novel one-step hydrothermal treatment method to produce elongated TiNTs&graphene-based composite materials. Elongated TiNTs grew in-situ on the surface of graphene-based materials. We are the first to introduce TiNTs&graphene-based composite materials as an anode for LIBs. Moreover, the utilization of elongated TiNTs with a nitrogen doped graphene composite has a potential for Li-ion batteries and we will continue that study in our future work.

5.3 Challenges & outlook

The main problem we faced in this study was obtaining a good contact between each component of the composite materials. This confined the potential capacity of those promising composites to a lower value than expected. Yet the battery test results still remain very promising based on the results obtained from TiNTs&GO-NH_2 at pH=4. Therefore, a further research effort should be put on modifying the synthesis process regarding the slurry preparation and the mixing ratio of the slurry components.

Based on the results obtained from the battery tests, we speculate that a poor electrical contact could form between components in the slurry on a microscopic scale. This, in turn, leads to further problems. For example, a poor electrical contact gives rise to lower conductivity of charge carriers. Thereby, local heat could be generated by the accumulated ions. In the end, this could cause unstable experimental results. Hence, it is necessary to conduct a more systematic study to address this speculation.

Acid washing is still a challenging procedure because it requires optimization of a multitude of parameters. But it must be addressed to obtain a pure hydrogen type of titanate which would enhance the battery capacity and prolong the battery life-time.

Bibliography

[1] A. S. Gozdz, C. N. Schmutz, J.-M. Tarascon, and P. C. Warren, "Rechargeable lithium battery construction," Dec. 26 1995. US Patent 5,478,668.

[2] M. Yoshio, R. J. Brodd, and A. Kozawa, *Lithium-Ion Batteries*, vol. 1. Springer, 2009.

[3] J. McDowall, "Conventional battery technologies-present and future," in *Power Engineering Society Summer Meeting, 2000. IEEE*, vol. 3, pp. 1538–1540, IEEE, 2000.

[4] D. Linden, "Handbook of batteries and fuel cells," *New York, McGraw-Hill Book Co., 1984, 1075 p. No individual items are abstracted in this volume.*, vol. 1, 1984.

[5] B. J. Landi, M. J. Ganter, C. D. Cress, R. A. DiLeo, and R. P. Raffaelle, "Carbon nanotubes for lithium ion batteries," *Energy & Environmental Science*, vol. 2, no. 6, pp. 638–654, 2009.

[6] F. Cheng-Hua, R. Xu, and C.-L. Han, "Lithium ion battery," Nov. 3 2011. US Patent App. 12/768,732.

[7] Y. Zhao, X. Li, B. Yan, D. Xiong, D. Li, S. Lawes, and X. Sun, "Recent developments and understanding of novel mixed transition-metal oxides as anodes in lithium ion batteries," *Advanced Energy Materials*, 2016.

[8] W. G. Howard, C. L. Schmidt, and E. R. Scott, "Lithium-ion battery," Oct. 5 2010. US Patent 7,807,299.

[9] Y. Shao-Horn, L. Croguennec, C. Delmas, E. C. Nelson, and M. A. O'Keefe, "Atomic resolution of lithium ions in licoo2," *Nature materials*, vol. 2, no. 7, pp. 464–467, 2003.

[10] C. M. Julien, A. Mauger, K. Zaghib, and H. Groult, "Comparative issues of cathode materials for li-ion batteries," *Inorganics*, vol. 2, no. 1, pp. 132–154, 2014.

[11] S. T. Mayer, "Mixed lithium manganese oxide and lithium nickel cobalt oxide positive electrodes," Dec. 28 1999. US Patent 6,007,947.

[12] C. Chen, J. Liu, M. Stoll, G. Henriksen, D. Vissers, and K. Amine, "Aluminum-doped lithium nickel cobalt oxide electrodes for high-power lithium-ion batteries," *Journal of power Sources*, vol. 128, no. 2, pp. 278–285, 2004.

[13] M. M. Doeff, *Battery Cathodes*, pp. 5–49. New York, NY: Springer New York, 2013.

[14] R. Pitchai, V. Thavasi, S. G. Mhaisalkar, and S. Ramakrishna, "Nanostructured cathode materials: a key for better performance in li-ion batteries," *Journal of Materials Chemistry*, vol. 21, no. 30, pp. 11040–11051, 2011.

[15] M. Tang, W. C. Carter, and Y.-M. Chiang, "Electrochemically driven phase transitions in insertion electrodes for lithium-ion batteries: examples in lithium metal phosphate olivines," *Annual Review of Materials Research*, vol. 40, pp. 501–529, 2010.

[16] T. Ohzuku and R. J. Brodd, "An overview of positive-electrode materials for advanced lithium-ion batteries," *Journal of Power Sources*, vol. 174, no. 2, pp. 449–456, 2007.

[17] S. Yang, H. Song, and X. Chen, "Electrochemical performance of expanded mesocarbon microbeads as anode material for lithium-ion batteries," *Electrochemistry communications*, vol. 8, no. 1, pp. 137–142, 2006.

[18] M. S. Islam and C. A. Fisher, "Lithium and sodium battery cathode materials: computational insights into voltage, diffusion and nanostructural properties," *Chemical Society Reviews*, vol. 43, no. 1, pp. 185–204, 2014.

[19] Y. Xing, W. He, M. Pecht, and K. L. Tsui, "State of charge estimation of lithium-ion batteries using the open-circuit voltage at various ambient temperatures," *Applied Energy*, vol. 113, pp. 106–115, 2014.

[20] J. K. Lee, D. Ryu, J. B. Ju, Y. Shul, B. Cho, and D. Park, "Electrochemical characteristics of graphite coated with tin-oxide and copper by fluidised-bed chemical vapour deposition," *Journal of power sources*, vol. 107, no. 1, pp. 90–97, 2002.

[21] P. B. Balbuena and Y. Wang, "Lithium-ion batteries," *Solid–Electrolyte Interphase*, 2004.

[22] M. Reddy, G. Subba Rao, and B. Chowdari, "Metal oxides and oxysalts as anode materials for li ion batteries," *Chemical reviews*, vol. 113, no. 7, pp. 5364–5457, 2013.

[23] K. Xu, S. Zhang, T. R. Jow, W. Xu, and C. A. Angell, "Libob as salt for lithium-ion batteries: a possible solution for high temperature operation," *Electrochemical and Solid-State Letters*, vol. 5, no. 1, pp. A26–A29, 2002.

[24] M. Wakihara, "Recent developments in lithium ion batteries," *Materials Science and Engineering: R: Reports*, vol. 33, no. 4, pp. 109–134, 2001.

[25] M. B. Pinson and M. Z. Bazant, "Theory of sei formation in rechargeable batteries: capacity fade, accelerated aging and lifetime prediction," *Journal of the Electrochemical Society*, vol. 160, no. 2, pp. A243–A250, 2013.

[26] C. Wei, W. He, X. Zhang, J. Shen, and J. Ma, "Recent progress in hybrid cathode materials for lithium ion batteries," *New Journal of Chemistry*, vol. 40, no. 4, pp. 2984–2999, 2016.

[27] A. Yoshino, "Development of the lithium-ion battery and recent technological trends," *Lithium-ion batteries(Elsevier, 2014)*, pp. 1–20, 2014.

[28] E. M. Sorensen, S. J. Barry, H.-K. Jung, J. M. Rondinelli, J. T. Vaughey, and K. R. Poeppelmeier, "Three-dimensionally ordered macroporous li4ti5o12: effect of wall structure on electrochemical properties," *Chemistry of Materials*, vol. 18, no. 2, pp. 482–489, 2006.

[29] K. Hoang and M. Johannes, "Defect physics and chemistry in layered mixed transition metal oxide cathode materials:(ni, co, mn) vs (ni, co, al)," *Chemistry of Materials*, vol. 28, no. 5, pp. 1325–1334, 2016.

[30] H. Liu, "Electrochemical performance of li (nmc) o2 cathode materials for li-ion batteries," 2010.

[31] P. Poizot, S. Laruelle, S. Grugeon, L. Dupont, and J. Tarascon, "Nano-sized transition-metal oxides as negative-electrode materials for lithium-ion batteries," *Nature*, vol. 407, no. 6803, pp. 496–499, 2000.

[32] A. R. Kamali and D. J. Fray, "Tin-based materials as advanced anode materials for lithium ion batteries: a review," *Rev. Adv. Mater. Sci*, vol. 27, no. 1, pp. 14–24, 2011.

[33] C. K. Chan, H. Peng, G. Liu, K. McIlwrath, X. F. Zhang, R. A. Huggins, and Y. Cui, "High-performance lithium battery anodes using silicon nanowires," *Nature nanotechnology*, vol. 3, no. 1, pp. 31–35, 2008.

[34] L. Yang, Q. Gao, L. Li, Y. Tang, and Y. Wu, "Mesoporous germanium as anode material of high capacity and good cycling prepared by a mechanochemical reaction," *Electrochemistry Communications*, vol. 12, no. 3, pp. 418–421, 2010.

[35] R. Yi, F. Dai, M. L. Gordin, S. Chen, and D. Wang, "Micro-sized si-c composite with interconnected nanoscale building blocks as high-performance anodes for practical application in lithium-ion batteries," *Advanced Energy Materials*, vol. 3, no. 3, pp. 295–300, 2013.

[36] D.-J. Xue, S. Xin, Y. Yan, K.-C. Jiang, Y.-X. Yin, Y.-G. Guo, and L.-J. Wan, "Improving the electrode performance of ge through ge@ c core–shell nanoparti-

cles and graphene networks," *Journal of the American Chemical Society*, vol. 134, no. 5, pp. 2512–2515, 2012.

[37] X.-L. Wang, W.-Q. Han, J. Chen, and J. Graetz, "Single-crystal intermetallic m-sn (m= fe, cu, co, ni) nanospheres as negative electrodes for lithium-ion batteries," *ACS applied materials & interfaces*, vol. 2, no. 5, pp. 1548–1551, 2010.

[38] S. Deng, L. Wang, T. Hou, and Y. Li, "Two-dimensional mno2 as a better cathode material for lithium ion batteries," *The Journal of Physical Chemistry C*, vol. 119, no. 52, pp. 28783–28788, 2015.

[39] A. Pan, J.-G. Zhang, Z. Nie, G. Cao, B. W. Arey, G. Li, S.-q. Liang, and J. Liu, "Facile synthesized nanorod structured vanadium pentoxide for high-rate lithium batteries," *Journal of Materials Chemistry*, vol. 20, no. 41, pp. 9193–9199, 2010.

[40] Y.-G. Guo, J.-S. Hu, and L.-J. Wan, "Nanostructured materials for electrochemical energy conversion and storage devices," *Advanced Materials*, vol. 20, no. 15, pp. 2878–2887, 2008.

[41] Z. Liang, P. Hui-Lin, H. Yong-Sheng, L. Hong, and C. Li-Quan, "Spinel lithium titanate (li4ti5o12) as novel anode material for room-temperature sodium-ion battery," *Chinese Physics B*, vol. 21, no. 2, p. 028201, 2012.

[42] J. Xu, S. Dou, H. Liu, and L. Dai, "Cathode materials for next generation lithium ion batteries," *Nano Energy*, vol. 2, no. 4, pp. 439–442, 2013.

[43] Y. Liu and Y. Yang, "Recent progress of tio 2-based anodes for li ion batteries," *Journal of Nanomaterials*, vol. 2016, p. 2, 2016.

[44] J. Banfield *et al.*, "Thermodynamic analysis of phase stability of nanocrystalline titania," *Journal of Materials Chemistry*, vol. 8, no. 9, pp. 2073–2076, 1998.

[45] P. Roy and S. K. Srivastava, "Nanostructured anode materials for lithium ion batteries," *Journal of Materials Chemistry A*, vol. 3, no. 6, pp. 2454–2484, 2015.

[46] S. Goriparti, E. Miele, F. De Angelis, E. Di Fabrizio, R. P. Zaccaria, and C. Capiglia, "Review on recent progress of nanostructured anode materials for li-ion batteries," *Journal of Power Sources*, vol. 257, pp. 421–443, 2014.

[47] Z. Liu, Y. G. Andreev, A. R. Armstrong, S. Brutti, Y. Ren, and P. G. Bruce, "Nanostructured tio 2 (b): the effect of size and shape on anode properties for li-ion batteries," *Progress in Natural Science: Materials International*, vol. 23, no. 3, pp. 235–244, 2013.

[48] M.-S. Wu, M.-J. Wang, J.-J. Jow, W.-D. Yang, C.-Y. Hsieh, and H.-M. Tsai, "Electrochemical fabrication of anatase tio 2 nanostructure as an anode material for aqueous lithium-ion batteries," *Journal of Power Sources*, vol. 185, no. 2, pp. 1420–1424, 2008.

[49] C. De las Casas and W. Li, "A review of application of carbon nanotubes for lithium ion battery anode material," *Journal of Power Sources*, vol. 208, pp. 74–85, 2012.

[50] X. Chen and A. Selloni, "Introduction: titanium dioxide (tio2) nanomaterials," *Chemical reviews*, vol. 114, no. 19, pp. 9281–9282, 2014.

[51] H. Wang, D. Ma, X. Huang, Y. Huang, and X. Zhang, "General and controllable synthesis strategy of metal oxide/tio2 hierarchical heterostructures with improved lithium-ion battery performance," *Scientific reports*, vol. 2, 2012.

[52] D. Datta, J. Li, N. Koratkar, and V. B. Shenoy, "Enhanced lithiation in defective graphene," *Carbon*, vol. 80, pp. 305–310, 2014.

[53] Z. Yang, G. Du, Q. Meng, Z. Guo, X. Yu, Z. Chen, T. Guo, and R. Zeng, "Synthesis of uniform tio 2@ carbon composite nanofibers as anode for lithium ion batteries with enhanced electrochemical performance," *Journal of Materials Chemistry*, vol. 22, no. 12, pp. 5848–5854, 2012.

[54] T. Shen, X. Zhou, H. Cao, C. Zheng, and Z. Liu, "Tio 2 (b)–cnt–graphene ternary composite anode material for lithium ion batteries," *Rsc Advances*, vol. 5, no. 29, pp. 22449–22454, 2015.

[55] X. Zhang, J. Zhang, Y. Liu, X. Wang, and B. Li, "Improving the anode performances of tio 2–carbon–rgo composites in lithium ion batteries by uv irradiation," *New Journal of Chemistry*, vol. 39, no. 12, pp. 9345–9350, 2015.

[56] X. Li, X. Meng, J. Liu, D. Geng, Y. Zhang, M. N. Banis, Y. Li, J. Yang, R. Li, X. Sun, *et al.*, "Tin oxide with controlled morphology and crystallinity by atomic layer deposition onto graphene nanosheets for enhanced lithium storage," *Advanced Functional Materials*, vol. 22, no. 8, pp. 1647–1654, 2012.

[57] T. Gao, H. Fjellvåg, and P. Norby, "Crystal structures of titanate nanotubes: a raman scattering study," *Inorganic chemistry*, vol. 48, no. 4, pp. 1423–1432, 2009.

[58] J. Selvaraj, S. Gupta, S. DelaCruz, and V. R. Subramanian, "Role of reduced graphene oxide in the critical components of a cds-sensitized tio2-based photoelectrochemical cell," *ChemPhysChem*, vol. 15, no. 10, pp. 2010–2018, 2014.

[59] Z. Xing, Z. Ju, Y. Zhao, J. Wan, Y. Zhu, Y. Qiang, and Y. Qian, "One-pot hydrothermal synthesis of nitrogen-doped graphene as high-performance anode materials for lithium ion batteries," *Scientific reports*, vol. 6, 2016.

[60] C. Zhao, K. Shu, C. Wang, S. Gambhir, and G. G. Wallace, "Reduced graphene oxide and polypyrrole/reduced graphene oxide composite coated stretchable fabric electrodes for supercapacitor application," *Electrochimica Acta*, vol. 172, pp. 12–19, 2015.

[61] J. N. Tiwari, R. N. Tiwari, and K. S. Kim, "Zero-dimensional, one-dimensional, two-dimensional and three-dimensional nanostructured materials for advanced electrochemical energy devices," *Progress in Materials Science*, vol. 57, no. 4, pp. 724–803, 2012.

[62] D. V. Bavykin, J. M. Friedrich, and F. C. Walsh, "Protonated titanates and tio2 nanostructured materials: synthesis, properties, and applications," *Advanced Materials*, vol. 18, no. 21, pp. 2807–2824, 2006.

[63] M. Yarali, "Novel expanded titanate based materials for energy applications," Master's thesis, Sabanci University, 2015.

[64] S. H. Lim, J. Luo, Z. Zhong, W. Ji, and J. Lin, "Room-temperature hydrogen uptake by tio2 nanotubes," *Inorganic Chemistry*, vol. 44, no. 12, pp. 4124–4126, 2005.

[65] T. Kasuga, M. Hiramatsu, A. Hoson, T. Sekino, and K. Niihara, "Formation of titanium oxide nanotube," *Langmuir*, vol. 14, no. 12, pp. 3160–3163, 1998.

[66] M. Yada and Y. Inoue, *Synthesis of Titanate and Titanium Dioxide Nanotube Thin Films and Their Applications to Biomaterials*. INTECH Open Access Publisher, 2012.

[67] H.-K. Seo, G.-S. Kim, S. Ansari, Y.-S. Kim, H.-S. Shin, K.-H. Shim, and E.-K. Suh, "A study on the structure/phase transformation of titanate nanotubes synthesized at various hydrothermal temperatures," *Solar Energy Materials and Solar Cells*, vol. 92, no. 11, pp. 1533–1539, 2008.

[68] D. V. Bavykin, V. N. Parmon, A. A. Lapkin, and F. C. Walsh, "The effect of hydrothermal conditions on the mesoporous structure of tio 2 nanotubes," *Journal of Materials Chemistry*, vol. 14, no. 22, pp. 3370–3377, 2004.

[69] X. Sun and Y. Li, "Synthesis and characterization of ion-exchangeable titanate nanotubes," *Chemistry–A European Journal*, vol. 9, no. 10, pp. 2229–2238, 2003.

[70] E. M. Neville, J. D. MacElroy, K. R. Thampi, and J. A. Sullivan, "Visible light active c-doped titanate nanotubes prepared via alkaline hydrothermal treatment of c-doped nanoparticulate tio 2: Photo-electrochemical and photocatalytic properties," *Journal of Photochemistry and Photobiology A: Chemistry*, vol. 267, pp. 17–24, 2013.

[71] Y. Chen, L. Wang, G. M. Lu, X. Yao, and L. Guo, "Nanoparticles enwrapped with nanotubes: a unique architecture of cds/titanate nanotubes for efficient photocatalytic hydrogen production from water," *Journal of Materials Chemistry*, vol. 21, no. 13, pp. 5134–5141, 2011.

[72] C. Huang, X. Liu, L. Kong, W. Lan, Q. Su, and Y. Wang, "The structural and magnetic properties of co-doped titanate nanotubes synthesized under hydrothermal conditions," *Applied Physics A*, vol. 87, no. 4, pp. 781–786, 2007.

[73] A. S. Arico, P. Bruce, B. Scrosati, J.-M. Tarascon, and W. Van Schalkwijk, "Nanostructured materials for advanced energy conversion and storage devices," *Nature materials*, vol. 4, no. 5, pp. 366–377, 2005.

[74] D. Fang, K. Huang, S. Liu, and J. Huang, "Fabrication and photoluminiscent properties of titanium oxide nanotube arrays," *Journal of the Brazilian Chemical Society*, vol. 19, no. 6, pp. 1059–1064, 2008.

[75] H. Zhang, G. Li, L. An, T. Yan, X. Gao, and H. Zhu, "Electrochemical lithium storage of titanate and titania nanotubes and nanorods," *The Journal of Physical Chemistry C*, vol. 111, no. 16, pp. 6143–6148, 2007.

[76] J. Li, Z. Tang, and Z. Zhang, "H-titanate nanotube: a novel lithium intercalation host with large capacity and high rate capability," *Electrochemistry Communications*, vol. 7, no. 1, pp. 62–67, 2005.

[77] Y. Zhu, S. Murali, W. Cai, X. Li, J. W. Suk, J. R. Potts, and R. S. Ruoff, "Graphene and graphene oxide: synthesis, properties, and applications," *Advanced materials*, vol. 22, no. 35, pp. 3906–3924, 2010.

[78] J. Zhang, H. Cao, X. Tang, W. Fan, G. Peng, and M. Qu, "Graphite/graphene oxide composite as high capacity and binder-free anode material for lithium ion batteries," *Journal of Power Sources*, vol. 241, pp. 619–626, 2013.

[79] H. Zhang, S. Jing, Y. Hu, H. Jiang, and C. Li, "A flexible freestanding si/rgo hybrid film anode for stable li-ion batteries," *Journal of Power Sources*, vol. 307, pp. 214–219, 2016.

[80] Z.-J. Lu, M.-W. Xu, S.-J. Bao, K. Tan, H. Chai, C.-J. Cai, C.-C. Ji, and Q. Zhang, "Facile preparation of nitrogen-doped reduced graphene oxide as a metal-free catalyst for oxygen reduction reaction," *Journal of Materials Science*, vol. 48, no. 23, pp. 8101–8107, 2013.

[81] C. Fu, C. Song, L. Liu, X. Xie, and W. Zhao, "Synthesis and properties of nitrogen-doped graphene as anode materials for lithium-ion batteries," *INTERNATIONAL JOURNAL OF ELECTROCHEMICAL SCIENCE*, vol. 11, no. 5, pp. 3876–3886, 2016.

[82] N. G. Sahoo, Y. C. Jung, H. H. So, and J. W. Cho, "Polypyrrole coated carbon nanotubes: synthesis, characterization, and enhanced electrical properties," *Synthetic Metals*, vol. 157, no. 8, pp. 374–379, 2007.

[83] X. Feng, Z. Yan, R. Li, X. Liu, and W. Hou, "The synthesis of shape-controlled polypyrrole/graphene and the study of its capacitance properties," *Polymer bulletin*, vol. 70, no. 8, pp. 2291–2304, 2013.

[84] X. Yang and L. Li, "Polypyrrole nanofibers synthesized via reactive template approach and their nh 3 gas sensitivity," *Synthetic Metals*, vol. 160, no. 11, pp. 1365–1367, 2010.

[85] S. Li, K. Shu, C. Zhao, C. Wang, Z. Guo, G. Wallace, and H. K. Liu, "One-step synthesis of graphene/polypyrrole nanofiber composites as cathode material for a biocompatible zinc/polymer battery," *ACS applied materials & interfaces*, vol. 6, no. 19, pp. 16679–16686, 2014.

[86] A. Navaee and A. Salimi, "Efficient amine functionalization of graphene oxide through the bucherer reaction: an extraordinary metal-free electrocatalyst for

the oxygen reduction reaction," *RSC Advances*, vol. 5, no. 74, pp. 59874–59880, 2015.

[87] S.-C. Wang, J. Yang, X.-Y. Zhou, and J. Xie, "The contribution of functional groups in carbon nanotube electrodes to the electrochemical performance," *Electronic Materials Letters*, vol. 10, no. 1, pp. 241–245, 2014.

[88] S. Stankovich, D. A. Dikin, R. D. Piner, K. A. Kohlhaas, A. Kleinhammes, Y. Jia, Y. Wu, S. T. Nguyen, and R. S. Ruoff, "Synthesis of graphene-based nanosheets via chemical reduction of exfoliated graphite oxide," *carbon*, vol. 45, no. 7, pp. 1558–1565, 2007.

[89] Q. Wan, H. Cai, Y. Liu, H. Song, H. Liao, S. Liu, and N. Yang, "Graphene nanoplatelets: Electrochemical properties and applications for oxidation of endocrine-disrupting chemicals," *Chemistry–A European Journal*, vol. 19, no. 10, pp. 3483–3489, 2013.

[90] S. Wang, L. Zhang, Z. Xia, A. Roy, D. W. Chang, J.-B. Baek, and L. Dai, "Bcn graphene as efficient metal-free electrocatalyst for the oxygen reduction reaction," *Angewandte Chemie International Edition*, vol. 51, no. 17, pp. 4209–4212, 2012.

[91] D.-Y. Yeom, W. Jeon, N. D. K. Tu, S. Y. Yeo, S.-S. Lee, B. J. Sung, H. Chang, J. A. Lim, and H. Kim, "High-concentration boron doping of graphene nanoplatelets by simple thermal annealing and their supercapacitive properties," *Scientific reports*, vol. 5, 2015.

[92] W. S. Hummers Jr and R. E. Offeman, "Preparation of graphitic oxide," *Journal of the American Chemical Society*, vol. 80, no. 6, pp. 1339–1339, 1958.

[93] T. Kuila, S. Bose, A. K. Mishra, P. Khanra, N. H. Kim, and J. H. Lee, "Chemical functionalization of graphene and its applications," *Progress in Materials Science*, vol. 57, no. 7, pp. 1061–1105, 2012.

[94] L. Shahriary and A. A. Athawale, "Graphene oxide synthesized by using modified hummers approach," *Int J Renew Energy Environ Eng*, vol. 2, pp. 58–63, 2014.

[95] S. H. Huh, *Thermal reduction of graphene oxide*. INTECH Open Access Publisher, 2011.

[96] S. Pei and H.-M. Cheng, "The reduction of graphene oxide," *Carbon*, vol. 50, no. 9, pp. 3210–3228, 2012.

[97] X. Li, H. Wang, J. T. Robinson, H. Sanchez, G. Diankov, and H. Dai, "Simultaneous nitrogen doping and reduction of graphene oxide," *Journal of the American Chemical Society*, vol. 131, no. 43, pp. 15939–15944, 2009.

[98] S. N. Alam, L. Kumar, and N. Sharma, "Development of cu-exfoliated graphite nanoplatelets (xgnp) metal matrix composite by powder metallurgy route," *Graphene*, vol. 4, no. 4, pp. 91–111, 2015.

[99] D. R. Dreyer, S. Park, C. W. Bielawski, and R. S. Ruoff, "The chemistry of graphene oxide," *Chemical Society Reviews*, vol. 39, no. 1, pp. 228–240, 2010.

[100] M. Danilov, I. Slobodyanyuk, I. Rusetskii, G. Dovbeshko, and G. Y. Kolbasov, "Influence of the synthesis conditions of reduced graphene oxide on the electrochemical characteristics of the oxygen electrode," *Nanoscience and Nanotechnology Research*, vol. 2, no. 1, pp. 12–17, 2014.

[101] H.-C. Tao, X.-L. Yang, L.-L. Zhang, and S.-B. Ni, "Reduced graphene oxide/porous si composite as anode for high-performance lithium ion batteries," *Ionics*, vol. 21, no. 3, pp. 617–622, 2015.

[102] L. Li, A. Kovalchuk, and J. M. Tour, "Sno2-reduced graphene oxide nanoribbons as anodes for lithium ion batteries with enhanced cycling stability," *Nano Research*, vol. 7, no. 9, pp. 1319–1326, 2014.

[103] Z. Lin, G. Waller, Y. Liu, M. Liu, and C.-P. Wong, "Facile synthesis of nitrogen-doped graphene via pyrolysis of graphene oxide and urea, and its electrocatalytic activity toward the oxygen-reduction reaction," *Advanced Energy Materials*, vol. 2, no. 7, pp. 884–888, 2012.

[104] M. Du, J. Sun, J. Chang, F. Yang, L. Shi, and L. Gao, "Synthesis of nitrogen-doped reduced graphene oxide directly from nitrogen-doped graphene oxide as a high-performance lithium ion battery anode," *RSC Advances*, vol. 4, no. 80, pp. 42412–42417, 2014.

[105] D. Li, D. Shi, Z. Liu, H. Liu, and Z. Guo, "Tio2 nanoparticles on nitrogen-doped graphene as anode material for lithium ion batteries," *Journal of nanoparticle research*, vol. 15, no. 5, pp. 1–10, 2013.

[106] R. Liu, Y. Liu, Q. Kang, A. Casimir, H. Zhang, N. Li, Z. Huang, Y. Li, X. Lin, X. Feng, *et al.*, "Synergistic effect of graphene and polypyrrole to enhance the sno 2 anode performance in lithium-ion batteries," *RSC Advances*, vol. 6, no. 12, pp. 9402–9410, 2016.

[107] Y. Yang, C. Wang, B. Yue, S. Gambhir, C. O. Too, and G. G. Wallace, "Electrochemically synthesized polypyrrole/graphene composite film for lithium batteries," *Advanced Energy Materials*, vol. 2, no. 2, pp. 266–272, 2012.

[108] S. S. Yoon, W. Lee, J. H. Byun, and J. U. Lee, "Preparation of graphene/gold nano-hybrid using diamine linker as effective surface-enhanced raman scattering platforms," *Journal of nanoscience and nanotechnology*, vol. 15, no. 11, pp. 8996–9001, 2015.

[109] C. Sun, Y. Deng, L. Wan, X. Qin, and G. Chen, "Graphene oxide-immobilized nh2-terminated silicon nanoparticles by cross-linked interactions for highly stable silicon negative electrodes," *ACS applied materials & interfaces*, vol. 6, no. 14, pp. 11277–11285, 2014.

[110] Q. Yang, Y. Tang, H. Zhang, C. Liu, and S. Luo, "Fabrication of reduced graphene oxide film by photocatalytic deposition," *Nanoscience and Nanotechnology Letters*, vol. 6, no. 1, pp. 57–61, 2014.

[111] M. Agostini, L. G. Rizzi, G. Cesareo, V. Russo, and J. Hassoun, "Characteristics of a graphene nanoplatelet anode in advanced lithium-ion batteries using ionic

liquid added by a carbonate electrolyte," *Advanced Materials Interfaces*, vol. 2, no. 8, 2015.

[112] D. W. Chang, E. K. Lee, E. Y. Park, H. Yu, H.-J. Choi, I.-Y. Jeon, G.-J. Sohn, D. Shin, N. Park, J. H. Oh, *et al.*, "Nitrogen-doped graphene nanoplatelets from simple solution edge-functionalization for n-type field-effect transistors," *Journal of the American Chemical Society*, vol. 135, no. 24, pp. 8981–8988, 2013.

[113] R. I. Jafri, N. Rajalakshmi, and S. Ramaprabhu, "Nitrogen doped graphene nanoplatelets as catalyst support for oxygen reduction reaction in proton exchange membrane fuel cell," *Journal of Materials Chemistry*, vol. 20, no. 34, pp. 7114–7117, 2010.

[114] Y. Guo, X. Sun, Y. Liu, W. Wang, H. Qiu, and J. Gao, "One pot preparation of reduced graphene oxide (rgo) or au (ag) nanoparticle-rgo hybrids using chitosan as a reducing and stabilizing agent and their use in methanol electrooxidation," *Carbon*, vol. 50, no. 7, pp. 2513–2523, 2012.

[115] G. Dawson, W. Chen, T. Zhang, Z. Chen, and X. Cheng, "A study on the effect of starting material phase on the production of trititanate nanotubes," *Solid State Sciences*, vol. 12, no. 12, pp. 2170–2176, 2010.

[116] H. G. Yang, C. H. Sun, S. Z. Qiao, J. Zou, G. Liu, S. C. Smith, H. M. Cheng, and G. Q. Lu, "Anatase tio2 single crystals with a large percentage of reactive facets," *Nature*, vol. 453, no. 7195, pp. 638–641, 2008.

[117] M. Yarali, Y. Alp, *et al.*, "The effect of ph on the interlayer distances of elongated titanate nanotubes and their use as a li-ion battery anode," *Nanotechnology*, vol. 27, no. 1, p. 015401, 2015.

[118] S. Zhang, Q. Chen, and L.-M. Peng, "Structure and formation of h 2 ti 3 o 7 nanotubes in an alkali environment," *Physical Review B*, vol. 71, no. 1, p. 014104, 2005.

[119] J. Yang, D. Li, X. Wang, X. Yang, and L. Lu, "Study on the synthesis and ion-exchange properties of layered titanate na2ti3o7 powders with different sizes," *Journal of materials science*, vol. 38, no. 13, pp. 2907–2911, 2003.

[120] B. C. Viana, O. P. Ferreira, A. G. Souza Filho, A. A. Hidalgo, J. Mendes Filho, and O. L. Alves, "Alkali metal intercalated titanate nanotubes: A vibrational spectroscopy study," *Vibrational Spectroscopy*, vol. 55, no. 2, pp. 183–187, 2011.

[121] L. Torrente-Murciano, A. A. Lapkin, and D. Chadwick, "Synthesis of high aspect ratio titanate nanotubes," *Journal of Materials Chemistry*, vol. 20, no. 31, pp. 6484–6489, 2010.

[122] M. H. Razali, A.-F. M. Noor, A. R. Mohamed, and S. Sreekantan, "Morphological and structural studies of titanate and titania nanostructured materials obtained after heat treatments of hydrothermally produced layered titanate," *Journal of Nanomaterials*, vol. 2012, p. 18, 2012.

[123] S. Konwer, R. Boruah, and S. K. Dolui, "Studies on conducting polypyrrole/graphene oxide composites as supercapacitor electrode," *Journal of electronic materials*, vol. 40, no. 11, pp. 2248–2255, 2011.

[124] T. A. Pham, J. S. Kim, J. S. Kim, and Y. T. Jeong, "One-step reduction of graphene oxide with l-glutathione," *Colloids and Surfaces A: Physicochemical and Engineering Aspects*, vol. 384, no. 1, pp. 543–548, 2011.

[125] T. Hu, X. Sun, H. Sun, G. Xin, D. Shao, C. Liu, and J. Lian, "Rapid synthesis of nitrogen-doped graphene for a lithium ion battery anode with excellent rate performance and super-long cyclic stability," *Physical Chemistry Chemical Physics*, vol. 16, no. 3, pp. 1060–1066, 2014.

[126] F. Tuinstra and J. L. Koenig, "Raman spectrum of graphite," *The Journal of Chemical Physics*, vol. 53, no. 3, pp. 1126–1130, 1970.

[127] R. Sitko, P. Janik, B. Feist, E. Talik, and A. Gagor, "Suspended aminosilanized graphene oxide nanosheets for selective preconcentration of lead ions and ultra-

sensitive determination by electrothermal atomic absorption spectrometry," *ACS applied materials & interfaces*, vol. 6, no. 22, pp. 20144–20153, 2014.

[128] S. P. Lim, A. Pandikumar, Y. S. Lim, N. M. Huang, and H. N. Lim, "In-situ electrochemically deposited polypyrrole nanoparticles incorporated reduced graphene oxide as an efficient counter electrode for platinum-free dye-sensitized solar cells," *Scientific reports*, vol. 4, 2014.

[129] P. Xu, J. Loomis, R. D. Bradshaw, and B. Panchapakesan, "Load transfer and mechanical properties of chemically reduced graphene reinforcements in polymer composites," *Nanotechnology*, vol. 23, no. 50, p. 505713, 2012.

[130] I.-Y. Jeon, H.-J. Choi, M. J. Ju, I. T. Choi, K. Lim, J. Ko, H. K. Kim, J. C. Kim, J.-J. Lee, D. Shin, *et al.*, "Direct nitrogen fixation at the edges of graphene nanoplatelets as efficient electrocatalysts for energy conversion," *Scientific reports*, vol. 3, 2013.

[131] T.-D. Nguyen-Phan, V. H. Pham, E. J. Kim, E.-S. Oh, S. H. Hur, J. S. Chung, B. Lee, and E. W. Shin, "Reduced graphene oxide–titanate hybrids: morphologic evolution by alkali-solvothermal treatment and applications in water purification," *Applied Surface Science*, vol. 258, no. 10, pp. 4551–4557, 2012.

[132] J. Wang, L. Shen, H. Li, X. Wang, P. Nie, B. Ding, G. Xu, H. Dou, and X. Zhang, "A facile one-pot synthesis of tio 2/nitrogen-doped reduced graphene oxide nanocomposite as anode materials for high-rate lithium-ion batteries," *Electrochimica Acta*, vol. 133, pp. 209–216, 2014.

[133] J. Wang, A. K. Mishra, Q. Zhao, and L. Huang, "Size effect on thermal stability of nanocrystalline anatase tio2," *Journal of Physics D: Applied Physics*, vol. 46, no. 25, p. 255303, 2013.

[134] S.-J. Kim, Y.-U. Yun, H.-J. Oh, S. H. Hong, C. A. Roberts, K. Routray, and I. E. Wachs, "Characterization of hydrothermally prepared titanate nanotube powders

by ambient and in situ raman spectroscopy," *The Journal of Physical Chemistry Letters*, vol. 1, no. 1, pp. 130–135, 2009.

[135] S. Yumitori, "Correlation of c1s chemical state intensities with the o1s intensity in the xps analysis of anodically oxidized glass-like carbon samples," *Journal of materials science*, vol. 35, no. 1, pp. 139–146, 2000.

[136] T. Allen, "Surface area and pore size determination," *Particle Size Measurement*, vol. 2, 1997.

[137] V. Štengl, S. Bakardjieva, T. M. Grygar, J. Bludská, and M. Kormunda, "Tio2-graphene oxide nanocomposite as advanced photocatalytic materials," *Chemistry Central Journal*, vol. 7, no. 1, pp. 1–12, 2013.

[138] L. Xiong, Y. Yang, J. Mai, W. Sun, C. Zhang, D. Wei, Q. Chen, and J. Ni, "Adsorption behavior of methylene blue onto titanate nanotubes," *Chemical Engineering Journal*, vol. 156, no. 2, pp. 313–320, 2010.

[139] J. Shen, Y. Hu, C. Li, C. Qin, and M. Ye, "Synthesis of amphiphilic graphene nanoplatelets," *small*, vol. 5, no. 1, pp. 82–85, 2009.

[140] Y. Wang, Y. Zhang, C. Hou, and M. Liu, "Ultrasensitive electrochemical sensing of dopamine using reduced graphene oxide sheets decorated with p-toluenesulfonate-doped polypyrrole/fe3o4 nanospheres," *Microchimica Acta*, vol. 183, no. 3, pp. 1145–1152, 2016.